

**SAMER NEMER**

**Fire buckling design of steel members:  
Overall Imperfection Method**

Doctoral Dissertation

Supervisor

**Prof. Ferenc Papp**

Doctor of the Hungarian Academy of Sciences

Department of Structural and Geotechnical Engineering

Modeling and Development of Infrastructural Systems

Doctoral School of Multidisciplinary Engineering Sciences

Győr, 2023.

## **Summary**

The Overall Imperfection Method is a well validated method for the assessment of the global stability resistance of steel structural members with any load and supporting conditions. The method has a strong mechanical background and is suitable for software implementation providing a fully automatic and economic way of buckling design for any structural steel member. In this dissertation I aim at proposing the OIM for fire design of steel members

The method uses the relevant elastic critical buckling mode shape as equivalent initial geometrical imperfection and gives universal procedure for the determination of the proper amplitude. The assessment of the global stability resistance of the proposed method is performed by checking of cross-sectional resistance using reduced value of the elastic modulus in the analysis and reduced yield strength for the cross-section checking at elevated temperatures.

First, I showed that the EN1993-1-2 buckling curve is not satisfactory in its current format for steel columns and needs to be recalibrated in order to obtain higher buckling capacities for members with low slenderness.

For proposing and validating the OIM for fire design a reference database is needed to which the OIM's results can be compared. Therefore, I developed a numerical model using ABAQUS software. Then, I validated it against several published numerical simulations and experimental tests results in the literature to guarantee its capability to accurately follow the response and predict the global buckling capacity of steel members at elevated temperatures.

I created a database using geometrically and materially nonlinear analysis with imperfections included 'GMNIA' using the developed ABAQUS model and a proper modified Matlab code.

Then I applied these values as loads on the investigated members in order to obtain the corresponding OIM results as a proportion of these values. In this way the comparison could be achieved easily.

I examined the accuracy of the OIM methodology on prismatic beams, columns and beam-columns. I showed that the OIM leads to accurate and consistent results if the imperfection factors applied for the pure buckling modes have the proper values.

Therefore, I examined the OIM with imperfection coefficients specified in the valid EN1993-1-2; the semi-probabilistic safety level assessment of the results shows that the proposed OIM has the better safety level than that of the interaction method given in EN1993-1-2.

I showed that both approaches may lead to unsafe design for the case of short columns. Therefore, I investigated the OIM with the new value of the imperfection coefficients of 0.85; by this proposal, the results show good agreement with the numerical results given by GMNIA

Furthermore, I showed how the proposed OIM is capable of providing accurate result for a studied class 4 cross-section beam column at elevated temperatures.

In addition to proposing the OIM for fire design, I investigated the influence of imperfections, namely, the initial geometrical imperfections (both global and local), and residual stress, upon the buckling load capacity of steel members subjected to axial force and bending moment at elevated temperatures.

Based on the imperfection sensitivity analysis, I found that the initial global imperfection value affects not only the buckling resistance but also the initial stiffness of steel beam-columns. The increase of the amplitude of the initial global imperfection resulted in a considerable decrease in the ultimate fire strength and initial stiffness.

Moreover, I studied the influence of different residual stress patterns at different temperatures. It was also observed that, at room temperature, ECCS residual stress pattern has the largest effect on the buckling resistance. However, at 500 °C considering Taras or ECCS residual stress patterns results in almost the same response, and Best-fit Prawel pattern has the biggest influence (the most conservative case).

# Table of contents

1. Introduction .....	1
1.1. Topic of the research .....	1
1.2. Problem statement .....	3
1.3. Objective of the research .....	3
1.4. Scientific methodology of the research.....	4
1.5. Importance of the research.....	4
1.6. Outline of the dissertation.....	5
2. Theoretical background.....	6
2.1. The background of the OIM methodology .....	6
2.1.1. Flexural buckling case: .....	6
2.1.2. Lateral torsional buckling case: .....	8
2.1.3. Coupled buckling case .....	11
2.2. Background study on the design of steel members under fire .....	15
2.2.1. Material behaviour at elevated temperature .....	15
2.2.2. Eurocode 3 formulae on buckling resistance of steel member at elevated temperatures .....	25
2.2.3. Experiments and numerical research review on fire resistance of steel members .....	29
3. Research methodology .....	33
3.1. General.....	33
3.2. Test program for statistical evaluation.....	33
3.3. Numerical model for GMNIA .....	34
3.3.1. Abaqus Element type and mesh size.....	34
3.3.2. Boundary conditions .....	36
3.3.3. Load conditions .....	36
3.3.4. Geometrical and material imperfections .....	36
3.3.5. Material properties.....	37
3.3.6. Numerical model validation.....	39
4. Testing the influence of imperfections on fire design of steel members.....	46
4.1. Sensitivity to imperfections analysis model.....	46
4.2. Sensitivity to initial geometrical imperfections .....	50
4.3. Sensitivity to residual stresses .....	51
4.4. Thesis 1.....	53
5. The effect of cross-section shape and slenderness ratio on buckling capacity of steel columns at elevated temperatures .....	54
5.1. The impact of cross-section shape on buckling capacity at elevated temperatures .....	54
5.2. Effect of the residual stress on different cross-sections at elevated temperatures .....	58

5.3. Influence of the material stress strain curve on buckling resistance .....	61
5.4. Thesis 2.....	63
<b>6. Overall Imperfection Method for fire design .....</b>	<b>64</b>
6.1. General.....	64
6.1.1. Universal Transformation (BS-1) .....	64
6.1.2. Analytical solution (BS-2).....	65
6.2. Main steps of OIM at elevated temperatures .....	66
6.2.1. ‘Structural Member → ERM’ transformation.....	66
6.2.2. The solution of the ERM .....	69
6.2.3. The ‘ERM → Structural Member’ transformation.....	71
6.2.4. Checking utilization of global buckling resistance .....	71
6.3. An illustrative example .....	74
6.4. Thesis 3:.....	77
<b>7. Statistical evaluation of the proposed OIM method for fire global buckling design.....</b>	<b>78</b>
7.1. Accuracy assessment of the OIM with exact imperfection factors .....	78
7.2. Thesis 4.....	81
7.3. Accuracy assessment of the OIM with imperfection factors specified by EN1993-1-2 .....	81
7.4. Accuracy assessment of the OIM with modified imperfection factor.....	84
7.5. Thesis 5.....	88
<b>8. Conclusion and future research .....</b>	<b>89</b>
8.1. Conclusion .....	89
8.2. Recommendations and future research .....	90

## Nomenclature

### Acronyms

OIM	Overall Imperfection Method – a method for the assessment of the global buckling resistance of structural members and structures using equivalent geometrical imperfection where the checking the cross-section resistance using geometrically nonlinear analysis involves the checking the global stability resistance.
GNIA	Geometrically Nonlinear Analysis with Imperfection – an elastic analysis using initial geometrical imperfection and assuming geometrically nonlinear behavior.
GMNIA	Geometrically and Materially Nonlinear Analysis with Imperfections – a materially and geometrically nonlinear analysis using relevant initial imperfections. Sometimes it is referred as ‘simulation’ since it is assumed that using characteristic model parameters the result of the analysis leads to characteristic value of the ultimate load.
LBA	Linear Bifurcation Analysis – a buckling analysis using linearly elastic material law and assuming linear relationship between the load factor and the internal forces and moments.
UGLI	Unique Global and Local Imperfection – an initial geometrical imperfection in the shape of a relevant buckling mode which shape involves both the bow and the sway type buckling modes.
ERM	Equivalent Reference Member – a simply supported, uniform and straight structural member with constant internal forces and moments, which member has the same critical load factor than the examined member has; the properties of the equivalent reference member are derived from the properties of the examined member at the equivalent point; in the equivalent point the utilization of the cross-sectional resistance calculated from the modal shape generated internal forces and moments has maximum.
APF	Ayrton-Perry Formula – an equation for buckling reduction factor related to the first yielding design state of a column with initial bow imperfection, assuming geometrically nonlinear behavior; the equation involves a parameter called imperfection factor which ensures the calibration of the formula.
BMC	Buckling Mode Class – a possible fundamental buckling mode (e.g. flexural buckling or lateral-torsional buckling) of the examined structural member.
ECCS	European Convention for Constructional Steelworks.

### Latin upper case letters

$A$	area of the cross-section;
$A_{eff}$	effective area for class 4 cross-sections;
$B''_{fi, \theta, Ed}$	internal bimoment calculated by GNIA at elevated temperature;
$B_{sec, \theta}$	warping cross-sectional resistance at elevated temperature;
$B''_{cr, \theta, ep}$	modal second order internal bimoment generated by the buckling mode shape at elevated temperature, taken in equivalent point;
$E$	modulus of elasticity;
$G$	shear modulus of elasticity;
$L_{eq}$	equivalent length of ERM;
$M_{cr}$	critical bending moment for lateral-torsional buckling mode;
$M_{fi, Ed}$	design bending moment load at fire design situation;
$M^l_y$	internal bending moment around the strong axis (y) calculated by linear elastic first-order analysis, in the paper it is always equal to the buckling-active internal bending moment $M^a$ ;
$M''_{cr, \theta, ep}$	modal second order internal bending moment generated by buckling mode shape at elevated temperature, taken in equivalent point;
$M''_{fi, \theta, Ed}$	internal bending moment about axis y or z calculated by GNIA at elevated temperature;
$\Delta M''_{fi, \theta, Ed}$	secondary internal bending moment in case of class 4 cross-sections at elevated temperature, due to shift of centroid;
$M_{fi, \theta, Rd}$	design cross-sectional resistance for pure bending at elevated temperature in fire design situation (see EN1993-1-2);
$M_{sec, \theta}$	bending cross-sectional resistance about axis y or z at elevated temperature;

$N_{fi,Ed}$	design axial load at fire design situation;
$N^I$	internal axial force calculated by linear elastic first-order analysis, in the paper it is always equal to the buckling-active internal axial force $N^a$ ;
$N_{cr}$	critical axial force for flexural buckling mode;
$N_{cr,z,\theta}$	critical axial force for flexural buckling mode around weak axis at elevated temperature;
$N_{cr,x,\theta}$	critical axial force for torsional buckling mode at elevated temperature;
$N_{fi,\theta,Ed}^I$	internal axial force calculated by GNIA at elevated temperature;
$N_{fi,\theta,Rd}$	design cross-sectional resistance for pure compression at elevated temperature in fire design situation (see EN1993-1-2);
$N_u$	ultimate value of compressive load of structural test;
$U_{sec}$	utilization of cross-sectional resistance;
$U_{max,\theta}$	maximum utilization of the cross-sectional resistance along the examined member at elevated temperature;
$U_{sec,cr,\theta}^{II}$	second order cross-section utilization from the model internal moments, which are generated by shape of buckling mode with arbitrary amplitude, at elevated temperature;
$W$	cross-sectional modulus about axis $y$ or $z$ , or for warping, considering class of section;
$W_{eff}$	effective sectional modulus about axis $y$ or $z$ , or for warping, in case of class 4 sections.

### Latin lower-case letters

$ep$	location of the equivalent point along the examined structure;
$v_{cr,\theta}$	flexural component of the shape of the elastic buckling mode at elevated temperature;
$y$	strong axis of the cross-section;
$z$	weak axis of the cross-section;
$f_y$	design yield strength;
$k_{y,\theta}$	reduction factor from section 3 for the yield strength of steel at elevated temperature $\theta$ ;
$k_{p0.2,\theta}$	reduction factor for the yield strength at elevated temperature in case of class 4 cross-sections;
$n$	number of test cases to be considered;
$r_e$	reduced ultimate load parameter calculated experimentally;
$r_t$	reduced ultimate load parameter calculated numerically.

### Greek lower case letters

$\alpha$	imperfection factor in the AP formula of the flexural buckling curve at fire design situation;
$\alpha_{ult}$	minimum load amplifier of the design load to reach the characteristic resistance of the most critical cross-section;
$\alpha_{LT}$	imperfection factor in the AP formula of the lateral torsional buckling curve at fire design situation;
$\delta_{eq}$	equivalent amplitude for the initial geometrical imperfection;
$\alpha_{cr,\theta}$	minimum force amplifier to reach the elastic critical buckling load at elevated temperature;
$\alpha_{sec,\theta}$	cross-sectional resistance multiplication factors taking the buckling active load (N, M or N+M) into account at elevated temperature;
$\bar{\lambda}$	non dimensional slenderness for the flexural buckling;
$\bar{\lambda}_\theta$	the reduced non-dimensional slenderness for the flexural buckling mode for the temperature $\theta$ ;
$\bar{\lambda}_{LT}$	non dimensional slenderness for the lateral torsional buckling;
$\bar{\lambda}_{LT,\theta}$	the reduced non-dimensional slenderness for the lateral-torsional buckling mode for the temperature $\theta$ ;
$\theta$	the temperature [ $^{\circ}\text{C}$ ];
$\varphi_{cr}$	torsional component of the shape of the elastic buckling mode;
$\mu_{cr,\theta}$	shape of elastic buckling mode with arbitrary amplitude;
$\mu_{cr,eq}$	equivalent geometrical imperfection in the shape of the elastic buckling mode with arbitrary amplitude;
$\mu_\theta$	interaction factor for interpolating the beam-column imperfection factor at elevated temperature;

$\eta_{N,\theta}$	shape of elastic critical buckling mode of the column member (pure compression);
$\eta_{M,\theta}$	shape of elastic critical buckling mode of the beam member (pure bending);
$\eta_{NM,\theta}$	shape of elastic critical buckling mode of the beam-column member (compression and bending).
$f$	modification factor for $\chi_{LT}$
$kc$	correction factor for moment distribution
$\psi$	ratio of moments in segment
$\gamma$	taper ratio

### Subscripts which refers to

$sec$	cross-sectional parameter;
$cr$	elastic buckling state;
$\theta$	elevated temperature;
$eq$	equivalent value;
$Ed$	design action calculated by elastic theory;
$fi$	fire design situation;
$y$	strong axis of cross-section;
$z$	weak axis of cross-section;
$\omega$	warping;
$N$	effect by axial force;
$M$	effect by bending moment;
$NM$	coupled axial force and bending moment effect;
$u$	ultimate load carrying capacity;
$el$	elastic cross-sectional property;
$pl$	plastic cross-sectional property;
$eff$	effective cross-sectional property of class 4 sections;
$LT$	lateral-torsional buckling mode.

### Superscripts which refers to

$a$	buckling-active effect (which directly causes the buckling);
$I$	calculated by linear elastic (1 <sup>st</sup> order) theory;
$II$	calculated by geometrically non-linear elastic (2 <sup>st</sup> order) theory;
$ERM$	calculated on the equivalent reference member.



## 1. Introduction

### 1.1. Topic of the research

Over the past few years, there has been growing interest in improving the rules used in structural fire design. The fire part of Eurocode ‘EN1993-1-2’ [1] adopts simple application rules for designing steel members at elevated temperatures following reduced values of material properties correspond to the investigated elevated temperatures. However, this method adopts only one buckling curve and limited to uniform members design. Moreover, numerous studies have demonstrated that the current design rules of steel members under elevated temperatures that are outlined in EN1993-1-2 are very approximate in most cases [2]. Moreover, it turned out that these rules are too conservative and also lead to uneconomical results [3]. Therefore, there is a need to explore alternative design methods that could provide more comprehensive and efficient solutions.

Under normal temperature condition, the current European standard EN1993-1-1 [4] provides formulae for calculating the buckling resistance of uniform steel members subjected to compression, bending, and combined axial compression and bending in its sections (6.3.1), (6.3.2) and (6.3.3), respectively. Additionally, two alternative methods are available for assessing the stability resistance of steel members subjected to either uniform or non-uniform loading conditions. These methods include the General Method (GM), which can be found in EN 1993-1-1: section 6.3.4, and the Overall Imperfection Method (OIM), as outlined in EN 1993-1-1: section 5.3.2(11) [4].

The Overall Imperfection Method (OIM) is the generalization of the Unique Global and Local Imperfection (UGLI) method introduced by the EN1993-1-1 [4] and initially published by Chladný et al. [5]. The original UGLI method was primarily valid for purely compressed members subjected to flexural buckling.

Later, Agüero et al. expanded the UGLI method for lateral-torsional buckling [6], while Papp extended it further to evaluate the buckling of structural members susceptible to the interaction of flexural and lateral-torsional buckling [7]. In [8], the OIM was introduced for beam-columns subjected to different load conditions at normal member temperature. The OIM methodology

assumes that all complex global buckling modes can be categorized into a finite numbers of fundamental buckling modes, such as flexural buckling or lateral-torsional buckling [9].

Furthermore, the efficacy of the method was examined for beam-columns subjected to various load conditions in [10]. The study concluded that the OIM at normal member temperature is reliable and provides a comparable safety level to the available design methods.

The most comprehensive description of the generalized OIM was published by Szalai and Papp [11]. The OIM was used by Papp et al. for design of irregular structural members and simple portal frames [12].

The Overall Imperfection Method OIM covers all types of buckling modes (flexural, torsional, flexural-torsional, lateral-torsional or any interaction thereof), which may be calculated by linear buckling analysis LBA of structural models composed of uniform or non-uniform members with any cross-sections and support conditions and subjected to complex loading [13].

In order to evaluate the stability resistance of steel members subjected to elevated temperatures, the proposed OIM methodology in this research employs the result of the Linear Buckling Analysis (LBA), including the elastic critical load factor, buckling mode shape, and second order internal moments induced by the modal geometric imperfection.

Similar to the OIM at normal temperature, the proposed approach assumes that, in case of elevated temperature, any complex global buckling mode can be classified into one of the finite number of fundamental buckling modes (e.g. flexural buckling, lateral-torsional buckling or interaction of them).

Moreover, it assumes that the Ayrton-Perry formula based standard buckling curves calibrated for elevated temperatures are available for the fundamental global buckling modes, and by using them the required reliability level can be ensured.

Previous works on the OIM have been limited to the stability design of steel members at normal temperatures. Therefore, the purpose of this research is to develop and validate the OIM methodology for checking the stability resistance of steel members at elevated temperatures.

## **1.2. Problem statement**

The rules available in the Eurocode standard for fire design of steel members are simplified. The method adopts only one buckling curve and limited to uniform members design. These rules are reported to be unsafe for some cases and very conservative for other cases. In other words, there is still a lack of certainty about the safety level and accuracy of the Eurocode procedure and the adopted imperfection factor. Therefore, there is a need to find more comprehensive and accurate methods. Besides, previous works have been limited to the use of the Overall Imperfection Method for the stability design of steel members at room temperatures.

In addition to that, there is a lack of adequate information regarding the influence of various factors, such as the cross-section shape, slenderness, and geometrical (global and local) and material imperfections on buckling capacity of steel members in fire conditions. Therefore, a deeper research on the effect of these factors on buckling strength at elevated temperatures is needed.

## **1.3. Objective of the research**

The primary objective of this research is to propose and validate the Overall Imperfection Method for global stability design of steel beams, columns, and beam-columns under elevated temperatures condition.

Moreover, the research aims to propose and examine a new suitable value of the imperfection factor given in EN1993-1-2.

Additionally, the research aims to determine real impact of several factors, including the structural geometrical and material imperfections on the ultimate load capacity of steel members at elevated temperatures in order to avoid oversimplification related to fire design of steel structures.

#### **1.4. Scientific methodology of the research**

In order to evaluate the accuracy of the proposed OIM, it is essential to have a reference database covering different load cases, temperatures, sections and slenderness ratios, against which the OIM's results can be compared.

To achieve this, a numerical model using ABAQUS software was developed, then its capability to correctly depict the real behavior of steel members at elevated temperatures and predicting the fire buckling capacities of different steel members were evaluated by comparing its results against real experimental and numerical studies results.

Following validation of the numerical model, the database was created using GMNIA and a structural model, taking into account characteristic parameters (especially the characteristic value of the yield strength).

This database created by this way can serve as a reference for calculating the capacities according to the proposed OIM for the purpose of comparison, . Based on statically evaluation of these results, the accuracy of the proposed OIM can be evaluated.

It is noted that nowadays this concept is widely accepted in the current research on steel structural engineering.

#### **1.5. Importance of the research**

Enhancing the level of accuracy of the fire design procedures for steel members is crucial for ensuring structural safety and reducing the fire protection costs. Therefore, there is a need for developing more accurate design methods to better predict the behavior of steel members at elevated temperatures.

The innovation of this research is a computer based formula for the equivalent initial imperfection for steel members subjected to buckling at elevated temperatures. The derived formula is consistent with the fundamental case adopted in the EN 1993-1-2, where the design equations for the assessment buckling resistances are based on the Ayrton–Perry formula.

## 1.6. Outline of the dissertation

**Chapter 2:** The scientific background and literature study is given, which is used throughout the research. First the proposed OIM is explained in details along with its adaptation to fire and secondly the current rules from the fire part of Eurocode, After this some discussion points on the effect of imperfections and other factors on the fire design of steel members is discussed.

**Chapter 3:** In this chapter, the research methodology including description of the developed Finite element model used in this research for the numerical study is elaborated along with the applied material properties, boundary conditions, load cases and imperfections including geometrical imperfections and residual stress pattern used is described.

**Chapter 4:** This section provides an investigation on the influence of imperfections, namely, the initial geometrical imperfections (both global and local), and residual stress, on the buckling load capacity of steel members subjected to axial force and bending moment at elevated temperatures.

**Chapter 5:** In this section, a study is presented that explores how various factors affect the buckling strength of steel members at elevated temperatures. The study specifically focuses on three parameters: slenderness ratio, residual stress, and material model, and their influence on the behavior of steel columns with different hot-rolled cross-sections (IPE, HEA) at elevated temperature conditions.

**Chapter 6:** The application of the OIM for the design of structural beam-columns subjected to elevated temperatures is presented in this chapter. The main steps of the method are explained, followed by a detailed step-by-step case study solved using the proposed Overall Imperfection Method on fire design of a steel beam-column is given.

**Chapter 7:** Numerical and statistical evaluation of the accuracy of the proposed Overall Imperfection method for different imperfection factor values is given through comparison between the proposed OIM's results, GMNIA and Eurocode results for different imperfection factor, load cases and temperatures.

**Chapter 8:** This section summarizes the key findings and contributions of the research and outline potential areas for future investigation that are suggested by the results.

## 2. Theoretical background

In this section, first, the studies on the Overall Imperfection Method (OIM) will be summarized for normal temperature, taking different fundamental buckling cases (flexural buckling, lateral-torsional buckling, interaction buckling) into consideration. After that, a review of the factors that affect the fire design of steel members will be discussed, with a focus on the material behavior at elevated temperatures.

### 2.1. The background of the OIM methodology

#### 2.1.1. Flexural buckling case:

The principles and applications of the Equivalent Unique Global and Local initial Imperfection (EUGLI) method for purely compressed members and frames were presented by Chladný and Štujberová in [5] and [15].

Basically, the amplitude of the equivalent imperfection should be based on both experimentally established and statistically evaluated imperfections for different types of frames. However, the experimentally established values were unavailable. Therefore, the amplitude of the equivalent imperfection in the shape of the elastic buckling mode was determined by the following fundamental requirement: The buckling resistance of the frame structure with axially loaded members shall be equal to the flexural buckling resistance of the equivalent member.

The equivalent member was defined as a structural member with pinned ends, it has the same cross-section and axial force as these in the critical cross-section ( $m$ ) of the frame, and its length is such that its critical force equals the axial force in the critical cross-section ( $m$ ) at the critical loading of the structure.

The position of the critical cross-section ( $m$ ) was determined by the following condition:

The utilization  $U_m$  with allowance for the effect of the axial force and bending moments due to imperfections at the critical cross-section  $m$ , is greater than the utilization  $U(x)$  at all other cross-sections of the verified member or frame:

$$U_m = \frac{N_{Ed,m}^{\parallel}}{N_{Rd,m}} + \frac{M_{\eta init,m,m}^{\parallel}}{M_{Rd,m}} = U_{N,m} + U_{M,\eta init,m,m} \quad (1)$$

In equation (1),  $M_{\eta_{init,m,m}}^{\parallel}$  is the bending moment at the critical cross-section ( $m$ ) of the compressed member or frame due to the imperfection  $\eta_{init,m}(x)$  calculated using a second-order analysis

The equivalent unique global and local initial imperfection  $\eta_{init,m}$  is given by:

$$\eta_{init,m}(x) = \eta_{init,m,max} \frac{\eta_{cr}(x)}{|\eta_{cr}|_{max}} \quad (2)$$

$\eta_{init,m,max}$  is the design value of the maximum amplitude of the  $\eta_{init,m}$  imperfection.

$|\eta_{cr}|_{max}$  is the maximum amplitude of the imperfection in the shape of the elastic critical buckling mode  $\eta_{cr}(x)$ .

The second-order deflection  $\eta^{\parallel}$ , as the effect of imperfection  $\eta_{cr}$  on the compressed member is given by:

$$\eta^{\parallel}(x) = \frac{1}{\alpha_{cr}-1} \eta_{cr}(x) ; \text{ where } \alpha_{cr} = \frac{N_{cr}(x)}{N_{Ed}(x)} \quad (3)$$

The second-order bending moment at the critical cross-section  $m$  of the member (which is bent into the shape of the  $\eta_{init,m}$ ) is:

$$M_{\eta_{init,m,m}}^{\parallel} = \eta_{init,m,max} \frac{1}{\alpha_{cr}-1} \frac{|EI_m \eta_{cr}^{\parallel}|_m}{|\eta_{cr}|_{max}} \quad (4)$$

The amplitude of the equivalent initial imperfection in the shape of buckling mode  $\eta_{init,m}$  is expressed in terms of the second order normal stress as follows:

$$\eta_{init,m,max} = \frac{\sigma_{M,\eta_{init,m,m}}^{\parallel}}{|\sigma_{\eta_{cr}}^{\parallel}|_m} |\eta_{cr}|_{max} \quad (5)$$

$|\sigma_{\eta_{cr}}^{\parallel}|_m$ : is the maximum second-order normal stress from bending as the effect of the  $N_{Ed}$  compressive force with initial imperfection in the shape of the elastic buckling mode

$\sigma_{M,\eta_{init,m,m}}^{\parallel}$ : is the maximum second-order normal stress from bending as the effect of the  $N_{Ed}$  compressive force with the calibrated value of the equivalent amplitude

### 2.1.2. Lateral torsional buckling case:

EN1993 specifies that the fundamental case of LTB can consider an equivalent initial imperfection through a lateral geometric out-of-straightness with an amplitude of  $(k e_{0d})$ , where  $k$  takes the value of 0.5. Later, Calgaro et al. proposed to change this factor to  $k = 1.0$  [16]. Boissonnade et al. determined the equivalent amplitude of the lateral initial imperfection based on the relevant reduction factor [17].

Later, Agüero et al. [6] presented a proposal for the design of steel structures sensitive to lateral-torsional buckling due to bending moment in order to fill the gaps in the Standard EN 1993-1-1 [4]. Thus, the proposal generalized the approach provided in clause 5.3.2(11) of EN 1993-1-1 for steel structures sensitive to flexural buckling under compression. He derived the comprehensive definition of the equivalent initial imperfection for Class 2 and Class 3 cross-sections.

the following assumptions were made by the authors:

- the Clause 6.3.2 of the standard EN 1993-1-1 allows designers to use the  $\chi_{LT}$  factor, originally deduced from compression-flexural buckling experiments, for members under lateral-torsional buckling due to bending. The approach proposed is valid if different  $\chi_{LT}$  factors were taken into account, which were proposed to flexural–torsional buckling by Taras in [18], [19], [20].
- the basic concept of the proposal is the same as in the method given in Clause 5.3.2(11) of EN1993-1-1 [4], using the elastic buckling mode as the shape of the imperfection and assuming the results of the equivalent member method, which extracts an equivalent member with the same buckling length but with pinned boundary conditions, and computes its buckling strength on the basis of beam buckling curves.

By this, a simplified method to obtain the geometric equivalent imperfection scaling the buckling mode consistent with clause 5.3.2(11) of the EN1993-1-1 was proposed, without considering the shear stresses due to Saint–Venant torsion.

According to Agüero proposal, for an I-section beam with fork supports on both ends subjected to uniform bending the shape of lateral imperfection in a side view and top view for three points (bottom flange, shear center and top flange) is shown in Fig. (1). The analytical expression of the geometrical imperfection is:



$$\frac{\eta_{init_v}(x)}{\left(\frac{H^2}{4} + \frac{L^2}{\pi^2} \frac{G I_t}{E I_z}\right)} = \eta_{init_{\theta x}}(x) \quad (6)$$

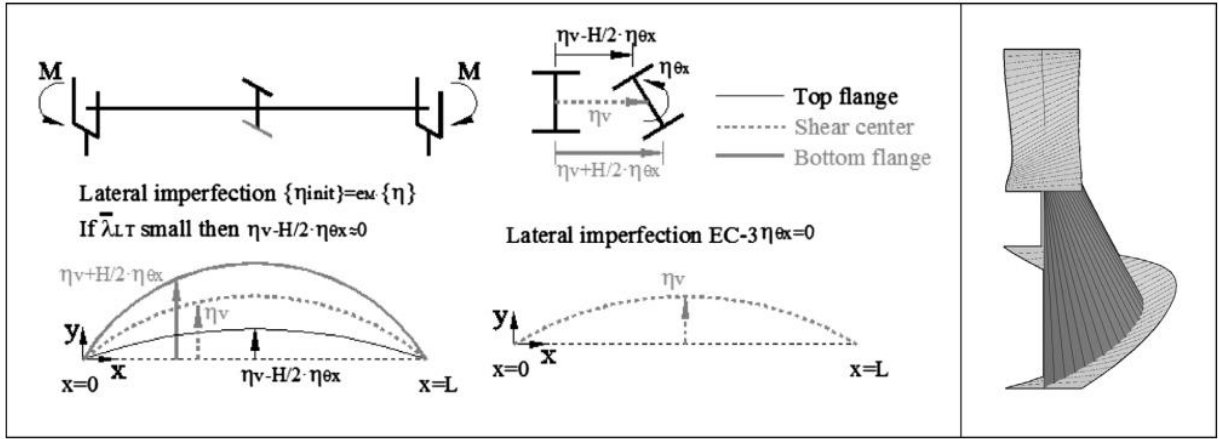


Fig. 1. Lateral imperfection according to the proposal in [6] and Eurocode 3.

Later, Papp [7] proposed the magnitude of the equivalent initial bow imperfection for members subjected to Lateral Torsional Buckling as follows:

$$v_{0d} = \frac{\eta_{LT}}{\frac{W_y}{W_\omega} + \frac{W_y}{W_z} \frac{N_{cr,z}}{M_{cr}} - \frac{N_{cr,z}}{M_{cr}^2} G I_t \frac{W_y}{W_\omega}} \quad (7)$$

$$\varphi_{0d} = v_{0d} \frac{N_{cr,z}}{M_{cr}} \quad (8)$$

$W_y, W_z, W_\omega$  = section modulus, regarding the class of cross-section

$N_{cr,z}$  : critical force for flexural buckling

$M_{cr}$ : critical moment for lateral-torsional buckling

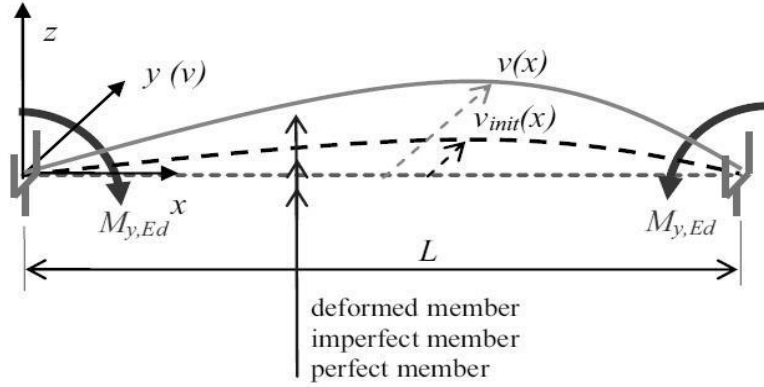


Fig. 2. Fundamental case of Lateral Torsional Buckling according to [7]

The equivalent initial imperfection formula:

$$v_{init}(x) = v_{init,max} \frac{v_{cr}(x)}{v_{cr,max}} \quad (9)$$

where:

$v_{cr}(x)$ : is the shape of the elastic buckling mode, and  $v_{cr,max}$  : is the arbitrary amplitude

$v_{init,max}$ : is the equivalent amplitude

The second-order deformation  $v^{\parallel}(x)$  is given by:

$$v^{\parallel}(x) = v_{init,max} \frac{1}{\alpha_{cr}-1} \frac{v_{cr}(x)}{v_{cr,max}} \quad (10)$$

where  $\alpha_{cr} = \frac{M_{cr}(x)}{M_{y,Ed}(x)}$

The second-order bending moment:

$$M_{z,v_{init}}^{\parallel}(x) = v_{init,max} \frac{1}{\alpha_{cr}-1} \frac{EI_z}{v_{cr,max}} v^{\parallel}_{cr}(x) \quad (11)$$

Papp proposed an alternative formula to calculate the magnitude of the equivalent initial imperfection in the shape of buckling mode  $\eta_{init,m}$  for which the second-order normal stress is used, as follows:

$$v_{init}(x) = \frac{\sigma_{z,v_{init,max}}^{\parallel}}{\sigma_{z,v_{cr,max}}^{\parallel}} v_{cr}(x) \quad (12)$$

$\sigma_{z,v_{cr},max}^{\parallel}$ : is the maximum second-order normal stress from around the z axis as the effect of the  $M_{y,Ed}$  bending moment with initial imperfection in the shape of the elastic buckling mode

$\sigma_{z,v_{init},max}^{\parallel}$ : is the maximum second-order normal stress from bending as the effect of the  $N_{Ed}$  compressive force with the calibrated value of the equivalent amplitude.

### 2.1.3. Coupled buckling case

#### 2.1.3.1. Generalized Ayrton-Perry formula

The Ayrton-Perry formula, in its original form, provides an analytical expression for determining the load-bearing capacity of columns under pure compression with geometric imperfections.

Szalai [21] presented consistent and generalized versions of the Ayrton-Perry formula (APF) that can be applied to different steel beam-column stability problems. According to the author, the generalized imperfection factor of the relevant Ayrton-Perry formula can be represented through linear interpolation between the fundamental cases.

To achieve a comprehensive solution suitable for the Overall Stability Design Method (OSDM) for members with doubly symmetric cross-sections, two new approaches were incorporated to amend the pure case solutions:

- In-plane effects can be effectively addressed by implementing the proposed strategy that involves active and passive loads.
- The interaction between the pure buckling cases can be accurately modeled using Equation (13), which represents a specialized combination of the solutions derived from the pure cases.

The amplitude of the imperfection is:

$$v_{0d,NM} = \frac{\alpha_{ult}}{\alpha_{ult,N}} e_{0,d} + \frac{\alpha_{ult}}{\alpha_{ult,M}} v_{0,d} \quad (13)$$

Where the minimum load amplifier of the design loads to reach the characteristic resistance of the most critical cross-section are given in equations (14 – 16):

$$\alpha_{ult,N} = \frac{N_{Rk}}{N_{Ed}} \quad (14)$$

$$\alpha_{ult,M} = \frac{M_{y,Rk}}{M_{y,Ed}} \quad (15)$$

$$\alpha_{ult} = \frac{1}{\frac{1}{\alpha_{ult,N}} + \frac{1}{\alpha_{ult,M}}} \quad (16)$$

The global buckling condition through the utilization of the cross-section resistance using linear approach:

$$U_{max} = \frac{N_{Ed}}{N_{Rd}} + \frac{M_{y,Ed}}{M_{y,Rd}} + \frac{M_{z,max}^{\parallel}}{M_{z,Rd}} + \frac{B_{max}^{\parallel}}{B_{Rd}} = 1 \quad (17)$$

The results of this paper hold significant value in the development of novel stability design approaches for beam-columns, particularly in the context of the Overall Stability Design Method (OSDM). In OSDM, the calculation of overall elastic critical buckling loads forms the foundation of the design process, making the results of this study given by Szalai relevant and practical.

### 2.1.3.2. Generalized Overall Imperfection Method

Later, Szalai and Papp in [11] provided a detailed explanation of the mechanical interpretation and calculation procedure of the OIM.

The Overall Stability Design methodology (OSDM) includes two design methods:

the Overall Strength Reduction Method (OSRM) and the Overall Imperfection Method (OIM).

Both of which have the same mechanical basis. This mechanical basis consists of two essential components: namely (1) a generalized form of the Ayrton-Perry or Perry-Robertson type strength reduction method for basic reference members and (2) a generalized transformation technique connecting the real members of the global structural model with the appropriate basic reference member. The methods are based on linear buckling analysis (LBA) of global structural models and use standard reduction curves.

The forward model transformation creates the Equivalent Reference Member (ERM) with the following properties (geometry: cross-section and member length; member loads; and buckling mode type) derived from the LBA results performed on the real structural model.

The transformation point where the second-order internal stress utilization effect from the buckling mode shape is the highest is called the equivalent point ( $ep$ )

The equivalent point is obtained by evaluating the internal forces and moments resulting from the deformation of the buckling mode shape along the longitudinal axes of the entire structural model (represented by  $x$ ) as  $S^{cr}(x)$ . Subsequently, the corresponding cross-section resistances are computed as  $R^T(x)$ . Finally, the linear utilization function is determined based on these internal forces and moments.

$$U_{sec,cr}(x) = R^T(x)S^{cr}(x) = \frac{1}{\alpha_{sec,cr}(x)} : x = ep \quad (18)$$

The analytical solution of any ERM is based on the generalized Ayrton-Perry model of a general reference member subjected to geometrical imperfection with a shape corresponding to the fundamental buckling mode and with a proper amplitude consistent with the standard buckling resistances

The most important parameter to correctly apply Ayrton-Perry formula and to estimate the second order effect is the imperfection factor. The imperfection factors are well-defined internal parameters of the Ayrton-Perry based standard reduction factors of the EC3 corresponding to the fundamental buckling mode types of pure loads (compression or bending only). The imperfection factors corresponding to coupled buckling modes are presented in [13]:

$$\eta_{coupled}^{ERM} = \frac{\frac{N^I}{N_{sec}}}{\frac{N^I}{N_{sec}} + \frac{M_y^I}{M_{y,sec}}} \eta_N^{ERM} + \mu \frac{\frac{M_y^I}{M_{y,sec}}}{\frac{N^I}{N_{sec}} + \frac{M_y^I}{M_{y,sec}}} \eta_{M_y}^{ERM} = \frac{\alpha_{sec,a}}{\alpha_{sec,N}} \eta_N^{ERM} + \mu \frac{\alpha_{sec,a}}{\alpha_{sec,M_y}} \eta_{M_y}^{ERM} \quad (19)$$

where  $\eta_N^{ERM}$  and  $\eta_{M_y}^{ERM}$  are the standard imperfection factors corresponding to the buckling modes,  $\alpha_{sec,N}$ ,  $\alpha_{sec,M_y}$  and  $\alpha_{sec,a}$  are the appropriate active LMFs and  $\mu$  is a modifying factor dependent on the pure elastic critical loads of the reference member (for OIM:  $\mu = 1$ ).

The equivalent reduction factor is the main result of the ERM

$$\chi^{ERM} = \frac{1}{\Phi + \sqrt{\Phi^2 - \lambda^{ERM^2}}} \quad (20)$$

Where:

$$\Phi = \frac{1}{2}(1 + \eta^{ERM} + \lambda^{ERM^2}) \quad (21)$$

The equivalent reduction factor and the second-order utilization of the ERM are the main results of the ERM and are used for backward result transformation to the real structural model.

$$U_{sec,cr}^{\parallel}(ep) = U_{sec,cr}^{\parallel,ERM} \quad (22)$$

Thus,

$$\delta_{eq} U_{sec,cr}(ep) \frac{1}{\alpha_{cr}-1} = \eta^{ERM} \frac{1}{\alpha_{sec,a}} \frac{1}{1-\frac{1}{\alpha_{cr}}} \quad (23)$$

where  $\delta_{eq}$  is the equivalent scale factor of the complex buckling mode shape which fulfils the equivalency relationship thus determines the correct amplitude of the equivalent geometrical imperfection of the real structural model.

The final step of the OIM involves running a second-order analysis and a cross-section check on the real structural model with the equivalent geometrical imperfection.

### 2.1.3.3. Parametric studies on the accuracy of Overall Imperfection Method

In order to assess the accuracy of the Overall Imperfection Method (OIM) for beam-columns under various load conditions, a comprehensive study was conducted as outlined in [9]. This involved performing a large number of geometrically and materially nonlinear analyses with imperfections (GMNIA) and conducting a semi-probabilistic safety level assessment of different available design methods to estimate the reliability of the OIM with different moment distributions. The results indicated that the OIM, when applied to beam-columns at normal temperature, demonstrates a satisfactory safety level without being excessively conservative. Furthermore, it was found to possess a comparable level of safety to other existing design methods.

Moreover, Hajdu and Papp in [22] conducted a parametric study to verify the accuracy of the overall imperfection method for beam-columns. The study involved performing numerical simulations on a member with an IPE360 cross-section using ConSteel software, under uniform compressive force and uniform bending moment, to evaluate the coupled buckling resistance. The results obtained from the advanced numerical simulation (GMNIA) were compared to those from the OIM. The coefficient of variation was found to be 4%, indicating the stability of the OIM results. The researchers also concluded that the OIM could be incorporated into design software that applies a 14 DOF thin-walled beam-column finite element method and supports geometrically nonlinear analysis on the buckled shape.

## **2.2. Background study on the design of steel members under fire**

The assessment of load-carrying resistance of steel members under fire situation is usually conducted on four levels:

Level 1: The material behavior at elevated temperatures

Level 2: The cross-sectional behavior, including local buckling

Level 3: The member behavior, including global buckling

Level 4: The global structural behavior (of the entire building or structure) that takes into account large deformations, changes in structural systems, and alternative load paths that may arise during a fire event. (nonlinear structural analysis)

However, this research specifically concentrates on the investigation of the global and local buckling of steel members at elevated temperatures, and therefore Level 4 is beyond the scope of this study. This following sub-sections discuss Levels 1, 2 and 3 in greater detail.

### **2.2.1. Material behaviour at elevated temperature**

Accurately predicting the behavior of steel members under fire conditions and constructing analytical models is heavily reliant on a thorough comprehension and effective application of

material behavior at elevated temperatures. Steel strength and stiffness experience a marked decrease as temperature rises. Moreover, carbon steel's clearly defined yield point and yield plateau at ambient temperature are no longer distinguishable, leading to a highly nonlinear stress-strain response.

#### **2.2.1.1. Material testing at elevated temperature**

There exist two conventional techniques for determining the mechanical characteristics (strength and stiffness) of steel under fire situation: isothermal (steady-state) and anisothermal (transient-state) tests.

Isothermal tests involve heating the specimen to the desired temperature, followed by loading the material at a steady pace until failure occurs. Conversely, anisothermal tests require subjecting the specimen to a predetermined constant load before raising the temperature at a controlled rate between 2-50°C/min (usually 10°C/min) until the material fails. The entire strain is measured with respect to temperature  $\theta$ , which can subsequently be transformed into stress-strain curves once the impact of thermal expansion is eliminated from the results via the appropriate coefficient of thermal expansion.

In steady-state tests, the strain rate and, in transient tests, the heating rate significantly influence the experimental outcomes. Therefore, to model structural fire behavior accurately or simulate fire tests, it is essential to use mechanical properties determined in a manner consistent with the projected fire conditions or the expected failure time in the tests [23].

It is worth noting that, in general, anisothermal (transient-state) tests on carbon steel produce marginally lower strength values than those obtained from isothermal (steady-state) tests. A comparison of results from steady-state tests and the minimum values from transient tests for temperatures ranging from 20 to 900 °C and plastic strains of 0.2%, 1.0%, 2.0%, and 5.0% was presented by Kirby and Preston [24]. The study evaluated contemporary U.K. structural carbon steels of grades 43A and 50B, with nominal yield strengths of 275 and 355 N/mm<sup>2</sup>, respectively, and the results were illustrated in Fig. 3.



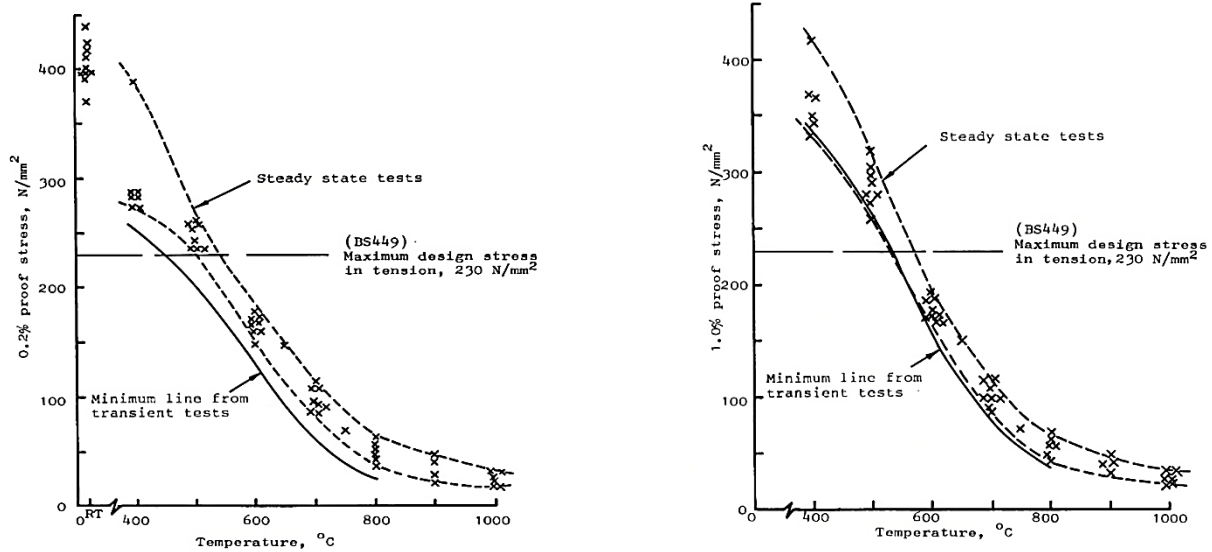


Fig. 3. Relationship between temperature and 0.2% (left) & 1.0% (right) proof stress for BS4360: Grade 50B structural steels [24]

As depicted in Fig. 3, the minimum 0.2% proof stress obtained from transient tests falls significantly below the steady-state range minimum between 400°C and 800°C, which is the range of temperatures under consideration. Nevertheless, for the 1.0% proof stress, the minimum from transient tests is nearly indistinguishable from the lower limit of the steady-state range.

### 2.2.1.2. Steel material model at elevated temperature

In this study, the EN 1993-1-2 material model is adopted, which incorporates Rubert and Schaumann's model developed based on anisothermal (transient state) tests performed on beams [25].

#### - Stress-strain relationship

The material model adopted in EN 1993-1-2:2005 [1] is a four-stage model, which is described below and illustrated in Fig. 4:

The first stage of the model is a linear elastic region, characterized by the elastic modulus ( $E_{a,\theta}$ ) which ranges from zero stress up to the proportional limit ( $f_{p,\theta}$ ). The proportional limit is defined as the point where the stress-strain curve transitions from elastic to plastic behavior.

The second stage which begins at the proportional limit ( $f_{p,\theta}$ ). The stress-strain curve in this region is represented by an elliptical curve until the maximum strength ( $f_{y,\theta}$ ) is obtained at a strain: ( $\varepsilon_{y,\theta} = 2\%$ ).

In the third stage, a constant strength is assumed between strain ( $\varepsilon_{y,\theta} = 2\%$ ) and ( $\varepsilon_{t,\theta} = 15\%$ ).

The fourth and final stage of the model assumes that the stress decreases to zero at the ultimate strain ( $\varepsilon_{u,\theta} = 20\%$ ).

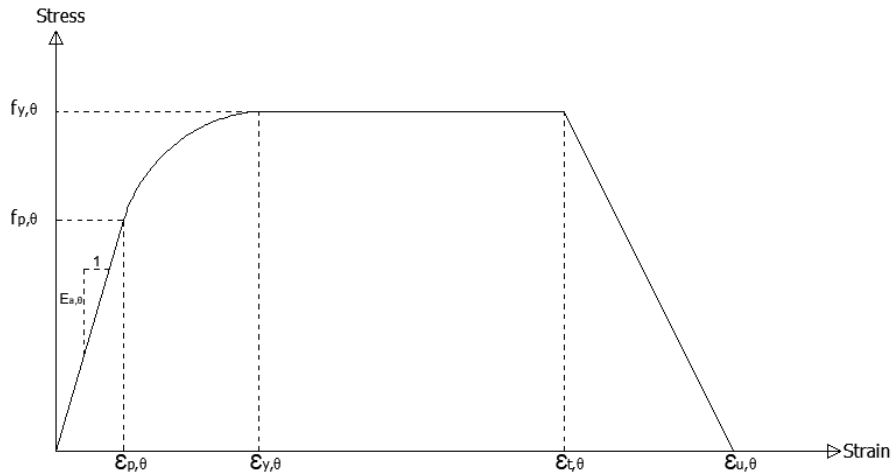


Fig. 4. Stress-strain model for steel at elevated temperature as shown in EN 1993-1-2:2005[1]

### - Stress-strain relationship with strain hardening

The annex A of EN 1993-1-2 [1] provides an additional stress-strain relationship that accounts for strain hardening at temperatures below 400°C. This relationship is presented in graphical form in Fig. 5.

- The stress-strain curve has a linear region from zero stress up to the point where the material begins to deform plastically, known as the proportional limit ( $f_{p,\theta}$ ). This linear region is defined by the material's elastic modulus ( $E_{a,\theta}$ ).
- A tangent ellipse by connecting the end point of the initial linear region (at  $f_{p,\theta}$ ,  $\varepsilon_{p,\theta}$ ) and the first point of the horizontal line at the yield where the strain is 2% and the stress is the degraded yield strength  $f_{y,\theta}$ .

- For temperatures below 400°C, the alternative model represents strain hardening with a straight line from the yield point to an ultimate stress of  $1.25 f_{y,\theta}$  at a strain  $\epsilon_{s,\theta}$  of 4%. A horizontal plateau then runs to  $\epsilon_{t,\theta}$ , again at 15%.
- Lastly, the stress-strain relationship enters a final phase with a negative-gradient linear behavior, which represents the final fracture process. At this stage, the stress decreases until it reaches zero at a strain  $\epsilon_{u,\theta}$  of 20%, indicating the occurrence of fracture.

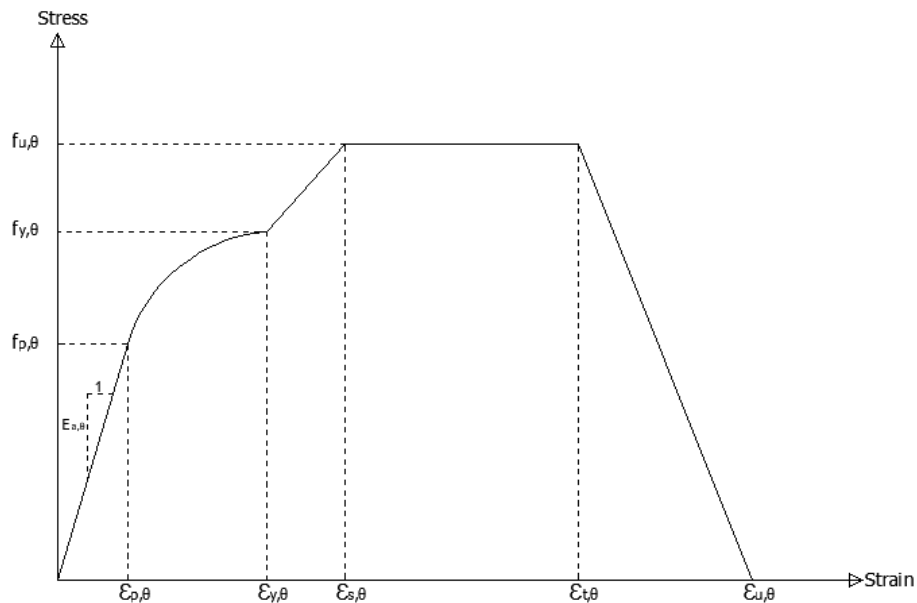


*Fig. 5. Alternative stress-strain relationship for steel allowing for strain hardening at temperatures below 400°C as shown in Appendix A of EN 1993-1-2:2005 [1]*

For  $\theta_a < 300 \text{ }^\circ\text{C}$  :  $f_{u,\theta} = 1.25 f_{y,\theta}$

For  $300 \text{ }^\circ\text{C} \leq \theta_a \leq 400 \text{ }^\circ\text{C}$  :  $f_{u,\theta} = f_{y,\theta}(2 - 0.0025\theta_a)$

For  $\theta_a \geq 400 \text{ }^\circ\text{C}$  :  $f_{u,\theta} = f_{y,\theta}$

### - Reduction factors

In EN1993-1-2, the degradation of steel strength and stiffness with increasing temperature is defined through reduction factors, where the property at elevated temperature is normalized with respect to the corresponding value at room temperature

Fig.6 and Table 1 present the reduction factors for the effective yield strength ( $k_{y,\theta} = f_{y,\theta}/f_y$ ), 0.2% proof strength ( $k_{0.2p,\theta} = f_{0.2p,\theta}/f_y$ ) and proportional limit ( $k_{p,\theta} = f_{p,\theta}/f_y$ ). The proportional limit degrades more rapidly, followed by the 0.2% proof strength and effective yield strength. The proportional limit degrades more rapidly than the 0.2% proof strength and effective yield strength. It is worth noting that the Eurocode assumes linear interpolation of material properties of steel at elevated temperatures between values provided at every 100°C.

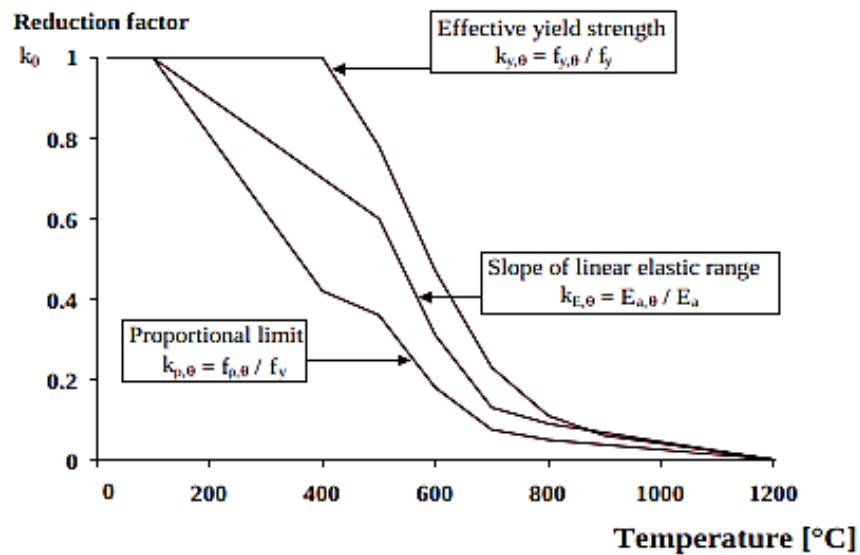


Fig. 6. Reduction factors for the stress-strain relationship of carbon steel at elevated temperatures

Table 1. Reduction factors for stress-strain relationship of carbon steel at elevated temperatures taken from EN1993-1-2 :2005 [1]

Steel Temperature $\theta_a$	Reduction factors at temperature $\theta_a$ relative to the value of $f_y$ or $E_a$ at 20°C			
	Reduction factor (relative to $f_y$ ) for effective yield strength $k_{y,\theta} = f_{y,\theta} / f_y$	Reduction factor (relative to $f_y$ ) for proportional limit $k_{p,\theta} = f_{p,\theta} / f_y$	Reduction factor (relative to $E_a$ ) for the slope of the linear elastic range $k_{E,\theta} = E_{a,\theta} / E_a$	Reduction factor (relative to $f_y$ ) for the design strength of hot rolled and welded thin walled sections (Class 4) $k_{0.2p,\theta} = f_{0.2p,\theta} / f_y$
20 °C	1.000	1.000	1.000	1.000
100 °C	1.000	1.000	1.000	1.000
200 °C	1.000	0.807	0.900	0.890
300 °C	1.000	0.613	0.800	0.780
400 °C	1.000	0.420	0.700	0.650
500 °C	0.780	0.360	0.600	0.530
600 °C	0.470	0.180	0.310	0.300
700 °C	0.230	0.075	0.130	0.130
800 °C	0.110	0.050	0.090	0.070
900 °C	0.060	0.0375	0.0675	0.050
1000 °C	0.040	0.0250	0.0450	0.030
1100 °C	0.020	0.0125	0.0225	0.020
1200 °C	0.000	0.0000	0.0000	0.000

NOTE: For intermediate values of the steel temperature, linear interpolation may be used.

### - Yield strength

Since the stress-strain response becomes increasingly nonlinear as the temperature rises, it becomes difficult to distinguish the strength at which the response changes from elastic linear to nonlinear; and owing to large strains exhibited at elevated temperatures in fire affected members, it is more usual to quote the 1.0% or 2.0% proof stress rather than the conventional ambient value of 0.2% proof stress. Some proposals are as follows:

- ECCS [26] suggests that when the temperature is higher than 400 °C, the 0.5% proof stress is used to determine the yield strength; when the temperature is lower than 400 °C, the proof stress is interpolated linearly between 0.2% (20 °C) and 0.5% (400 °C). The fire test of a steel beam and steel column showed that the 0.5% proof stress is too conservative.

- BS5950 Part 8 [27] specified that a strain limit of 0.5% should be used for columns, a strain limit of 1.5% for beams whose protection materials remain intact in a fire and a strain limit of 2.0% for composite beams.
- EN 1993-1-2 [1] use the 2% proof stress to determine the yield strength.
- Kirby and Preston [28] suggest that the 1% proof stress should be used to determine the yield strength.

EN 1993-1-2:2005 adopts the term “effective” yield strength in many structural fire design calculations, and is defined as the strength at 2.0% total strain. When there is a greater chance of buckling (i.e. class 4 sections), it specifies that the 0.2% proof strength should be used.

**- Strain rate:**

The material model adopted in EN1993-1-2 is a conservative approach regarding strain rate as it takes into account the effect of creep on yield strength without specifying heating rates. In this research, the strain rate is not taken into consideration as well.

### 2.2.1.3. Modified Ramberg-Osgood model

The Ramberg-Osgood material model provides a flexible way to express the stress-strain curves as continuous functions for numerical analysis [29].

Modified Ramberg-Osgood model has been used to characterise the stress stress-strain response of conventional steel grades (Saab and Nethercot, 1991; Outinen, 1996; Knobloch et al., 2013), as well as various HSS (Chen and Young, 2008; Choi et al., 2014; Ma et al., 2015) at elevated temperatures.

The original Ramberg-Osgood model was first proposed to characterize the stress-strain behavior of materials such as aluminum, stainless steels, and certain carbon steels (e.g. chromium nickel steels) which do not follow a bilinear stress-strain response [30]. This “simple” equation presented in Equation (24), describes the stress-strain behavior with three parameters: the elastic modulus  $E$  and two constants  $K$  and  $n$ , derived from experiments.

The total strain is the summation of the elastic and plastic strains, and the curvature of the stress-strain curve is defined through the exponential  $n$  which is called the strain hardening parameter.

The lower the strain hardening parameter, the more gradual the transition from elastic (linear) to the plastic (nonlinear) part of the stress-strain curve.

$$\varepsilon = \left(\frac{\sigma}{E}\right) + k \left(\frac{\sigma}{E}\right)^n \quad (24)$$

One year later, Hill (1944) modified the Ramberg-Osgood model by substituting the constant  $k$  and elastic modulus  $E$  with the plastic strain 0.002 and the 0.2% proof strength  $f_{0.2p}$ , respectively, as shown in Equation (25). The strain hardening parameter  $n$  is often determined from two fixed points on the stress-strain curve.

To determine the strain hardening parameter in this Equation, the first point is taken close to the origin of the stress-strain curve (e.g. the 0.01% proof strength and corresponding strain), whilst the second point is the 0.2% proof strength  $f_{0.2p}$  and corresponding strain (0.002).

$$\varepsilon = \left(\frac{\sigma}{E_0}\right) + 0.002 \left(\frac{\sigma}{f_{0.2p}}\right)^n \quad (25)$$

The modified Ramberg-Osgood model fire situation is based on real transient test

The equation to calculate the stress-strain curve of steel at elevated temperatures proposed by W. Ramberg and W. R. Osgood [31], is the following:

$$\varepsilon_i = \frac{\sigma_i}{E_{a,\theta}} + \beta \cdot \left( \frac{f_{y,\theta}}{E_{a,\theta}} \right) \cdot \left( \frac{\sigma_i}{f_{y,\theta}} \right)^{n_\theta} \quad (26)$$

$\sigma_i, \varepsilon_i$ : represent stress and corresponding strain, respectively, at temperature  $\theta$

$n_\theta$ : coefficient that enables the curvature to be adjusted;  $\beta = 6/7$ .

Outinen et al. [31] proposed simple formulas to determine the parameters of Ramberg-Osgood equation (27,28,29) based on the test results for steel grade S355, as follows:

for  $200^\circ\text{C} \leq \theta \leq 700^\circ\text{C}$ :

$$E_\theta = 263000 - 325\theta \quad (27)$$

for  $200^\circ\text{C} \leq \theta \leq 700^\circ\text{C}$ :

$$f_{y,\theta} = 352 - 0.54(\theta - 200) \quad (28)$$

for  $200^\circ\text{C} \leq \theta \leq 700^\circ\text{C}$ :

$$n_\theta = 0.000231 \theta^2 - 0.231 \theta + 62.5 \quad (29)$$

Fig. 7 shows the modified Ramberg-Osgood stress-strain curves for steel S355 at three different temperatures (400°C, 500°C, 600°C).

Thus, the parameters for this model for fire design case were presented by Outinen et al. [31] based on real test, but was not investigated or verified later by other researchers



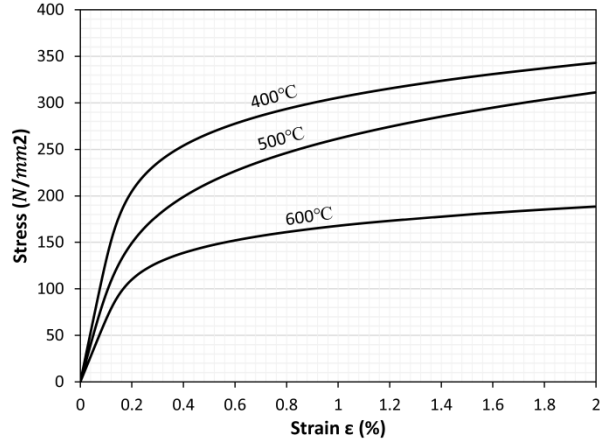


Fig. 7. Modified Ramberg-Osgood material model for steel S355 [31]

## 2.2.2. Eurocode 3 formulae on buckling resistance of steel member at elevated temperatures

### 2.2.2.1. Flexural buckling

Currently, different equations are used to design structures under fire situations compared to those under normal room temperature design. As per guidelines specified in the EN1993-1-2 [1], calculation of the design buckling resistance  $N_{b,fi,t,Rd}$  of a compressed member with a Class 1, Class 2, or Class 3 cross-section with a uniform temperature  $\theta_a$  at time  $t$  should be determined using the following formula:

$$N_{b,fi,t,Rd} = \chi_{fi} A k_{y,\theta} f_y / \gamma_{M,fi} \quad (30)$$

where

$\chi_{fi}$ : is the reduction factor for flexural buckling in the fire design situation.

$k_{y,\theta}$ : is the reduction factor for the yield strength of steel at the steel temperature  $\theta_a$  reached at time  $t$ .

$\gamma_{M,fi}$ : is the safety factor for the fire design situation.

$A$ : is the area of the cross-section.

The calculation of the reduction coefficient for cross-sectional compression capacity should be determined using the following equation:

$$\chi_{fi} = \frac{1}{\varphi_{\theta} + \sqrt{\varphi_{\theta}^2 - \bar{\lambda}_{\theta}^2}} \quad (31)$$

where  $\varphi_{\theta} = \frac{1}{2}[1 + \alpha \bar{\lambda}_{\theta} + \bar{\lambda}_{\theta}^2]$ , the imperfection factor is given as  $\alpha = \beta \sqrt{235/f_y}$ , where  $\beta = 0.65$ .

The non-dimensional slenderness  $\bar{\lambda}_{\theta}$  at the temperature  $\theta_a$  is given as:

$$\bar{\lambda}_{\theta} = \bar{\lambda}[k_{y,\theta}/k_{E,\theta}]^{0.5} \quad (32)$$

where  $k_{E,\theta}$  is the reduction factor for the slope of the linear elastic range at the steel temperature  $\theta_a$  reached at time t, and  $\bar{\lambda}$  is the nondimensional slenderness at ambient temperature, which can

be calculated according to EN1993-1-1 as:  $\bar{\lambda} = \sqrt{\frac{A f_y}{N_{cr}}}$

and  $N_{cr}$  is the lowest elastic critical load at ambient temperature.

### 2.2.2.2. Lateral-torsional buckling

The calculation of the design lateral-torsional buckling resistance  $M_{b,fi,t,Rd}$  for a laterally unrestrained with a Class 1, Class 2, or Class 3 cross-section with a uniform temperature  $\theta_a$  at time t should be determined using the following formula:

$$M_{b,fi,t,Rd} = \chi_{LT,fi} W_y k_{y,\theta} f_y / \gamma_{M,fi} \quad (33)$$

where

$W_y$ : is the plastic section modulus,  $W_{pl,y}$  for Class 1 and Class 2 cross sections or the elastic section modulus  $W_{el,y}$  for Class 3 cross sections.

$k_{y,\theta}$ : is the reduction factor for the yield strength of steel at the steel temperature  $\theta_a$  reached at time t.

$\gamma_{M,fi}$ : is the safety factor for the fire design situation.

$\chi_{LT,fi}$ : is the reduction factor fire design situation;

The calculation of the reduction coefficient  $\chi_{LT,fi}$  should be determined using the following equation:

$$\chi_{LT,fi} = \frac{1}{\varphi_{LT,\theta} + \sqrt{\varphi_{LT,\theta}^2 - \bar{\lambda}_{LT,\theta}^2}} \quad (34)$$

where  $\varphi_{LT,\theta} = \frac{1}{2} [1 + \alpha \bar{\lambda}_{LT,\theta} + \bar{\lambda}_{LT,\theta}^2]$ , the imperfection factor is given as  $\alpha = \beta \sqrt{235/f_y}$ , where  $\beta = 0.65$ .

The non-dimensional slenderness  $\bar{\lambda}_\theta$  at the temperature  $\theta_a$  is given as:

$$\bar{\lambda}_{LT,\theta} = \bar{\lambda}_{LT} [k_{y,\theta}/k_{E,\theta}]^{0.5} \quad (35)$$

where  $k_{E,\theta}$  is the reduction factor for the slope of the linear elastic range at the steel temperature  $\theta_a$  reached at time t, and  $\bar{\lambda}_{LT}$  is the nondimensional slenderness at ambient temperature, which can be calculated according to EN1993-1-1 as:

For class 1 and 2 cross-sections:  $\bar{\lambda}_{LT} = \sqrt{\frac{W_{pl,y} f_y}{M_{cr}}}$

For class 3 cross-sections:  $\bar{\lambda}_{LT} = \sqrt{\frac{W_{el,y} f_y}{M_{cr}}}$

### 2.2.2.3. Coupled buckling

The design buckling resistance at temperature  $\theta$  for a member with a Class 1, Class 2 or Class 3 doubly symmetric cross section subject to combined bending and axial compression should be verified by satisfying expressions (36) and (37):

$$\frac{N_{fi,Ed}}{\chi_{fi} A k_{y,\theta} \frac{f_y}{\gamma_{M,fi}}} + \frac{k_y M_{y,fi,Ed}}{W_y k_{y,\theta} \frac{f_y}{\gamma_{M,fi}}} + \frac{k_z M_{z,fi,Ed}}{W_z k_{y,\theta} \frac{f_y}{\gamma_{M,fi}}} \leq 1 \quad (36)$$

$$\frac{N_{fi,Ed}}{\chi_{z,fi} A k_{y,\theta} \frac{f_y}{\gamma_{M,fi}}} + \frac{k_{LT} M_{y,fi,Ed}}{\chi_{LT,fi} W_y k_{y,\theta} \frac{f_y}{\gamma_{M,fi}}} + \frac{k_z M_{z,fi,Ed}}{W_z k_{y,\theta} \frac{f_y}{\gamma_{M,fi}}} \leq 1 \quad (37)$$

Where

$$k_y = 1 - \frac{\mu_y N_{fi,Ed}}{\chi_{y,fi} A k_{y,\theta} \frac{f_y}{\gamma_{M,fi}}} \leq 3 \quad (38)$$

$$\mu_y = (2\beta_{M,y} - 5)\bar{\lambda}_{y,\theta} + 0.44 \beta_{M,y} + 0.29 \leq 0.8 \quad (39)$$

$$k_z = 1 - \frac{\mu_z N_{fi,Ed}}{\chi_{z,fi} A k_{y,\theta} \frac{f_y}{\gamma_{M,fi}}} \leq 3 \quad (40)$$

$$\mu_z = (1.2\beta_{M,y} - 3)\bar{\lambda}_{z,\theta} + 0.71 \beta_{M,z} - 0.29 \leq 0.8 \quad (41)$$

$$k_{LT} = 1 - \frac{\mu_{LT} N_{fi,Ed}}{\chi_{z,fi} A k_{y,\theta} \frac{f_y}{\gamma_{M,fi}}} \leq 1 \quad (42)$$

$$\mu_{LT} = 0.15\bar{\lambda}_{z,\theta}\beta_{M,LT} - 0.15 \leq 0.9 \quad (43)$$

For the equivalent uniform moment factors  $\beta_M$ , see Fig. 8.

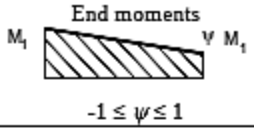
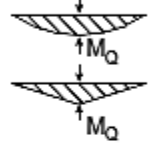
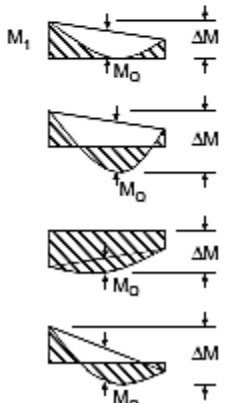
Moment diagram	Equivalent uniform moment factor $\beta_M$
 <p>End moments  <math>M_1</math> <math>\psi M_1</math>  <math>-1 \leq \psi \leq 1</math></p>	$\beta_{M,\psi} = 1.8 - 0.7\psi$
 <p>Moments due to in-plane lateral loads</p>	$\beta_{M,Q} = 1.3$  $\beta_{M,Q} = 1.4$
 <p>Moments due to in-plane lateral loads plus end moments</p>	$\beta_M = \beta_{M,\psi} + \frac{M_Q}{\Delta M} (\beta_{M,Q} - \beta_{M,\psi})$  $M_Q =  \max M  \text{ due to lateral load only}$  $\Delta M \left\{ \begin{array}{l}  \max M  \text{ for moment diagram without change of sign} \\  \max M  +  \min M  \text{ for moment diagram with change of sign} \end{array} \right.$

Fig. 8. Equivalent uniform moment factor to EN1993-1-2 [1]

### 2.2.3. Experiments and numerical research review on fire resistance of steel members

This section presents several studies that have made significant progress in research regarding steel members under elevated temperature through experimental tests, numerical simulations, and analytical models.

One of the most notable work has been achieved by Zhao et al [3], who investigated experimentally and numerically the behavior of steel members with class 4 cross-sections at elevated temperatures. A total of sixteen experimental tests at elevated temperatures and a big number of numerical simulations were conducted in this parametric study which has permitted to cover several parameters, including sizes of cross-section, slenderness, steel grades, and account

of initial residual stresses or not. The researchers established experimental database which may be employed for validation of the numerical models used for investigating the behavior of steel members at elevated temperatures.

For a big number of the simulated cases it was observed that the EN1993-1-2 provisions propose very conservative fire design, but it was also noticed that, for other cases, the EN1993-1-2 could lead to an unsafe design of the member. Moreover, it was noted that the initial residual stresses do not influence the final cross-sectional resistance of the beam at elevated temperatures.

The authors also proposed improvements to the design rules in terms of design strength of steel at elevated temperatures is  $f_{y,\theta}$ , and the effective cross-section of thin-wall steel members which is calculated based on the wall slenderness.

The experimental research conducted by Pauli et al. [32] at the Swiss Federal Institute of Technology in Zurich is significant because it investigates the behavior of steel columns under fire conditions, particularly the interaction of material, cross-sectional, and member behavior.

The authors noted that the buckling curves in EN1993-1-2, commonly used for determining the ultimate load of steel columns at elevated temperatures, do not accurately predict the ultimate load of steel columns due to incorrect determination of the cross-sectional capacity, and neglecting the non-linearity of steel behavior at high temperatures and fail to correctly estimate the ultimate loads of the columns. This highlights the need for more accurate methods for predicting the behavior of steel columns in fire conditions.

While the research by Pauli et al. offers valuable insights into the behavior of steel columns under fire conditions, it should be noted that their study only considered the behavior of centrally loaded columns. Therefore, more research is required to examine the behavior of eccentrically loaded columns in similar scenarios. Nonetheless, the findings emphasize the significance of developing more accurate methods for predicting the ultimate load of steel columns at high temperatures, which can ultimately result in safer and more dependable designs of steel structures in fire conditions.

The effect of local buckling on the behavior of steel members at ambient temperature is well documented and integrated into current design codes. However, this is not the case when such elements are exposed to fire.

Couto C et al. [33] showed that Eurocode procedures lack consistency and typically overestimate the capacity of laterally restrained beams-columns with class 4 cross-sections due to local buckling. The research found that local buckling limits the capacity of the beam-column to bear additional load, stating that the current Eurocode 3 procedure may not be entirely safe. Furthermore, the study demonstrated that the current interaction curve does not adequately account for cases related to non-uniform bending diagrams.

In his study, C. Maraveas in 2018 also supported the conclusion that the Eurocode procedures may not be entirely safe in all cases, particularly when calculating the failure load of heated steel sections prone to local buckling. He noted that the Eurocode procedures are not always conservative and may be unsafe in certain cases [34].

The initial out of straightness value of 1/1000 is used as a calibration to represent the effects of all other imperfections in a member. However, for more accurate ultimate strength analyses, a combination of both local and global imperfections should be considered. O. Kaitila [35] conducted preliminary work on this and concluded that the magnitude of local imperfections affects the compression stiffness of the members, while the magnitude of global flexural imperfections has a larger effect on the ultimate strength obtained in the analyses.

It is important to consider that there are several factors that can affect the buckling behavior of steel members in fire conditions. One of these factors is the bending moment distribution along the member, which can have a significant impact on the lateral-torsional buckling of steel beams as noted by Vila Real et al. [36].

Typically, the effect of high-temperature creep is not accounted for in material models used for numerical analysis. However, neglecting this phenomenon may lead to underestimated deflections and overstated restraint stresses, resulting in unsafe results, as suggested by Kodur et al. [38]. This claim is supported by Morovat et al. [38], who investigated the influence of material creep on the strength of steel columns at elevated temperatures. Additionally, analytical solutions

have been proposed to account for the effects of material creep on the overall time-dependent buckling.

In their study, Yang et al. [39] investigated the variations in ultimate strength of steel columns at specified elevated temperatures due to different width-to-thickness ratios. A total of 24 stub column specimens, including both box columns and H columns, were tested under fire conditions until reaching their limit states due to axial load. The experimental results showed that the ultimate strength and ductility of steel columns decrease with increasing width-to-thickness ratios or temperature. However, the effect of the width-to-thickness ratio on ultimate strength decreases with increasing temperature. Additionally, it was found that the effect of the width-to-thickness ratio on ultimate strength is more significant for box columns at elevated temperature compared to H columns.



### **3. Research methodology**

#### **3.1. General**

In order to assess the accuracy of the proposed OIM a reference database is needed, to which the OIM's results at elevated temperatures can be compared. In this research it is assumed that the appropriate database can be created by geometrically and materially nonlinear analyses with imperfections included (GMNIA) using a numerical model developed in ABAQUS software with characteristic parameters (especially the characteristic value of the yield strength), the resulted ultimate loads will be characteristic values.

In order to perform the numerical test program given in the next subsection, a proper code for the implementation of the OIM has been developed in GNU Octave software. The validation of this developed program for normal temperature design was published in [9] and [40].

The program uses 14 degrees of freedom thin-walled beam-column finite element method according to [41]. The program runs the steps of the proposed OIM defined in Section 4. The basic ultimate load for any examined structural member is generated by GMNIA, and an iteration procedure resulting in the ultimate load factor is used within the OIM.

The database created by this way may be considered as reference for comparing. It is noted that nowadays this concept is generally accepted in the steel structural engineering research.

#### **3.2. Test program for statistical evaluation**

The evaluation of the accuracy of proposed OIM for global buckling design of steel members is based on a numerical test program. Different conditions should be considered to verify the applicability of the proposed OIM method at elevated temperatures. Therefore, the numerical program of this research covers:

- ten different cross-sections (see Table 2);
- seven different non-dimensional slenderness ranging from 0.50 to 2.30 (only global buckling resistance is investigated here);
- three different elevated temperatures (400°C, 500°C, 600°C)

Steel grade S235 is used for all examined members.

It is worthy to mention that the focus of this statistical study is to propose the OIM for global buckling capacity of steel members at elevated temperatures. Therefore, only stocky (class 1, class 2 and class3) cross-sections are considered here in order to avoid any local effects and imperfections.

*Table 2. Properties of the cross-sections used in the numerical investigation*

cross-section	h (mm)	b (mm)	$t_w$ (mm)	$t_f$ (mm)	A ( $mm^2$ )
IPE 100	100	55	4.1	5.7	1032
IPE 160	160	82	5.0	7.4	2009
IPE 180	180	91	5.3	8	2395
IPE 240	240	120	6.2	9.8	3912
IPE 300	300	150	7.1	10.7	5381
HE300A	290	300	8.5	14	11253
HEB 300	300	300	11	19	14908
HEB 340	340	300	12	21.5	17090
HEB 500	500	300	14.5	28	23864

### 3.3. Numerical model for GMNIA

#### 3.3.1. Abaqus Element type and mesh size

The GMNIA method is employed to calculate the reference ultimate load, using the Abaqus software [42]. For the structural member models, the Abaqus software utilizes the S4R shell element, which is a general-purpose element with reduced integration to prevent shear and membrane locking. The cross-sectional mesh size is determined as follows: 16 elements are used in the flange, and 16 elements are used in the web depth. In terms of longitudinal meshing, the element size is set to 20 mm along the length of the member. The maximum aspect ratio of the elements was equal to 4. Fig. 9 provides a closer view of the ABAQUS model, illustrating the meshing details for the members under investigation.

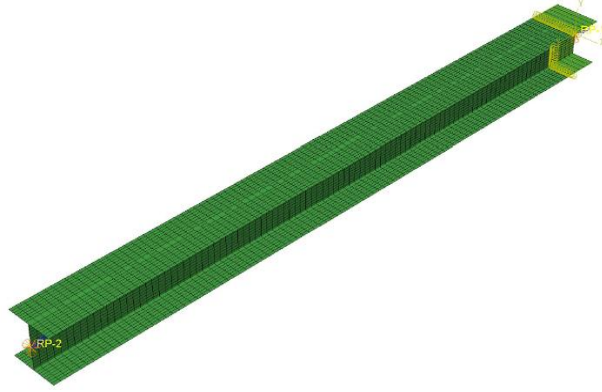


Fig. 9. ABAQUS model and meshing details

Due to the limitations of shell element modeling in ABAQUS, the cross-section representation may not perfectly match the actual hot-rolled I-shaped members. Specifically, the fillet radius at the intersections of the web and flange cannot be accurately modeled. Furthermore, there is a small region at the web-flange intersection in the modeled cross-section that is accounted for twice. To address these issues, additional beam elements with a square hollow section (SHS) cross-section (designated as B31) were incorporated at the web-flange intersections. The width and thickness of the added SHS profile ( $b_{SHS}, t_{SHS}$ ) were calculated to compensate for the moments around the y-axis ( $I_{y,lac}$ ) and the torsional moment of inertia ( $I_{t,lac}$ ) that were lacking between the actual rolled cross-section and the modeled cross-section, where  $h_0$  is the distance between the center lines of flanges of the cross-section.

$$b_{SHS} = \sqrt{\frac{I_{t,lac} \cdot h_0^2}{I_{y,lac} - \frac{2}{3}I_{t,lac}}} \quad (44)$$

$$t_{SHS} = \frac{I_{t,lac}}{b_{SHS}^3} \quad (45)$$

Fig. 10 shows the cross-section of the members modelled in ABAQUS with A calculated profile assigned to compensate for the lacking stiffness properties

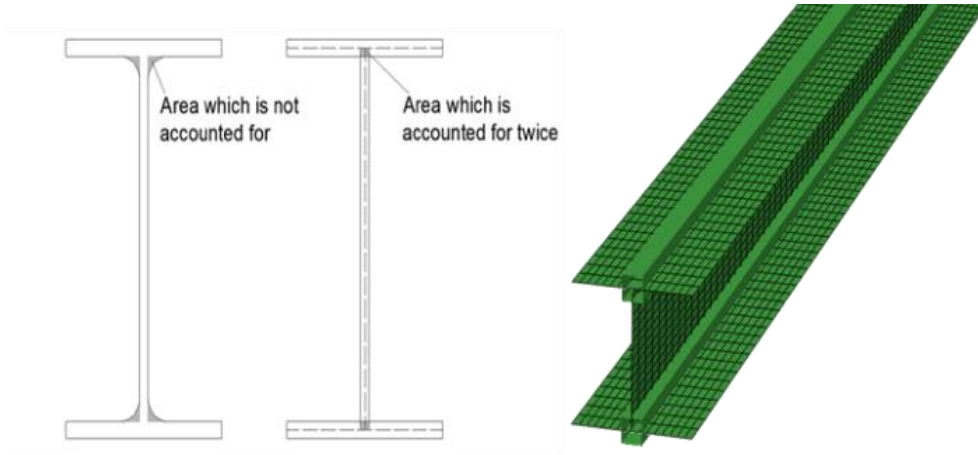


*Fig. 10. (Left) Real section vs. FE model section; (Right) modelled cross-section*

### **3.3.2. Boundary conditions**

In this study, all analysed members were considered to be pin-supported. To model this boundary condition in ABAQUS, a reference point was assigned at each end of the member. These reference points were then coupled with the corresponding nodes on the end surfaces of the members using kinematic coupling restraints. By doing so, the boundary conditions were applied through these reference points. Specifically, the reference points were constrained in all degrees of freedom, except for the longitudinal displacement at the loaded end (i.e., displacement in the direction of the applied load), as well as rotations about the axes of buckling at both ends.

### **3.3.3. Load conditions**

To simulate the load, distributed forces were applied on the flanges and web of the loaded end using nodal forces in ABAQUS. The modified RIKS tool (Arc length method) was employed for this purpose. This tool is available in the ABAQUS library [42].

### **3.3.4. Geometrical and material imperfections**

Regarding the imperfections, the initial geometrical imperfections of the studied members are introduced in the numerical analysis by first performing a linear buckling analysis (LBA) on the perfect prismatic member with given boundary conditions, then the relevant normalized global buckling mode is extracted. In this way, the first global buckling mode shape (corresponding to

the lowest elastic critical load) derived by the linear buckling analysis is introduced into the non-linear finite element model (GMNIA), multiplying this by the amplitude of initial geometrical (bow) imperfection and updating the nodal coordinates of the model by adding the established nodal imperfections. The amplitude of initial geometrical imperfection of the column is taken equals to  $L/1000$ , which is used in most studies in the literature and corresponds to 75% of the recommended tolerance value of  $L/750$  for steel column in Annex D of EN1090-2:2008 [43], where  $L$  is the member length.

The ECCS type residual stress model for hot-rolled cross-sections is taken into account [44] in this investigation. This model is the basis for the European buckling curves, and this is the most commonly used residual stress pattern in the literature. The magnitude of the initial stress depends on height to width ratio of the section analyzed, as illustrated in Fig. 11.

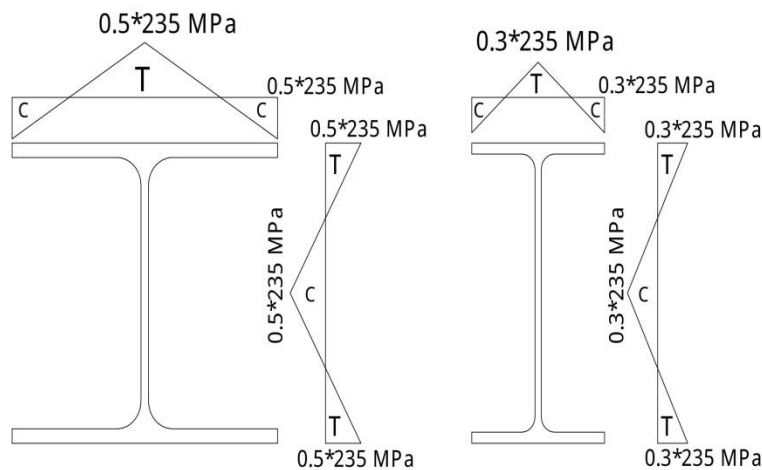


Fig. 11. Considered residual stress patterns for  $h/b \leq 1.2$  (left) and  $h/b > 1.2$  (right) [49]

Residual stress was introduced as initial stresses at normal temperature, and a static analysis step with temperature varies from normal to the temperature under consideration was performed as described by Franssen [45].

### 3.3.5. Material properties

S235 steel grade ( $\sigma_y = 235 \text{ N/mm}^2$ ) is considered in this study. The temperature introduced to the numerical model is considered to be uniformly distributed along the member. Thus, it is possible to compare the GMNIA results to the result of the proposed OIM and of the valid EN1993-1-2 formula.

For linear buckling analysis, linear elastic material law with Young's modulus  $E= 2.1 \cdot 10^5$  N/mm<sup>2</sup> is used. The Poisson's ratio is set to 0.3.

For the non-linear analysis at elevated temperatures, the reduction factors for carbon steel are used, according to the Table 3.1 of EN1993-1-2 [1], and as shown in Fig. 12.

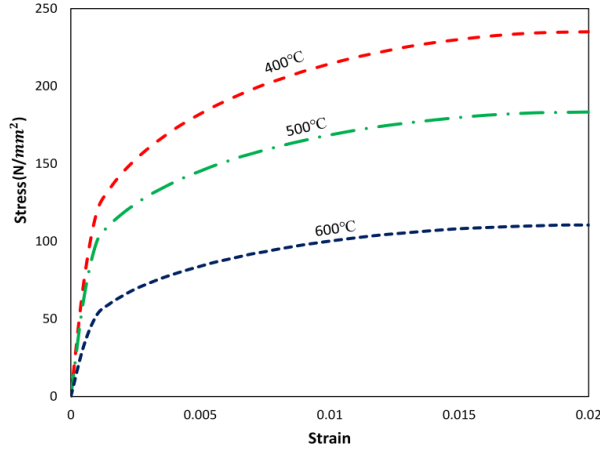


Fig. 12. EN1993-1-2 Stress-strain relationship for S235 carbon steel at elevated temperatures

Note: In the finite element models, "True stress versus plastic strain" instead of engineering stress and strain should be adopted. Therefore, the following equations are used to represent the relationship between true strain and stress.

$$\sigma_{\text{true}} = \sigma_{\text{nom}}(1 + \varepsilon_{\text{nom}}) \quad (46)$$

$$\varepsilon_{\text{true}} = \ln(1 + \varepsilon_{\text{nom}}) \quad (47)$$

The plastic strain is defined as the total strain minus the elastic logarithmic strain:

$$\varepsilon_{\text{pl}} = \ln(1 + \varepsilon_{\text{nom}}) - \frac{\sigma_{\text{true}}}{E} \quad (48)$$

Where:

$\sigma_{\text{true}}$ ,  $\varepsilon_{\text{true}}$ : the true stress and true strain, respectively.

$\sigma_{\text{nom}}$ ,  $\varepsilon_{\text{nom}}$ : the nominal (engineering) stress and nominal (total) strain, respectively.

### 3.3.6. Numerical model validation

#### 3.3.6.1. Column tests at elevated temperatures

The ultimate loads obtained from the GMNIA model described above are compared with the ultimate loads measured in the test performed by Pauli et al. [32]. The test was implemented on both stub (short) and slender (long) columns made of HEA100 cross-section. All structural members were made from hot finished. The experiments were performed at temperatures of 400, 550 and 700°C. . The simulated stub column is assumed to have initial local geometrical imperfections of 0.15 mm, and no residual stresses were taken into account in the finite element analysis. It can be seen from Table 4 that the predicted buckling loads are generally in good agreement with the test results with maximum difference of 7.6% and average difference of 5.7%.

Moreover, The GMNIA model underestimates the ultimate load of steel columns at elevated temperatures for all cases, and thus it provides a safe prediction for the fire resistance of steel columns.

*Table 3. Comparison of FE and experimental results from Pauli et al. [32]*

Column ID	Temperature	End conditions		$N_{u,test}$	$N_{u,GMNIA}$	Difference
	°C	y	z	(kN)	(kN)	
S19	400	tie	tie	996	964	3.3%
S13	550	tie	tie	511	472	7.6%
M02	400	tie	pin	646	615	5.1%
M03	550	tie	pin	405	375	7.4%

Fig. 13 shows the buckling load-axial deflection curves derived from the numerical model of the S19 member which is compared to its respective test responses.

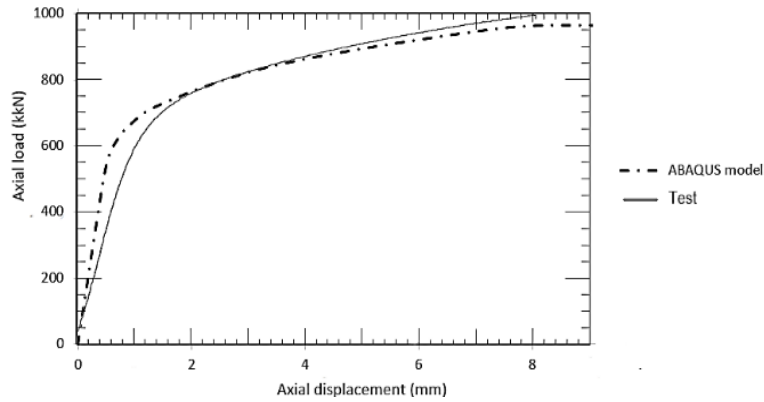


*Fig. 13. Comparison of the axial load- displacement curves for S19 column [9]*

It should be mentioned that the difference between the numerical and the experimental study may be interpreted due to many factors, such as human errors, the scale of the member, accurate specifications of materials, software errors, mesh dimensions, and differences between the material model and the real material properties. These factors can all lead to errors in the results between analysis and testing. Therefore, additional validations against other experimental and numerical results found in the literature are presented hereafter.



### 3.3.6.2. Beam tests at elevated temperatures

Moreover, the numerical model (GMNIA) is validated against the elevated temperature tests on beams reported by Prachar et al. in [46], Fig. 14 shows three comparisons of the load-displacement curves of three different beams subjected to: simple bending (section resistance) at 450°C (Test 3), simple bending at 650°C (Test 4), lateral torsional buckling at 450°C (Test 6).

No residual stresses were considered in the validation. Geometrical imperfections, both local and global, were incorporated into the analysis, according to the actual measured imperfections amplitudes of the beams given in [46].

The GMNIA curve (solid line) is given by the ABAQUS model described above. The shown displacement is the vertical displacement of the bottom flange at mid-span.

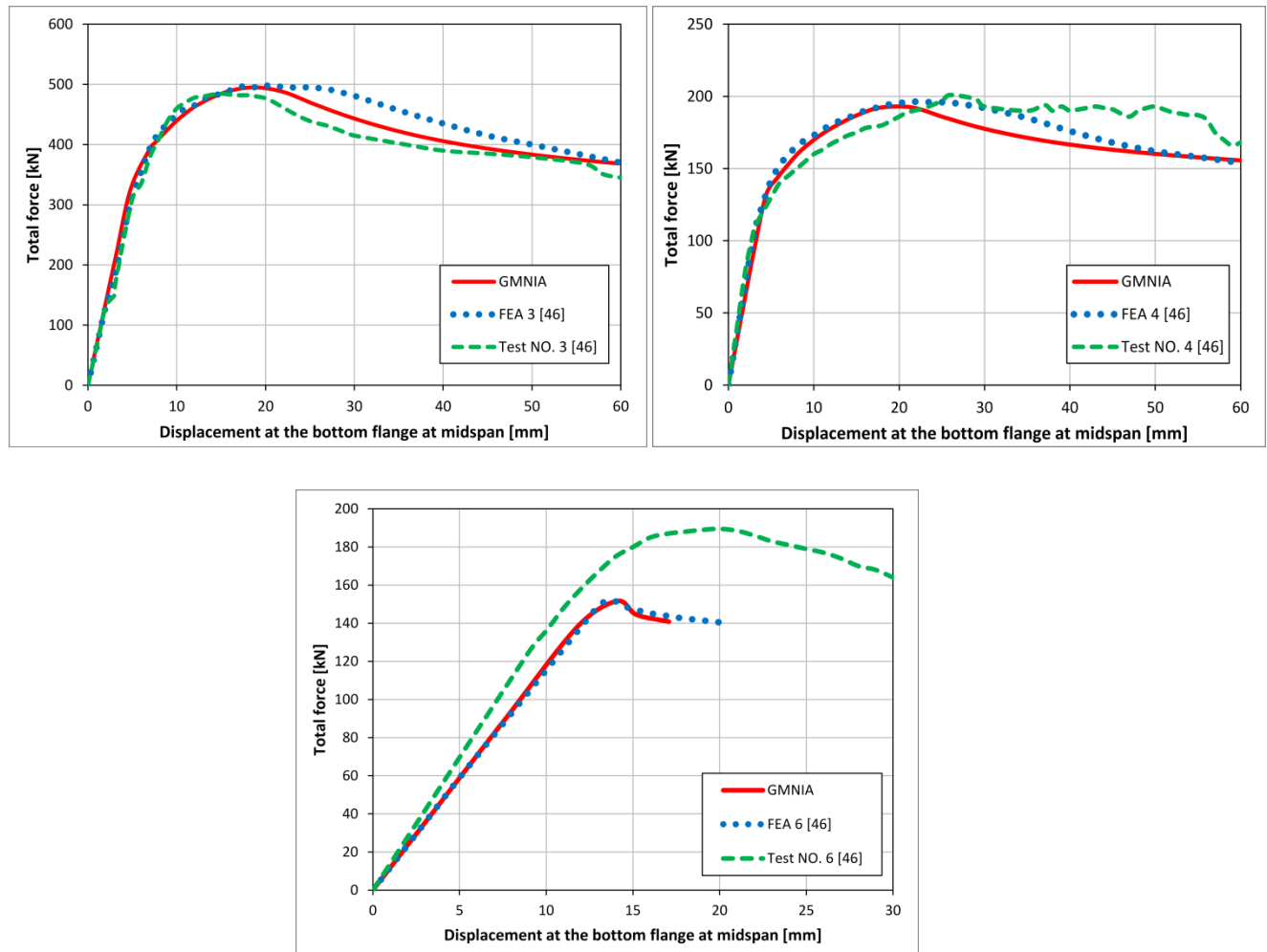


Fig. 14. Comparisons of numerical load–vertical displacement curves for three different tests given in [46]

### 3.3.6.3. Beams and columns test using SAFIR software

Fig. 15 illustrates the buckling load factors obtained from pin-ended column models with IPE220 cross-sections and S235 steel. These load factors were computed using the SAFIR software by Vila Real et al. [47], as well as the self-developed GMNIA model. In these numerical simulations, A lateral geometric global imperfection of  $L/1000$  was considered, where  $L$  is the member length. The ECCS type [44] residual stress model for hot-rolled cross-sections with a maximum value of  $0.3 \times 235$  MPa was used. Fig. 16 presents the lateral-torsional buckling load factors determined for the same members depicted in Fig. 15, but under the influence of a constant bending moment.

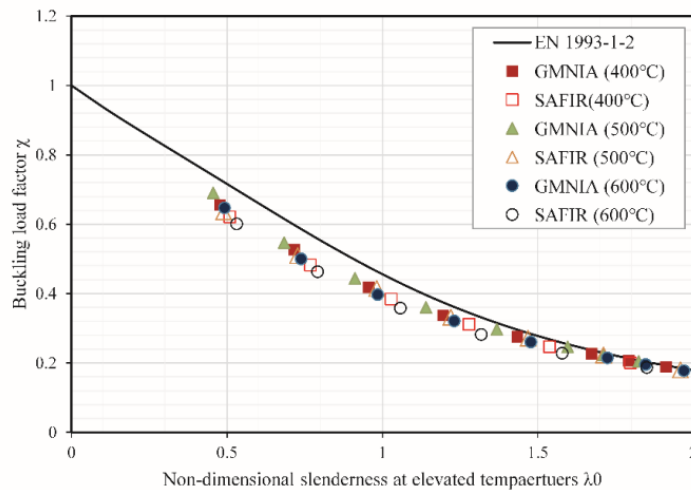


Fig. 15. Comparison of results obtained by Vila Real et al. [47] using SAFIR, and the results of the developed GMNIA model for the IPE220 cross-section steel column

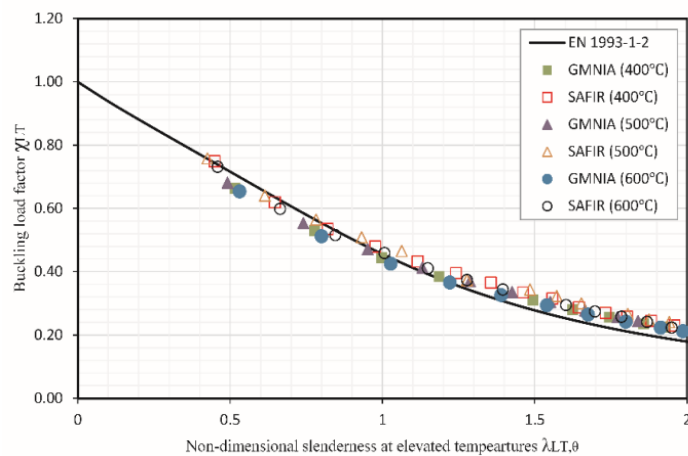


Fig. 16. Comparison of results obtained by Vila Real et al. [47] using SAFIR, and the results of the developed ABAQUS model for the IPE220 cross-section steel beam

As it can be observed from Fig. 15, and Fig. 16, there is a good agreement between the current numerical model and the one used in [47]. These good predictions from the model indicate that the model is capable of predicting buckling capacity of steel members at elevated temperatures, and thus can be used for the comparative investigation presented in this research.

### 3.3.6.4. LTB of class 4 steel plate girders under fire conditions

In the framework of project FIDESC4, a number of experimental tests were carried out in the Czech Technical University in Prague to study the LTB of Class 4 beams in case of fire [46].

A simply supported beam with two equal concentrated loads shown in Fig. 17. The intermediary span, which is therefore subjected to pure bending, is the only heated part (450 °C). The fire tests were performed on steady state, meaning the beam is heated and later the load was applied until failure. The beam was of the steel grade S355. The two load application points were laterally restrained and point pinned supports were applied at the beams end extremities.

End plates were used with thicknesses of 10 mm and stiffeners at the load application points had 20 mm of thickness.

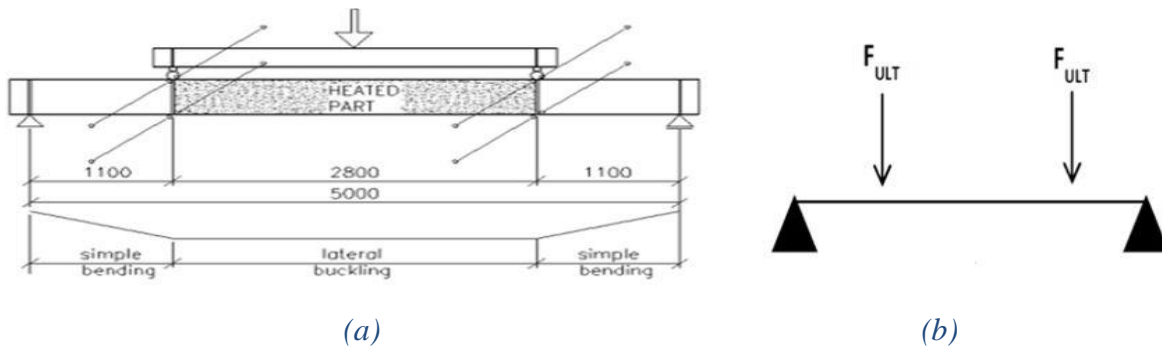


Fig. 17. Tested beam: a) scheme; b) test set-up

The beam was made of a welded cross-section, with the dimensions shown in Table 5.

Table 4. Dimensions of the cross-section of the studied member [46]

<b>Dimensions</b>	<b><math>h</math></b>	<b><math>b</math></b>	<b><math>t_f</math></b>	<b><math>t_w</math></b>
(mm)	460	150	5	4

All material properties (Young modulus, yield strength) which were adopted into the model are based on EN1993-1-2, the thermal expansion was not considered. The residual stresses were neglected. The initial global and local imperfections were considered using following amplitudes:

- global =  $L/1000$  where  $L$  is the distance between lateral supports
- local =  $H/100 * 0.8 * 0.7$ , where  $H$  is the web height

The failure deformed shape obtained from the self-developed ABAQUS model, and the failure shape from the test, are illustrated in Figs 18(a), 18(b) respectively.



Fig. 18. Deformed shape of beam from both a) ABAQUS model and b) real test [46]

Moreover, a comparison of Load-displacement curves for the beam as obtained from different numerical analysis by the researcher [46] with the ABAQUS model described previously, is shown in Fig. 19.

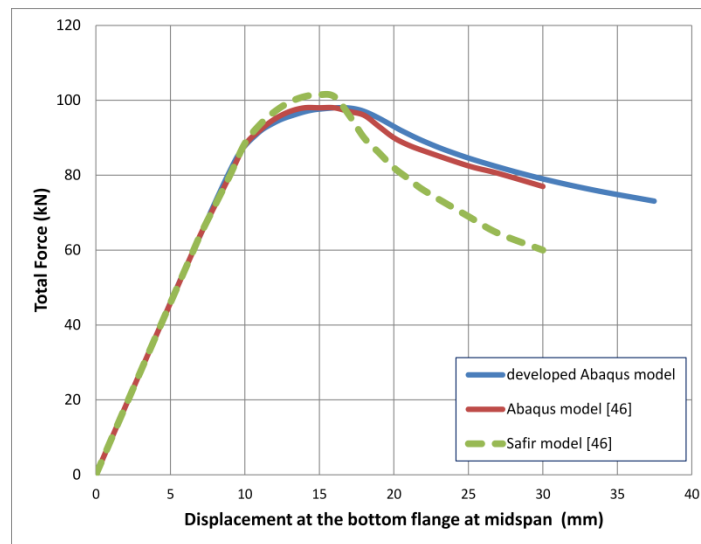


Figure 19. Comparison of load–displacement curves as obtained from different numerical analyses [46]

### 3.3.6.5. Numerical results on LTB of class 3 welded beams

In this section, the results of the numerical study performed by Couto et al. [48] on lateral–torsional buckling of steel beams with slender cross sections in case of fire are compared with the developed ABAQUS model results.

Table 5. Dimensions of the cross-section of the studied member [48]

Cross-section	$h_w$	$t_w$	$b$	$t_f$
mm	450	6	150	8

The ECCS type [44] residual stress model for welded cross-sections was used. a combination of global and local imperfections was considered. The global imperfection amplitude was scaled to 80% of  $L/750$  and the local imperfection amplitude to 80% of  $b/100$ , where  $b$  is the flange width of the cross section.

Fig. 20 shows a comparison between the numerical results obtained in SAFIR [48] and the self-developed ABAQUS model, for welded cross-section with the dimensions given in Table 6:

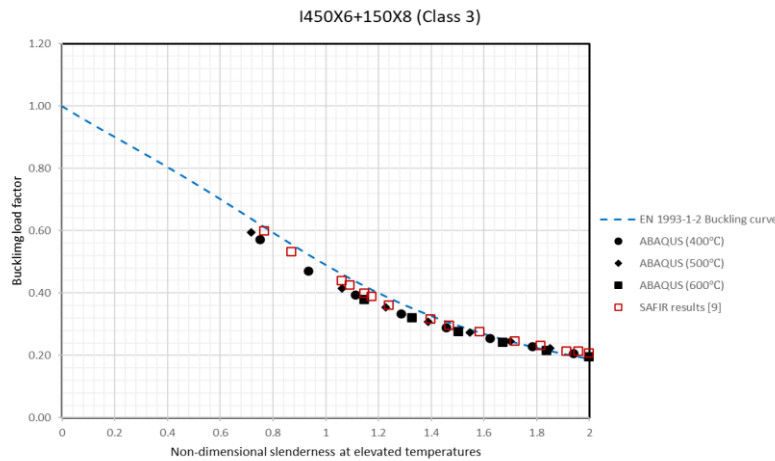


Fig. 20. Comparison of numerical results obtained by Couto et al. [48], and the results of the developed ABAQUS model steel beams with slender cross section.

In conclusion, the developed ABAQUS model has undergone a comprehensive validation process to assess its ability to replicate the behaviour and predict the load-bearing capacity of steel members under elevated temperature conditions. By comparing our numerical model with a wide range of published numerical simulations and experimental test results, and based on the close

match between the results, it can be stated that the model is verified and can be used this model to create an important reference database.

#### **4. Testing the influence of imperfections on fire design of steel members**

Before proposing the OIM for fire design, it was observed that there is a wide range of factors (i.e., structural imperfections, residual stress, etc) affecting the buckling capacity of steel members when exposed to high temperatures. It is important to accurately take into account these factors in order to avoid oversimplification. Moreover, there is a lack of sufficient and consistent information about the impact of these factors on class 4 I-section steel members at elevated temperatures. Thus, one goal of the research is to analyze how the structural geometrical (global and local) imperfections and material (residual stress) imperfections, affect the buckling capacity of steel beam-columns at elevated temperatures. To achieve this, a numerical model was created in Abaqus, incorporating different amplitudes of geometrical imperfections and residual stress patterns gathered from existing literature.

##### **4.1. Sensitivity to imperfections analysis model**

To examine how initial geometrical imperfections and residual stresses affect the ultimate load capacity of steel welded beam-columns with a class 4 cross-section at elevated temperatures, different magnitudes of global and local (plate) imperfections were taken into account. In this study, the validated finite element model, which was described in Section 3.3, was utilized to assess the buckling resistance of the steel welded beam-column at elevated temperatures. The material properties specified in EN1993-1-2 were employed for the analysis.

The specific member under investigation is a simply supported I-shaped welded steel beam-column, consisting of three steel plates (top and bottom flanges and web). It has an overall length of 6000 mm and is composed of steel grade S235. Fig. 21 depicts the member being studied along with the applied loads, which include an axial load of 95.8 kN and a bending moment of 13.10 kN/m.

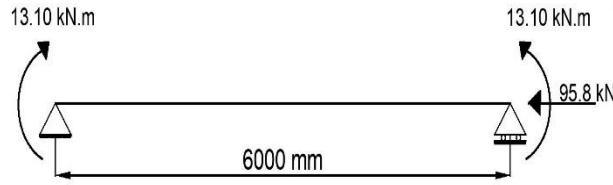


Fig. 21. Details of the beam-column with the applied loads used for residual stress sensitivity analysis

Table 3 displays the geometry of the welded cross section, as well as the temperatures considered, the patterns of residual stresses, and the magnitudes of initial imperfections examined in this study. The overall span of the member is represented by " $L$ ," and " $b$ " refers to either the flange width or web height, depending on which dimension corresponds to the maximum displacement in the respective local buckling mode. The residual stress patterns were incorporated into the Abaqus model as "initial conditions: type=stress" [42]. These same residual stress patterns were previously compared in [49] for beams featuring slender I-shaped welded sections at ambient temperature.

Regarding the geometrical imperfections, for normal ambient temperature, Annex C of EN 1993-1-5 [50] introduces guidance on the use of Finite Element (FE) methods. It states that both initial global and local (plate) imperfections should be included in the FE-model in a way that one type of imperfection should be chosen as a leading imperfection, and the accompanying imperfections may be reduced to 70%. Moreover, geometric imperfections may be based on the shape of the first buckling modes. Thus, the Eigen-modes obtained from the elastic buckling analysis are used; as the initial geometric imperfection shape for the post-buckling analysis.

Both first (lowest) global and first (lowest) local buckling mode shapes are shown in Fig. 22. As mentioned before, superposition of overall buckling mode as well as local buckling mode is achieved for accurate finite element analysis, and particularly in this study for the purpose of comparison.

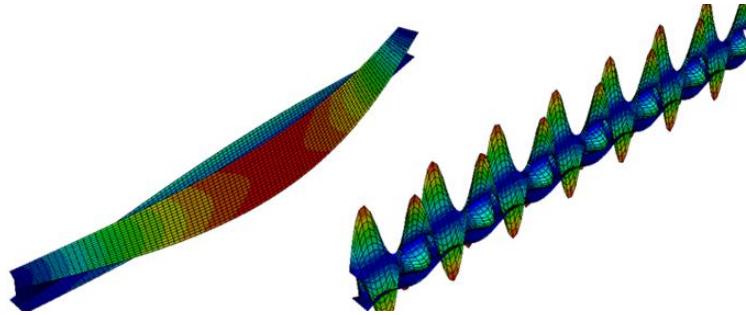


Fig. 22. First global and first local buckling modes of the studied member

Regarding the amplitude of these imperfections, recent research was carried out by Couto et al. [49] investigated the effect of material and geometrical imperfections on the capacity of welded slender I-shaped beams. a value of  $b/100$  was recommended for the maximum effect of the local imperfection. Moreover, a preliminary work on imperfection sensitivity of cold formed steel lipped channel columns at high temperatures was carried out by Kaitila [35]. the author proposed  $L/500$  and  $h/200$  as suitable values for global and local imperfections, respectively.

Therefore, the chosen values in this comparison fell within the established range commonly found in the existing literature.

Table 6. Parameters used for residual stress sensitivity analysis

Geometry		Temperatures	Residual stress patterns	global imperfection	Local imperfection
$h$	300 (mm)	20 °C	Taras [51].	$L/2000$	$b/100$
$b$	240 (mm)	400 °C	ECCS [52].	$L/1000$	$b/200$
$t_w$	4 (mm)	500 °C	Barth and White [53]	$L/800$	
$t_f$	6 (mm)		Chacón [54]	$L/600$	
$A$	4032 (mm <sup>2</sup> )		Best-fit Prawel [55]	$L/400$	

The combinations of the initial global and local geometrical imperfections considered are presented in Table 7. The ECCS residual stress pattern [44] is considered in the numerical simulations. The results show the direct correlation between the amplitude of the initial



imperfections and the buckling resistance of the studied member. The bigger the imperfection values, the smaller the buckling capacity. The load capacity difference between the case when initial global imperfection is equal to  $L/2000$  and the case when it equals to  $L/400$  (with fixed local imperfection  $b/100$ ) is:  $(118.924-106.953)/106.953 \approx 11\%$  at 500 °C, while it is equal to 9.9% at room temperature. On the other hand, the amplitude of initial local imperfection, especially when accompanied by a relatively big initial global imperfection amplitude (e.g.  $L/400$ ), has a smaller effect on the load capacity of the member.

*Table 7. Results of initial global and local imperfections sensitivity analysis*

Model ID	Global imperfection	Local imperfection	Temperature (°C)	Load Capacity (kN)
NL 1	L/2000	b/100	0	185.042
			400	134.251
			500	118.924
NL 2	L/2000	b/200	0	188.204
			400	136.847
			500	121.696
NL 3	L/1000	b/100	0	179.9
			400	130.404
			500	115.273
NL 4	L/1000	b/200	0	183.341
			400	132.880
			500	117.429
NL 5	L/800	b/100	0	177.667
			400	128.745
			500	113.625
NL 6	L/800	b/200	0	181.143
			400	131.107
			500	115.460
NL 7	L/600	b/100	0	174.259
			400	126.258
			500	111.113
NL 8	L/600	b/200	0	177.786
			400	128.545
			500	112.449
NL 9	L/400	b/100	0	168.31
			400	122.082
			500	106.953
NL 10	L/400	b/200	0	171.76
			400	124.582
			500	106.662

## 4.2. Sensitivity to initial geometrical imperfections

Fig. 23 shows the different buckling resistance at 500°C for all cases that have fixed initial local imperfection ( $b/200$ ) and different initial global imperfection amplitudes. It can be seen that the initial global imperfection value affects not only the ultimate strength but also the initial stiffness. When increasing the initial global imperfection with fixed initial local imperfection amplitude, the ultimate strength and initial stiffness decrease significantly.

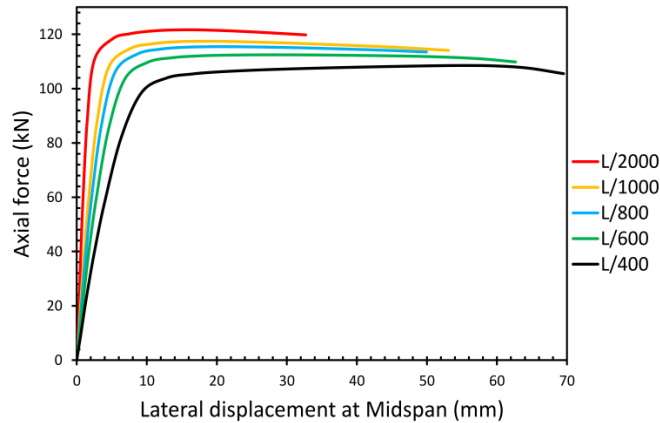


Fig. 23. Load capacity of the studied member at 500 °C with initial local imperfection  $b/200$  and different initial global imperfection values

Fig. 24 shows the different buckling capacities at 500°C for cases with fixed initial global imperfection and two different local imperfection amplitudes. It shows clearly that the initial local imperfection has no influence on the initial stiffness of the member. It is worthy to mention that axial force and bending moment increase proportionally, so that only the axial force-displacement relationship is presented.

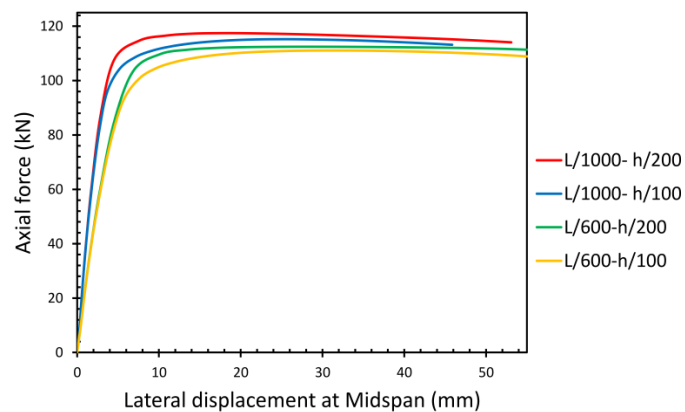


Fig. 24. Load capacity of the studied member at 500 °C with fixed global imperfection and two different initial local imperfection values

### 4.3. Sensitivity to residual stresses

This section presents an analysis of the impact of residual stress on the ultimate strength of the beam-column at 500°C, (the section geometry and residual stress patterns are given in Table 3). The initial global and local imperfections were set at 80% of  $L/750$  for the global mode and (70-80% of  $b/100$ ) for the local mode, following the recommendations provided in Annex C of EN1993-1-5. Fig. 25 illustrates that the response is nearly identical when considering Taras and ECCS residual stress patterns at 500°C. Additionally, the 'Best-fit Prawel' pattern yields the most conservative scenario with the worst outcome, while the 'Barth and white' pattern has the least influence.

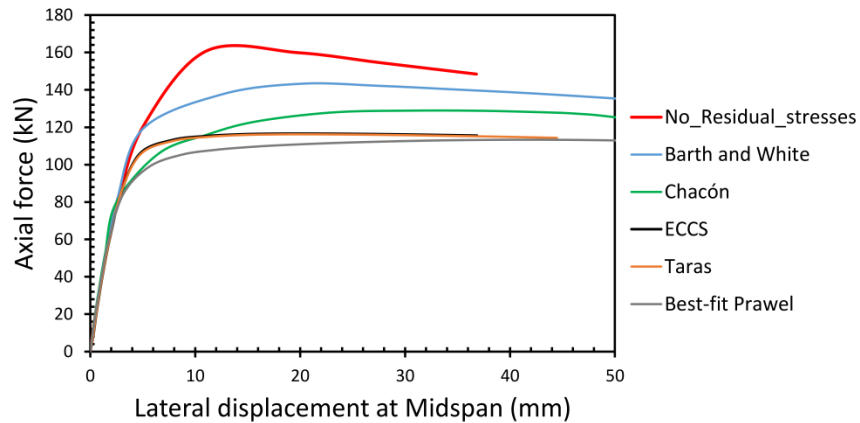


Fig. 25. Influence of different residual stresses distributions at 500°C

Table 8 shows the influence of the residual stress on the ultimate strength of the beam-columns at room temperature, 400 °C, and 500 °C. At room temperature, ECCS residual stress pattern gives the lowest ultimate strength and it represents the most conservative scenario. However, at 400 °C, Taras and ECCS residual stress patterns give almost the same ultimate strength, and for higher temperatures, considering 'Best-fit Prawel' pattern results in the most conservative result (the least buckling resistance). Moreover, it can be seen that the effect of residual stress at 500°C is about 13% less than its effect at ambient temperature which is illustrated in Fig. 26.

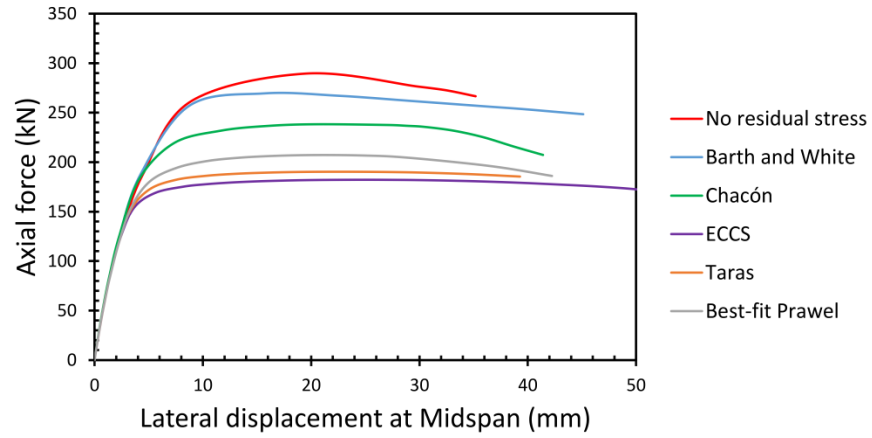


Fig. 26. Influence of different residual stresses distributions at ambient temperature

Table 8. Results of residual stress sensitivity analysis

Temperature (°C)	Barth and White (kN)	Taras (kN)	Best-fit Prawel (kN)	Chacón (kN)	ECCS (kN)	NO residual stress (kN)
500	143.28	116.22	113.34	128.88	116.58	160.81
400	169.38	132.62	135.14	153.16	132.03	187.57
0	269.49	190.32	207.21	238.29	182.24	289.48

#### 4.4. Thesis 1

I explored the impact of structural imperfections, namely initial global and local geometrical imperfections, as well as residual stress, on the local buckling capacity of class 4 steel beam-columns at elevated temperatures (400°C and 500°C).

I showed that initial global geometrical imperfections have a slightly larger effect on the studied class 4 steel beam-column at elevated temperatures. These imperfections not only affect the buckling resistance but also the initial stiffness of the member.

Moreover, a sensitivity analysis of residual stresses revealed that the local buckling resistance of the class 4 beam-column becomes slightly less sensitive to residual stresses as temperatures rise. Nonetheless, the influence of residual stresses remains significant and should be properly considered.

Finally, through the analysis of the effect of various residual stress patterns at different temperatures on the same member, it was observed that the ECCS residual stress pattern had the greatest impact on buckling resistance at room temperature. However, at 500°C, both the Taras and ECCS patterns produced similar responses, while the Best-fit Prawel pattern had the most significant influence, representing a more conservative scenario. Consequently, I recommend the use of the "Best-fit Prawel" pattern in further research for local buckling fire design of class 4 steel beam-columns, instead of the widely used "ECCS" pattern. [S1]

## 5. The effect of cross-section shape and slenderness ratio on buckling capacity of steel columns at elevated temperatures

### 5.1. The impact of cross-section shape on buckling capacity at elevated temperatures

The impact of various factors on the global buckling capacity of steel columns at elevated temperatures is diverse. To avoid oversimplification, these factors must be accurately considered. Furthermore, the available information regarding the effects of these factors on **hot-rolled I-section steel columns at elevated temperatures** is insufficient and even contradictory in some cases. Therefore, there is still a need to analyze **these members** under these conditions. Consequently, this section presents a study that investigates the influence of different factors on the buckling strength of steel **columns** at elevated temperatures. The study focuses on three parameters: slenderness ratio, residual stress, and material model, and their impact on the response of steel columns with different hot-rolled cross-sections (IPE, HEA) at elevated temperatures. The investigation includes four cross-sections and examines ten different non-dimensional slenderness values  $\bar{\lambda}$  ranges between (0.25 to 2.00) for modeling the columns at three different temperatures (400°C, 500°C, 600°C). A total of 500 numerical simulations were conducted, utilizing steel grade S235 for all members. The load-carrying capacities of columns with different non-dimensional slenderness  $\bar{\lambda}_z$  values were calculated using the GMNIA model, as described in Section 3.4.

The following results were obtained:

Local buckling occurred at the mid-height of the column when the non-dimensional slenderness value of the IPE180 column was below  $\bar{\lambda}_z < 0.4$ , at temperatures of 400°C ( $\bar{\lambda}_{400^\circ\text{C}} = 0.478$ ), 500°C ( $\bar{\lambda}_{500^\circ\text{C}} = 0.456$ ), and 600°C ( $\bar{\lambda}_{600^\circ\text{C}} = 0.493$ ). Similarly, for the HE240A column, local buckling occurred when the non-dimensional slenderness value was below  $\bar{\lambda}_z < 0.44$ , at temperatures of 400°C ( $\bar{\lambda}_{400^\circ\text{C}} = 0.538$ ), 500°C ( $\bar{\lambda}_{500^\circ\text{C}} = 0.513$ ), and 600°C ( $\bar{\lambda}_{600^\circ\text{C}} = 0.554$ ). Conversely, when the non-dimensional slenderness ratio was higher, the steel columns exhibited global buckling as the failure mode. Figures 27 and 28 illustrate the deformed shapes of the steel columns under global and local failure modes, respectively. In these figures, U1 represents the horizontal displacement of the steel column.

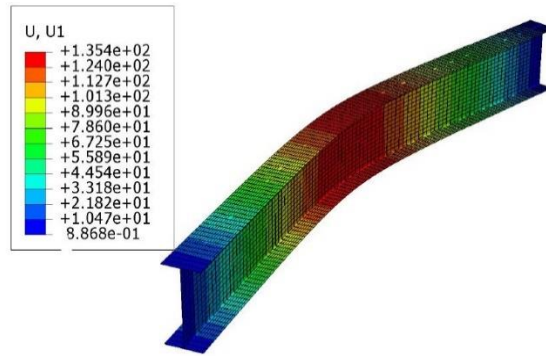


Fig. 27. Global failure mode of columns

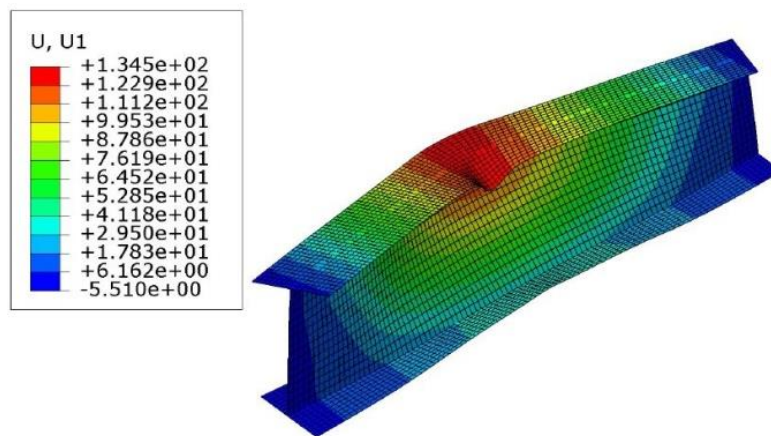


Fig. 28. Local failure mode of columns

Figures 29, 30, 31, and 32 depict similar behavior among columns with the same cross-section type (HEA). Additionally, it is evident that the EN1993-1-2 buckling curve overestimates the buckling reduction factors for all cases where the non-dimensional slenderness of the columns at elevated temperatures is below 1.5. However, as the non-dimensional slenderness values increase, the difference between the EN1993-1-2 buckling curve and the numerical results diminishes. Furthermore, the simplified method presented in EN1993-1-2 for calculating the buckling capacities of steel columns at elevated temperatures completely disregards the shape and dimensions of the cross-section. This approach does not appear to be suitable or appropriate.

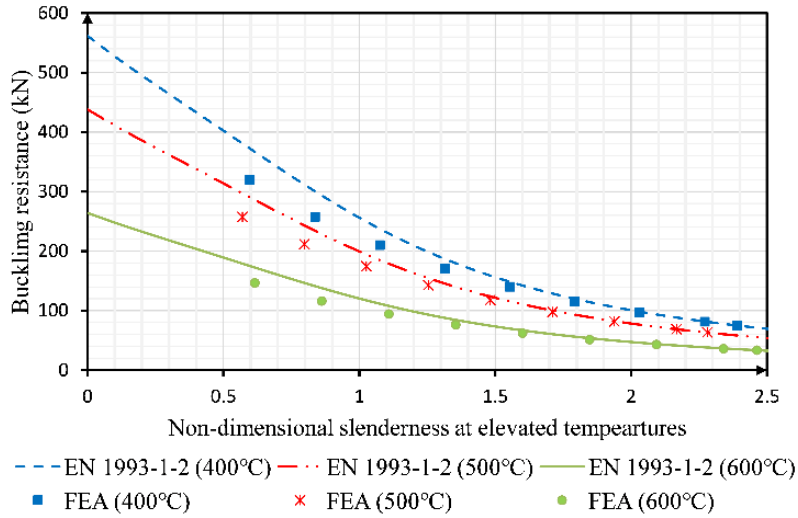


Fig. 29. Comparison of EN 1993-1-2 buckling curves and GMNIA results for IPE180 cross section

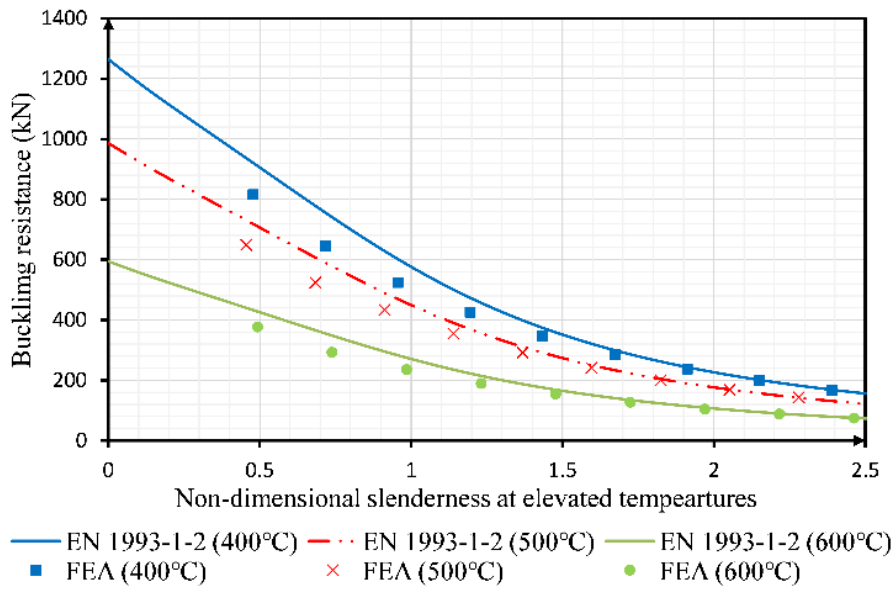


Fig. 30. Comparison of EN 1993-1-2 buckling curves and GMNIA results for IPE300 cross section



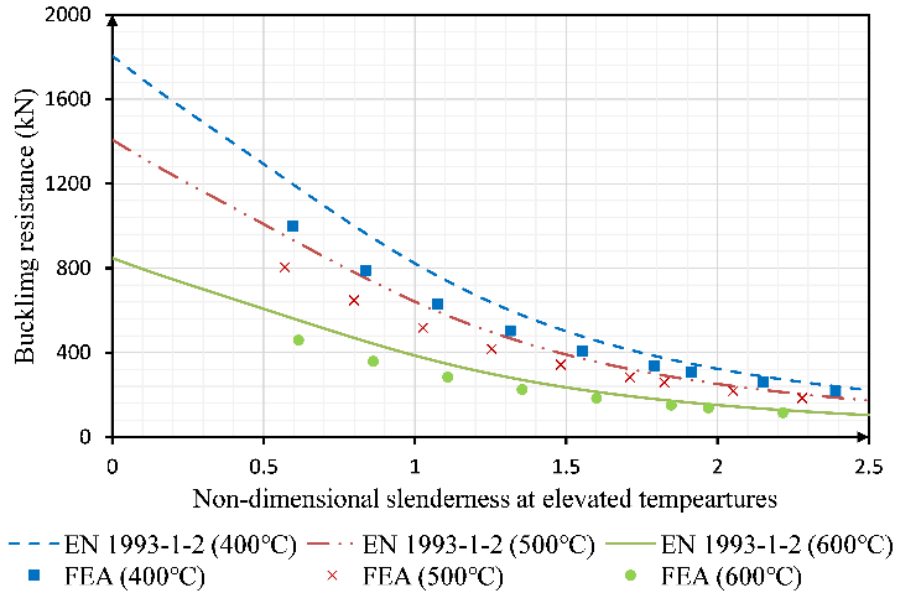


Fig. 31. Comparison of EN 1993-1-2 buckling curves and GMNIA results for HE240A cross-section

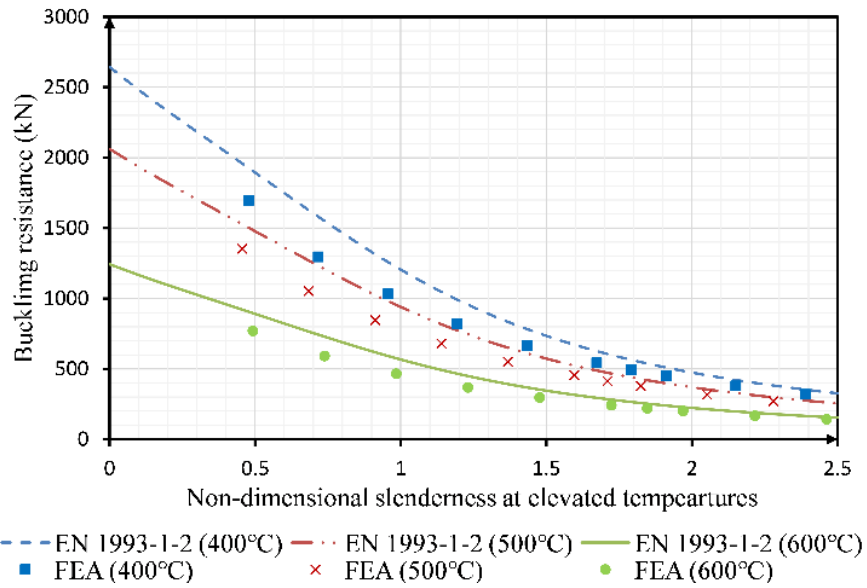


Fig. 32. Comparison of EN 1993-1-2 buckling curves and GMNIA results for HE300A cross-section

## 5.2. Effect of the residual stress on different cross-sections at elevated temperatures

In order to demonstrate the impact of residual stress, finite element analyses were conducted for columns with and without residual stress. The resulting overall buckling resistances of IPE180, IPE300, HE240A, and HE300A at elevated temperatures are displayed in Figures 33-36, respectively. Additionally, the influence of residual stress on various cross-sections at a temperature of 500 °C is illustrated in Figure 37.

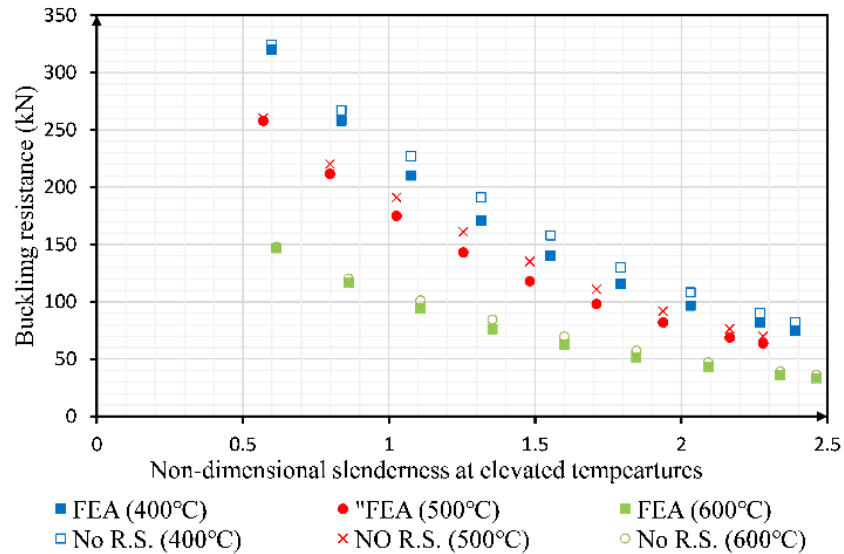


Fig. 33. Influence of residual stress on buckling resistance of columns with IPE180 cross section

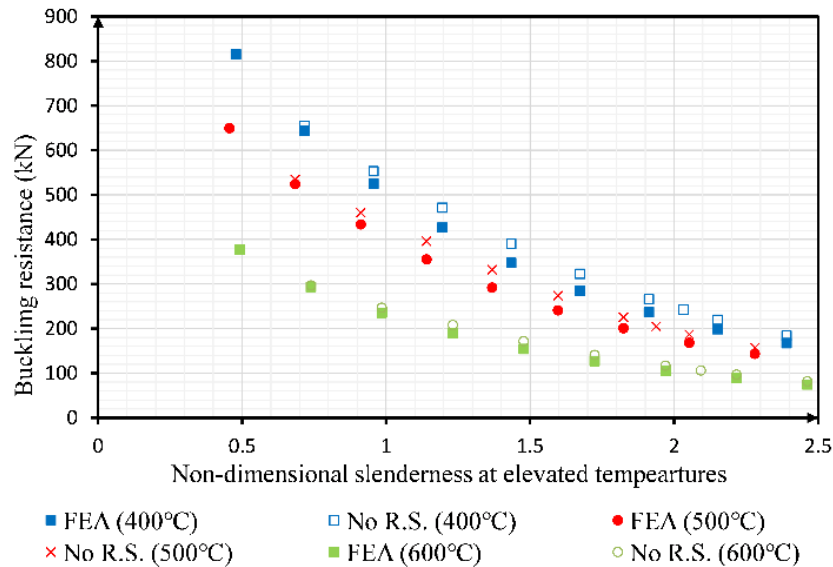


Fig. 34. Influence of residual stress on buckling resistance of columns with IPE300 cross section

The impact of residual stress on the buckling resistance of steel hot-rolled section columns varies depending on the section type and steel temperature, as outlined below:

- Residual stress has a more pronounced effect on columns with HEA cross-sections, resulting in a maximum reduction of up to 19% in buckling resistance. In contrast, columns with IPE cross-sections experience a maximum reduction of approximately 10% due to residual stress.
- The influence of residual stress is slightly greater on columns at 500 °C compared to those at 400 °C or 600 °C.
- The residual stress has the most significant influence on overall buckling resistance when the non-dimensional slenderness at elevated temperatures is equal to  $\bar{\lambda}_{600\text{ °C}} = 1.6$  for *IPE180* cross-section,  $\bar{\lambda}_{600\text{ °C}} = 1.47$ , for IPE300,  $\bar{\lambda}_{600\text{ °C}} = 1.84$  for HE240A. and  $\bar{\lambda}_{600\text{ °C}} = 1.72$  for HE300A, as depicted in Fig. 38. Generally, the impact of residual stress on buckling capacity is most significant for intermediate non-dimensional slenderness ratios ( $\bar{\lambda}_z$ ) ranging from 1.2 to 1.6, while it becomes smaller for other slenderness ratios.
- The effect of residual stress on columns with a slenderness ratio of  $\bar{\lambda}_{z,\theta} \leq 0.65$  is negligible.

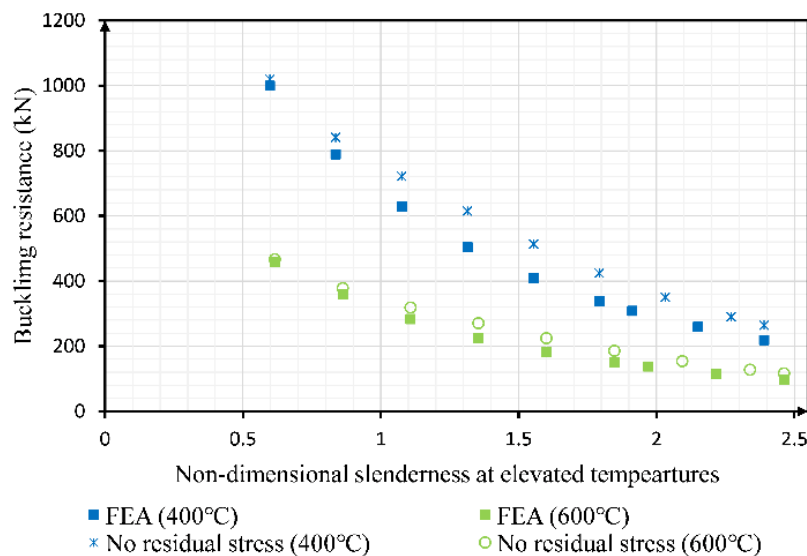


Fig. 35. Influence of residual stress on buckling resistance of columns with HE240A cross section

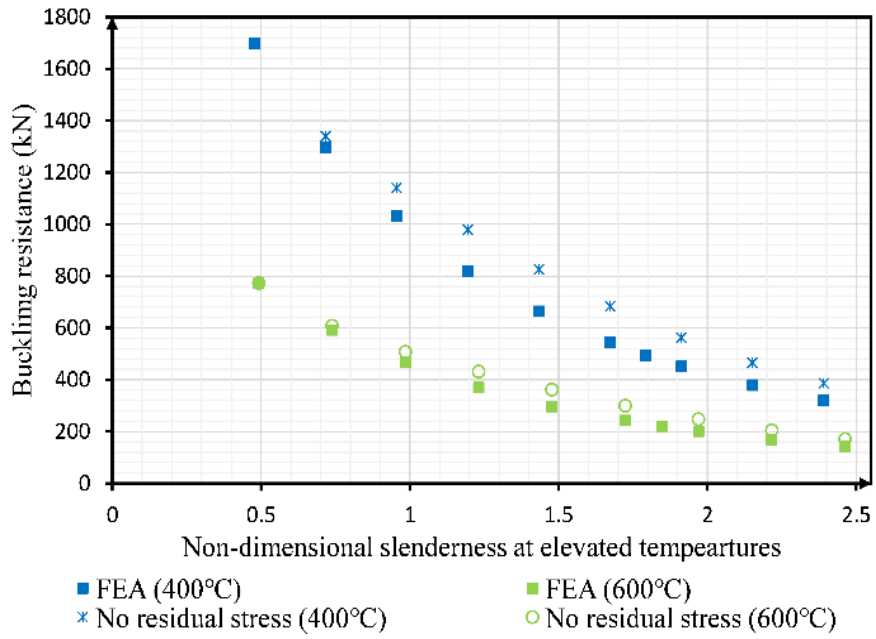


Fig. 36. Influence of residual stress on buckling resistance of columns with HE300A cross section

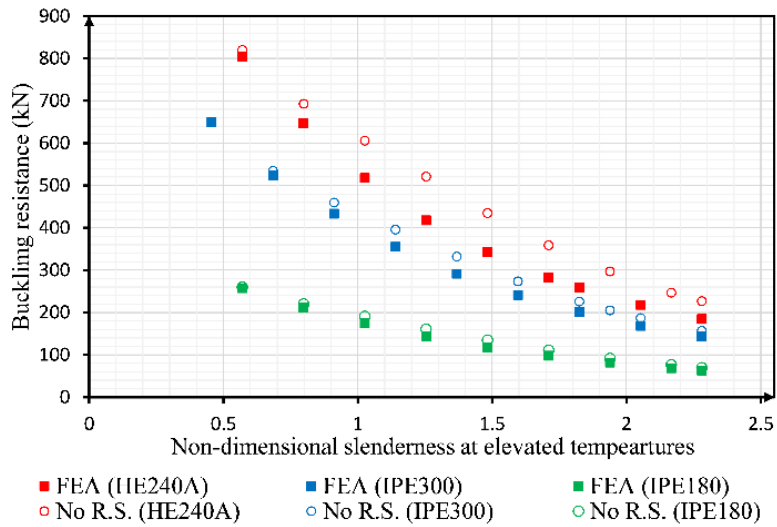


Fig. 37. Influence of residual stress on buckling resistance of columns with different cross sections at 500°C

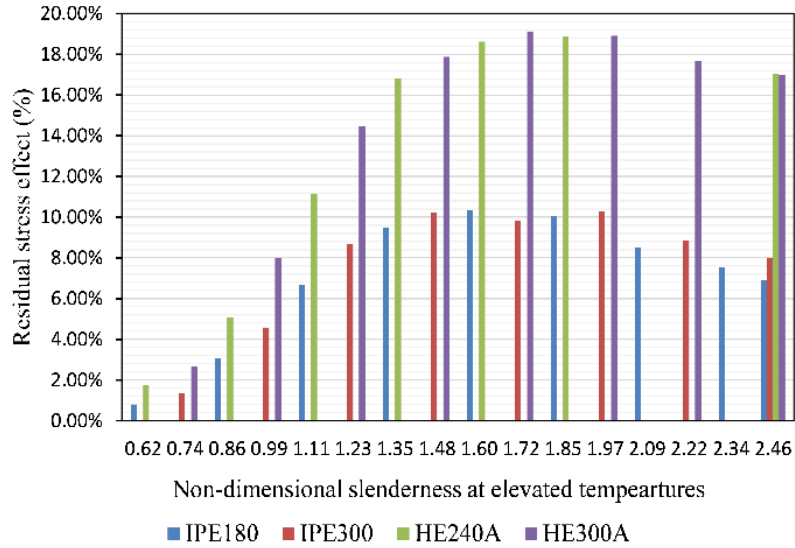


Fig. 38. Influence of residual stress on buckling resistance of columns with different cross-sections at 600°C

### 5.3. Influence of the material stress strain curve on buckling resistance

To examine how mechanical properties of the material affect the overall buckling resistance of steel hot-rolled I-section axial compressed columns at elevated temperatures, two stress-strain constitutive relations are employed in the finite element models: EN1993-1-2 and the Bilinear model. The resulting overall buckling resistances of steel columns with IPE300 and HE300A cross-sections, calculated using these two stress-strain relationships, are depicted in Fig. 39 and Fig. 40, respectively. Additionally, Fig. 41 illustrates the impact of mechanical properties on the buckling resistance of columns with IPE180 and HE240A cross-sections at a temperature of 500 °C.

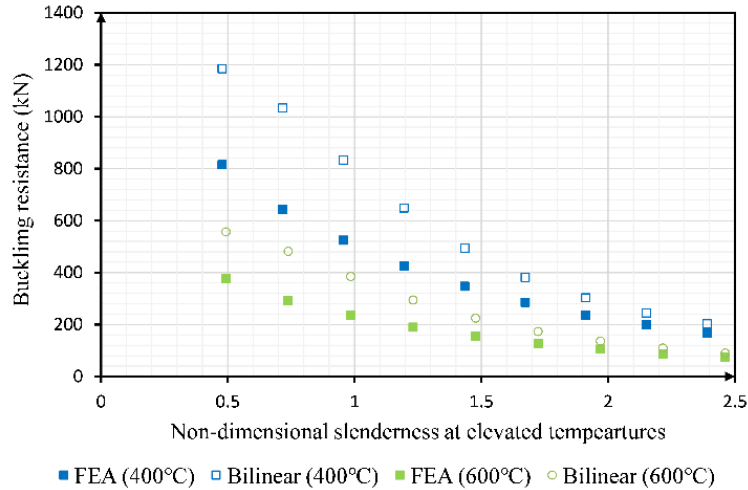


Fig. 39. Influence of residual stress on buckling resistance of column with of IPE300 cross section

In general, when there is high material nonlinearity in steel, it causes a decrease in the Young's modulus of the material. This, in turn, leads to early development of plasticity, increased deformation, and ultimately a reduction in the buckling capacity of the structure.

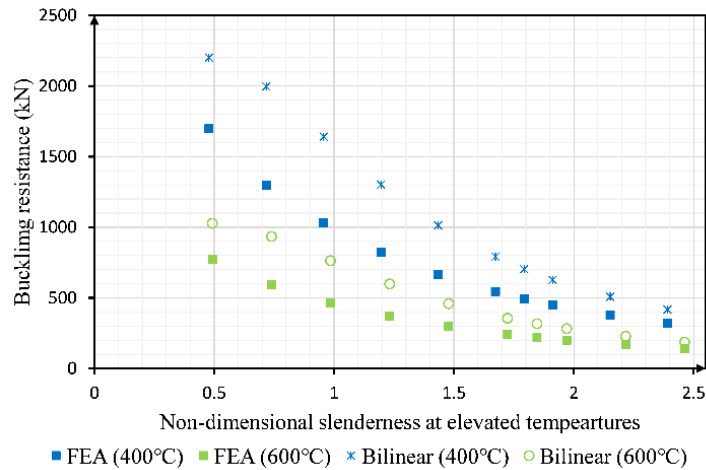


Fig. 40. Influence of residual stress on buckling resistance of column with of HE300A cross section

The EN1993-1-2 stress-strain curve for structural steel at elevated temperature adopted in the numerical model has a relatively low proportionality limit, and that leads to much lower buckling loads compared to those calculated using the bilinear material model in which the proportional limit is assumed to be the yield stress.

The yield plateau and material nonlinearity have a significant influence on the buckling capacity of hot-rolled I-section steel columns, and especially for columns with low slenderness ratio (short columns).

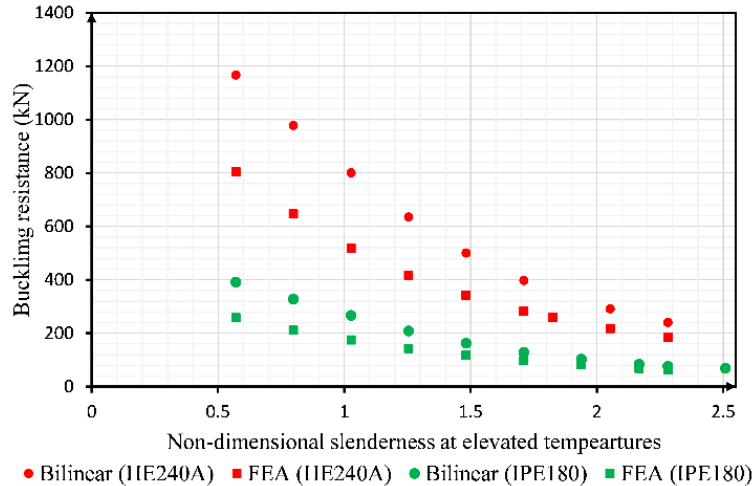


Fig. 41. Influence of residual stress on buckling resistance of column with different cross sections at 500 °C

#### 5.4. Thesis 2

I investigated the global design of steel columns with different hot-rolled cross-sections (IPE, HEA) at three different elevated temperatures (400°C, 500°C, 600°C) with different slenderness ratios ( $\bar{\lambda}$ ) ranging from 0.25 to 2.00.

The results obtained from the finite element model demonstrated that the simplified method specified in EN 1993-1-2 generally produces unsafe estimation of the buckling capacity for steel columns with non-dimensional slenderness ratios ( $\bar{\lambda}_\theta$ ) of 1.5 or less. However, as the non-dimensional slenderness ratio increases, the discrepancy between the EN1993-1-2 buckling curve and the FEM results diminishes.

Furthermore, I found that residual stresses have a more significant impact on the global buckling capacity of steel columns with HEA cross-sections, resulting in a maximum reduction of up to 19% in the buckling resistance. Conversely, for IPE cross-sections, the maximum reduction in buckling resistance due to residual stresses is approximately 10%.

Additionally, the influence of residual stresses on the buckling capacity of columns is bigger for intermediate slenderness ratios ( $\bar{\lambda}_z = 1.2 - 1.6$ ), while it becomes less significant for other slenderness ratios and negligible for short columns ( $\bar{\lambda}_{z,\theta} \leq 0.65$ ). [S2]

## **6. Overall Imperfection Method for fire design**

### **6.1. General**

In this section, the application of the OIM in designing structural members that are subjected to high temperatures is presented. The methodology involves using the results from Linear Buckling Analysis (LBA), which encompasses the elastic critical load factor, the buckling mode shape, and the second-order internal moments resulting from modal geometric imperfections. Moreover, the approach assumes that complex global buckling modes can be categorized into a finite number of fundamental buckling modes, such as flexural buckling or lateral-torsional buckling. Additionally, it presumes that the standard buckling curves for all fundamental buckling modes at elevated temperatures have been calibrated and can be integrated into the proposed methodology to ensure the required level of design reliability.

The OIM involves two fundamental blocks of steps:

- Universal Transformation
- Analytical solution

#### **6.1.1. Universal Transformation (BS-1)**

The universal Transformation, indicated as BS-1 block in Table 9, is employed to transform a structural member with a complex buckling problem into an appropriately defined equivalent reference member (ERM). This ERM serves as a prototype model representing the corresponding fundamental buckling mode. This process can be considered as the most comprehensive extension of the effective length (or equivalent member) method for addressing any buckling problem, as previously demonstrated by Szalai et al. in [11].

Initially, numerical analyses should be conducted on the perfect model of the structural member under the applied loads. These analyses include Linear Elastic Analysis (LA) and Linear Buckling Analysis (LBA). Subsequently, the equivalent point of the member is determined, which is located at the cross-section where the utilization is highest due to second-order modal internal forces.



The properties of the equivalent reference member (ERM), such as cross-section, internal forces, and buckling mode type, are derived from this equivalent point. The length of the ERM is determined to ensure that the critical load factors of the structural member being examined and of the corresponding ERM are equal.

The validity of the Universal Transformation method was previously verified by Hajdú [10] for ambient temperature conditions, validating its suitability for practical applications. In this research, it is assumed that the established conclusion remains valid when considering elevated temperatures.

### **6.1.2. Analytical solution (BS-2)**

The OIM methodology utilizes the Analytical Solution (referred to as the BS-2 block in Table 9), which employs closed-form equations derived from the theory of elastic stability, as described in references such as [56]. Moreover, the standard buckling curves corresponding to the equivalent global buckling mode [1] are incorporated. This approach represents a generalization of the interaction equations commonly used in design standards like EN1993.

In the OIM method, imperfection factors from the Ayrton-Perry Formula based standard design curves are employed to determine the initial equivalent amplitude for the geometric imperfection described by the buckling mode shape. To achieve this, the amplitude scale factor for the buckling shape is first calculated to derive the equivalent geometric imperfection. By subjecting the design model of the analyzed member to the aforementioned initial equivalent geometric imperfection and calculating the internal forces and moments using geometrically nonlinear analysis (GNIA), the determination of the cross-section resistance through a conservative interaction approach becomes equivalent with evaluating the overall buckling resistance.

Within this chapter, a comprehensive overview and detailed explanation of the essential stages involved in the proposed OIM for fire design is presented. These steps are outlined in a step-by-step manner, ensuring clarity and coherence. Furthermore, to show the practical application of the method, an illustrative example is provided, along with a comparison of the obtained results to those obtained through geometrically and materially nonlinear analysis with imperfections

(GMNIA). This example serves to demonstrate the effectiveness and reliability of the proposed OIM for fire design situation.

Table 9. The scheme of the generalized OIM

Phase 1 Structural Member	Phase 2 Transformations	Phase 3 Analytical solution	Standard Buckling Curves
<b>BS-1</b> Linear Elastic Analysis Linear Buckling Analysis	<b>Structural Member → ERM</b>	<b>ERM</b>	
		<b>BS-2</b> Elastic Stability Equation	<b>Imperfection Factors of AP formulas</b>
Checking utilization of Global Buckling Resistance	<b>ERM → Structural Member</b>	Equivalent Amplitude	

## 6.2. Main steps of OIM at elevated temperatures

Before explaining the steps of the method, it is worth mentioning that the adaptation to fire was primarily achieved by integrating adjustments to steel material properties in the original formulation of the Overall Imperfection Method based on EN 1993-1-2. Furthermore, the critical parameter in the formula is the imperfection factor, responsible for addressing second-order effects and forming the basis for standard safety calibration. In the following, we will proceed with the step-by-step procedure at elevated temperatures.

### 6.2.1. ‘Structural Member → ERM’ transformation

The ‘Structural Member → ERM’ transformation technique is utilized to simplify complex buckling problems, as depicted in Fig. 42.

The specific details of this transformation for structural members under ambient temperature conditions are outlined in the publication by Szalai and Papp [11].

The transformation technique is based on the underlying assumption that the essential mechanical characteristics of the actual complex buckling problem can be extracted from a particular point on the structural model. This point is identified as the one where the utilization of cross-section resistance, calculated from the modal second-order internal moments generated by the buckling mode shape, reaches its maximum. In other words, it corresponds to the location with the highest second-order flexural curvature of the compressed flange, as defined in paragraph 5.3.1 (11) of

the EN 1993-1-1. It is assumed that this maximum modal utilization is equal to the one calculated on the ERM, establishing an equivalence between the examined structural model and the ERM.

$$U_{sec,cr,\theta}^{II}(ep) = U_{sec,cr,\theta}^{II,ERM} \quad (49)$$

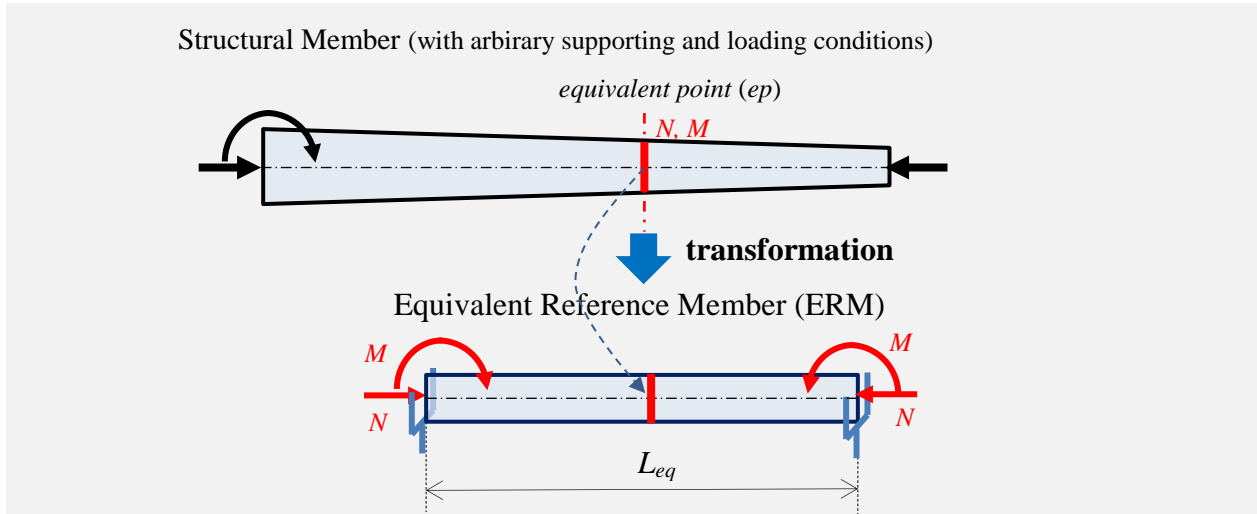


Fig. 42. The illustration of the 'Structural Member  $\rightarrow$ ERM' transformation

In Equation (49), the left-hand side corresponds to the modal utilization calculated at the equivalent point (ep) of the analyzed structural model. On the other hand, the right-hand side represents the modal utilization of the ERM (located at the mid-span and determined using the second-order theory) with the subscript II denoting the second-order theory and the subscript  $\theta$  denoting elevated temperature. The determination of the equivalent point's location in the analyzed structural model is based on the following condition:

$$U_{sec,cr,\theta}^{II}(ep) = \max U_{sec,cr,\theta}^{II}(x) \rightarrow x = ep \quad (50)$$

In general, the Equivalent Reference Member (ERM) is a straight member with a uniform cross-section, simply supported, and subjected to a constant compressive force and/or bending moments. To determine the specific characteristics of the ERM, such as its cross-section, length, loading, and buckling mode, the information obtained from the equivalent point of the analyzed structural model is utilized. Here are the key considerations for the ERM:

- The cross-section of the ERM will be identical to that of the structural member at the equivalent point.

- The constant axial force and moments acting on the ERM will be the same as the internal axial force and moments calculated at the equivalent point of the analyzed structural member.

Table 10. The fundamental Buckling Mode Classes (BMC) in case of double symmetric cross-sections

BMC	Cross-section at the $ep$	Active load components at the $ep$	Buckling mode shape displacement(s)* at the $ep$	Buckling mode
BMC_01	doubly symmetric	$N^I$	$w_{cr}$	flexural buckling about strong axis (FB $y$ )
BMC_02		$N^I$	$v_{cr}$	flexural buckling about weak axis (FB $z$ )
BMC_03		$N^I$	$\varphi_{cr}$	torsional buckling (TB)
BMC_04		$M_y^I$	$v_{cr}; \varphi_{cr}$	lateral-torsional buckling (LTB)
BMC_05		$N^I; M_y^I$	$v_{cr}; \varphi_{cr}$	coupled buckling (FB $z$ + LTB)

\*  $v$  and  $w$  denote the displacements in directions of the principle axes of the cross-section, while  $\varphi$  denotes the rotation around the member axis.

To determine the equivalent length  $L_{eq}$  of the ERM, the appropriate fundamental buckling mode must first be selected from Table 10. Since the cross-section and the loading at the equivalent point of the studied structural member are identical to those of the ERM, the elastic critical load factors must equal to satisfy Eq. (49). The elastic critical load of the ERM can be calculated using the well-known analytical formulas for each fundamental buckling modes (e.g. see [56]) from which the equivalent length of the ERM can be determined based on the equivalency of the elastic critical load factors. By following this procedure, the ERM can be fully defined.

To determine the equivalent length  $L_{eq}$  of the ERM, the appropriate fundamental buckling mode must first be selected from Table 10. Since the cross-section and the loading at the equivalent point of the studied structural member are identical to those of the ERM, the elastic critical load factors must equal to satisfy Eq. (50). The elastic critical load of the ERM can be calculated using the well-known analytical formulas for each fundamental buckling modes (e.g. see [58]) from which the equivalent length of the ERM can be determined based on the equivalency of the elastic critical load factors. By following this procedure, the ERM can be fully defined.

### 6.2.2. The solution of the ERM

Once the Equivalent Reference Member (ERM) has been thoroughly defined, the analytical solution offers the essential information required to address the buckling problem of the analyzed structural member. The analytical solution for the ERM relies on the utilization of the generalized Ayrton-Perry Formula (APF). The imperfection factor plays a crucial role in accurately accounting for the second-order effects and ensuring standard safety calibration. Szalai [21] introduced an imperfection coefficient specifically designed for coupled flexural and lateral-torsional buckling under elevated temperature conditions, which can be mathematically expressed as follows:

$$\eta_{NM,\theta} = \frac{\alpha_{sec,NM,\theta}}{\alpha_{sec,N,\theta}} \eta_{N,\theta} + \mu \frac{\alpha_{sec,NM,\theta}}{\alpha_{sec,M,\theta}} \eta_{M,\theta} \quad (51)$$

In Eq.(51)  $\eta_{N,\theta}$  and  $\eta_{M,\theta}$  are the calibrated standard imperfection factors corresponding to the buckling modes for flexural buckling and lateral-torsional buckling at elevated temperature respectively,  $\alpha_{sec,N,\theta}$   $\alpha_{sec,M,\theta}$  and  $\alpha_{sec,NM,\theta}$  are the cross-sectional resistance multiplication factors taking the buckling active loads into account, and  $\mu_{\theta}$  is an interaction factor dependent on the pure elastic critical loads of the equivalent reference member [21]:

$$\mu_{\theta} = \sqrt{\frac{1 - \alpha_{cr,\theta} N^I / N_{cr,z,\theta}}{1 - \alpha_{cr,\theta} N^I / N_{cr,x,\theta}}} \quad (52)$$

In Eq. (52)  $\alpha_{cr,\theta}$  is the critical load factor of the structural member,  $N_{cr,z,\theta}$  and  $N_{cr,x,\theta}$  are the flexural and the torsional critical load of the ERM at elevated temperature. The imperfection factors are determined in the EN 1993-1-2 for all the classes of cross-sections [1], see Table 11 and Table 12.

Table 11. Imperfection factor for flexural buckling at elevated temperature

parameter	class of cross-section (EN1993-1-2)	
	class 1; class 2; class 3	class 4
reduced slenderness	$\bar{\lambda}_{\theta} = \bar{\lambda} \sqrt{\frac{k_{y,\theta}}{k_{E,\theta}}}$ where $\bar{\lambda} = \sqrt{\frac{Af_y}{N_{cr}}}$	$\bar{\lambda}_{\theta} = \bar{\lambda} \sqrt{\frac{k_{p0.2,\theta}}{k_{E,\theta}}}$ where $\bar{\lambda} = \sqrt{\frac{A_{eff} f_y}{N_{cr}}}$
imperfection coefficient	$\alpha = 0.65 \sqrt{\frac{235}{f_y}}$	
imperfection factor	$\eta_{N,\theta} = \alpha \bar{\lambda}_{\theta}$	
<p>Note:</p> <p><math>A_{eff}</math> must be calculated using <math>\varepsilon = \sqrt{235/f_y}</math></p>		

Table 12. Imperfection factor for lateral-torsional buckling at elevated temperature

parameter	class of cross-section (EN1993-1-2)	
	class 1; class 2; class 3	class 4
reduced slenderness	$\bar{\lambda}_{LT,\theta} = \bar{\lambda}_{LT} \sqrt{\frac{k_{y,\theta}}{k_{E,\theta}}}$ ; $\bar{\lambda} = \sqrt{\frac{Wf_y}{M_{cr}}}$	$\bar{\lambda}_{LT,\theta} = \bar{\lambda}_{LT} \sqrt{\frac{k_{p0.2,\theta}}{k_{E,\theta}}}$ ; $\bar{\lambda}_{LT} = \sqrt{\frac{W_{eff} f_y}{M_{cr}}}$
imperfection coefficient	$\alpha_{LT} = 0.65 \sqrt{\frac{235}{f_y}}$	
imperfection factor	$\eta_{M,\theta} = \alpha_{LT} \bar{\lambda}_{LT,\theta}$	
<p>Notes:</p> <p>(i) <math>W</math> should be calculated according to the class of cross-section</p> <p>(ii) <math>W_{eff}</math> should be calculated using <math>\varepsilon = \sqrt{235/f_y}</math></p>		

### 6.2.3. The ‘ERM → Structural Member’ transformation

The  $\delta_{eq}$  equivalent amplitude of the initial geometrical imperfection must be determined for the shape of the elastic buckling mode  $\eta_{cr,\theta}$  of the examined structural member. It is done using again Eq. (53), where the left-hand side of the equation can be evaluated as follows:

$$U_{sec,cr,\theta}^{II}(ep) = \delta_{eq} U_{sec,cr,\theta}(ep) \frac{1}{\alpha_{cr,\theta} - 1} \quad (53)$$

In Eq. (53)  $U_{sec,cr,\theta}(ep)$  represents the modal cross-sectional utilization at the equivalent point computed from the buckling mode shape with arbitrary amplitude. The calculation of the right-hand side of the Eq. (53) can be performed by employing the imperfection coefficient given in Eq. (54) and the generalized APF defined in [11] and [21]:

$$U_{sec,cr,\theta}^{II,ERM} = \eta_{NM,\theta} \frac{1}{\alpha_{sec,NM,\theta}} \frac{1}{1 - \frac{1}{\alpha_{cr,\theta}}} \quad (54)$$

Using the equivalency relationship of Eqs. (49) with Eqs. (53-54) the standard conform equivalent imperfection amplitude can be calculated:

$$\delta_{eq} = \eta_{NM,\theta} \frac{\alpha_{cr,\theta}}{\alpha_{sec,NM,\theta}} \frac{1}{U_{sec,cr,\theta}(ep)} \quad (55)$$

### 6.2.4. Checking utilization of global buckling resistance

the last stage of the Overall Imperfection Method (OIM), focuses on assessing the utilization of cross-sectional resistances in the structural member under study. To achieve this, an essential step involves calculating the internal forces and moments using GNIA (Geometrically Nonlinear Analysis) and incorporating the initial equivalent geometrical imperfection. This calculation is outlined in Equation 56, as follows:

$$\eta_{cr,eq}(x) = \delta_{eq} \mu_{cr,\theta}(x) \quad (56)$$

If the maximum utilization of the cross-sectional resistance along the examined structural member ( $U_{max,\theta}$ ) is equal to or less than 1.0, it indicates that the structural member is adequate for the global buckling mode at elevated temperature. Therefore, the fundamental requirement of the APF is to calculate  $U_{max,\theta}$  using the provided linear interaction formulas specific to the cross-

section class. These formulas are presented in equations (57), (58), and (59) as follows:

- class 1 and class 2 cross-sections:

$$U_{max\theta} = \max \left[ \frac{N_{fi,\theta,Ed}^II}{k_{y,\theta} A f_y} + \frac{M_{y,fi,\theta,Ed}^II}{k_{y,\theta} W_{pl,y} f_y} + \frac{M_{z,fi,\theta,Ed}^II}{k_{y,\theta} W_{pl,z} f_y} + \frac{B_{fi,\theta,Ed}^II}{k_{y,\theta} W_{pl,B} f_y} \right] \quad (57)$$

- class 3 cross-sections:

$$U_{max\theta} = \max \left[ \frac{N_{fi,\theta,Ed}^II}{k_{y,\theta} A f_y} + \frac{M_{y,fi,\theta,Ed}^II}{k_{y,\theta} W_{el,y} f_y} + \frac{M_{z,fi,\theta,Ed}^II}{k_{y,\theta} W_{el,z} f_y} + \frac{B_{fi,\theta,Ed}^II}{k_{y,\theta} W_{el,B} f_y} \right] \quad (58)$$

- class 4 cross-sections:

$$U_{max\theta} = \max \left[ \frac{N_{fi,\theta,Ed}^II}{k_{p0.2,\theta} A_{eff} f_y} + \frac{M_{y,fi,\theta,Ed}^II + \Delta M_{y,fi,\theta,Ed}}{k_{p0.2,\theta} W_{eff,y} f_y} + \frac{M_{z,fi,\theta,Ed}^II + \Delta M_{z,fi,\theta,Ed}}{k_{p0.2,\theta} W_{eff,z} f_y} + \frac{B_{fi,\theta,Ed}^II}{k_{p0.2,\theta} W_{eff,\omega} f_y} \right] \quad (59)$$

Equations (57) to (59) take into account the potentially significant effect of the B bimoment associated with warping torsion. This consideration is based on the relevant background paper for the second generation of Eurocode 3 [57]. Additionally, the cross-section properties represented by 'eff' can be determined by applying the calculation procedure outlined in EN1993-1-2 E.2 (2). To guide the design process for elevated temperature cases, the step-by-step procedure of the Overall Imperfection Method (OIM) is conveniently summarized in Table 13. This table provides a concise and organized outline of the OIM implementation specific to the elevated temperatures design.

Table 13. The step-by-step procedure of the OIM at design situation of elevated temperature

<b>BS-1</b>
<b>Step 1:</b> Structural analysis of perfect model of structural member or structure with material properties at elevated temperature
1.1 Linear Elastic Analysis (LA) $\rightarrow N_{\theta}^I; M_{y,\theta}^I$
1.2 Linear Buckling Analysis (LBA) $\rightarrow \alpha_{cr,\theta}; \eta_{cr,\theta}$
<b>Step 2:</b> Determination of the equivalent point
2.1 Calculation of internal second order moments generated by buckling mode deformation $\rightarrow M_{z,cr,\theta,ep}^II; B_{cr,\theta,ep}^II$
2.2 Calculation of cross-section resistances $\rightarrow M_{z,sec,\theta}; B_{sec,\theta}$



2.3 Calculation of cross-section utilizations $\rightarrow U_{Mz,sec,cr,\theta}^{II}; U_{B,sec,cr,\theta}^{II}; U_{sec,cr,\theta}^{II}$
2.4 Determination of location of equivalent point $\rightarrow ep$
<b>Step 3: Buckling mode classification through the equivalent point</b>
3.1 Determination of buckling active force and moment $\rightarrow N_{,ep,\theta}^a; M_{y,ep,\theta}^a$
3.2 Classify the actual buckling mode into appropriate fundamental case (Table 1) $\rightarrow BMC$
<b>Step 4: Equivalent length of the equivalent reference member</b>
Calculation of length of ERM from equality of critical load factors of ERM and examined structure $\rightarrow L_{eq}$
<b>BS-2</b>
<b>Step 5: Buckling-active cross-sectional load multiplication factor</b>
Calculation of linear cross-sectional load multiplication factor from buckling-active loads $\rightarrow \alpha_{sec,NM,\theta}$
<b>Step 6: Equivalent imperfection factor</b>
Calculation of the equivalent <i>standard</i> imperfection factor of the ERM considering the relevant BMC and Eq. (3) $\rightarrow \eta_{NM,\theta}$
<b>Step 7: Equivalent geometrical imperfection</b>
7.1 Calculation of the equivalent scale factor $\rightarrow \delta_{eq}$
7.2 Calculation of the equivalent geometrical imperfection as the scaled buckling mode shape $\rightarrow \eta_{cr,eq}$
<b>Final</b>
<b>Step 8: Checking global buckling resistance</b>
8.1 Geometrically Nonlinear Analysis with Imperfection (GNIA) executed on the examined structural member with the equivalent geometrical imperfection computed in Step 7.2 $\rightarrow N_{fi,\theta,Ed}^{II}; M_{y,fi,\theta,Ed}^{II}; M_{z,fi,\theta,Ed}^{II}; B_{fi,\theta,Ed}^{II}$
8.2 Checking cross-sectional utilizations using conservative interaction formula according to Eq. (9), Eq. (10) or Eq. (11), which is the relevant $\rightarrow U_{max,\theta}$

### 6.3. An illustrative example

To show the practical implementation of the described Overall Imperfection Method (OIM) at elevated temperatures, a numerical example is presented here [58].

The example involves a simply supported beam-column member with a class 4 welded I cross-section (flanges: 240-6; web: 288-4) mm, as illustrated in Fig. 43. The member is subjected axial force and bending moment, leading to uniformly distributed internal forces along its length. The material for the member is steel grade S235, and it is subjected to an elevated temperature of 500 °C.

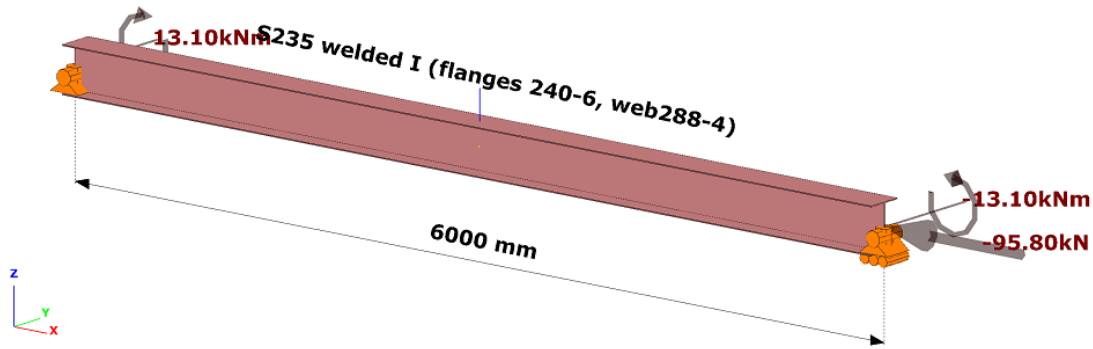


Fig. 43. The structural model of the examined structural member (beam-column)

It should be emphasized that the structural member analyzed in this example is identical to the ERM being examined. At an elevated temperature of 500 °C, the steel material exhibits the following properties: yield strength  $f_{y,\theta}=183.3 \text{ N/mm}^2$ , elastic moduli  $E_\theta=126000 \text{ N/mm}^2$ , and shear moduli  $G_\theta= 48462 \text{ N/mm}^2$ .

The summarized step-by-step numerical procedure is given in Table 14, accompanied by essential notes for each step in Table 15 to facilitate better understanding.

Table 14. The results of the step-by-step OIM calculation in case of the example in Fig. 43.

Steps of OIM	Notation	Dimension	Value
Step 1.1 Linear elastic analysis (LA)			
- Axial force (in the equivalent point given in Step 2.4)	$N^l$	kN	95.80
- Bending moment (in the equivalent point given in Step 2.4)	$M^l_y$	kNm	13.10
Step 1.2 Linear buckling analysis (LBA)			
- Elastic critical load factor	$\alpha_{cr}$		2.830

- Amplitude of buckling shape (in the center of cross-section)	$v_{cr,max}$	mm	37.60
Step 2.1 Internal forces and moment due to buckling mode shape			
- Bending moment (in the equivalent point given in Step 2.4)	$M^{cr,z}$	kNm	9.840
- Bimoment (in the equivalent point given in Step 2.4)	$B^{cr}$	kNm <sup>2</sup>	1.170
Step 2.2 Cross-section utilization (in the equivalent point given in Step 2.4)			
- Due to bending around minor axis	$U_{cr,Mz}$	kNm	0.853
- Due to bimoment	$U_{cr,B}$	kNm <sup>2</sup>	0.690
Step 2.3 Linear load multiplication factor (in the equivalent point)	$\alpha_{sec,cr}$		0.648
Step 2.4 Location of the equivalent point (measured from the member end)	$ep$	mm	3000
Step 3.1 Buckling-active internal forces and moments			
- Axial force	$N^a(ep)$	kN	95.80
- Bending moment around the major axis	$M^a_y(ep)$	kNm	13.10
Step 3.2 Classification of the buckling mode	"Coupled FB and LTB"		
Step 4 Equivalent length of the ERM	$L_{eq}$	mm	6000
Step 5 Equivalent imperfection factor for ERM			
- Slenderness for flexural buckling	$\lambda_z$		0.740
	$\lambda_{z,\theta}$		0.844
- Slenderness for lateral-torsional buckling	$\lambda_{LT}$		0.682
	$\lambda_{LT,\theta}$		0.778
- Imperfection coefficients	$\alpha_z$		0.550
	$\alpha_{LT}$		0.650
- Imperfection factor	$\eta_{N,\theta}$		0.464
	$\eta_{M,\theta}$		0.560
- Cross-sectional resistance multiplication factors	$\alpha_{sec,N}$		7.715
	$\alpha_{sec,M}$		6.549
	$\alpha_{sec,NM}$		3.542
- Modifying factor	$\mu$		0.954
- Equivalent imperfection factor	$\eta_{NM,\theta}$		0.474
Step 6 Buckling-active linear multiplication factor ( $\alpha_{sec,NM}$ in step 5)	$\alpha_{sec,a}$		3.542
Step 7.1 Equivalent scale factor	$\delta_{eq}$		0.263
Step 7.2 Equivalent amplitude	$\eta_{cr,eq}$	mm	9.870
Step 8.1 Internal forces and moments due to second order analysis with equivalent geometric imperfection (GNIA) in the critical point			
- axial compression	$N^{II}_{fi,Ed,\theta}$	kN	95.80
- bending moments	$M^{II}_{y,fi,Ed,\theta}$	kNm	13.71
	$M^{II}_{z,fi,Ed,\theta}$	kNm	2.410

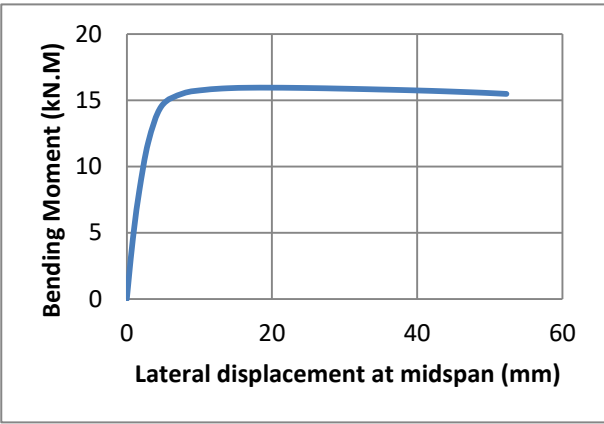
- additional bending moments due to shifting of centroid	$\Delta M''_{y,fi,Ed,\theta}$	kNm <sup>2</sup>	1.859
	$\Delta M''_{z,fi,Ed,\theta}$	kNm	1.159
- bimoment	$B''_{fi,Ed,\theta}$	kNm	0.281
Step 8.2 Cross-section utilization in the critical cross-section	$U^*$		0.788
<b>Buckling load factor by OIM</b> (100% cross-section utilization)	$\alpha_b$		<b>1.220</b>

\*The applied 'eff,new' cross-sectional properties:  $A=2600\text{mm}^2$ ;  $W_y=346646\text{mm}^3$ ;  $W_z=86298\text{mm}^3$ ;  $W_\omega=13.22 \cdot 10^6\text{mm}^4$

Table 15 : Notes to the steps in Table 14

Step 1.1	The analysis may be evaluated on the structural member with material properties at elevated temperature.
Step 1.2	
Step 2.1	These forces are computed from the modal deformation (strains) of the structural member.
Step 2.2	The cross-sectional utilizations are calculated using the internal moments calculated in the Step 2.1 with elastic cross-section properties.
Step 2.3	The load multiplication factor is the reciprocal of the linear sum of the utilizations calculated in the Step 2.2.
Step 2.4	In this example the location of the equivalent point was known (middle of the member). In general this point should be find discussing the utilization distribution along the structural member, given in Step 2.3
Step 3.1	The buckling active forces and bending moments are those first order ones that directly cause the buckling (usually the first order $M_z$ moment and all the second order ones are passive) .
Step 4	In this example the equivalent length is equal to the member length since the examined member itself is the equivalent reference member. In other cases the formulas of theory of elastic stability can be used.
Step 5	The calculation of these parameters is based on the EN1993-1-2 and the research report by Zhao et al. 2014. In any case the elastic cross-sectional properties were used.
Step 6	In this case the buckling-active linear multiplication factor is equal to the $\alpha_{sec,NM}$ factor calculated in in the Step 5.
Step 8.2	The Integrated effective cross-sectional model was used, following the research report by Zhao et al. 2014.

Table 16. Comparing the buckling load factors computed with different methods

method	$\alpha_b$
<p>GMNIA (using Abaqus software)</p>  <div style="border: 1px solid black; padding: 5px; margin-top: 10px;"> <p>According to Annex C of EN1993-1-5 for the geometrical imperfection a combination of global and local buckling modes were used. Amplitude for global mode was the 80% of <math>L/750</math> and for local imperfection was the 80% of <math>b/100</math>.</p> <p>(<math>L</math> is the member length, <math>b</math> is the flange width or web height depending which is the greater)</p> </div>	1.217
EN1993-1-2 4.2.3.2	0.937
<b>Overall Imperfection Method (OIM)</b>	<b>1.220</b>

In Table 16, the buckling load factors are compared calculated with GMNIA, interaction design formula of EN1993-1-2 4.2.3.2 and the presented OIM. It can be seen that the OIM is very close to the GMNIA result.

### 6.4. Thesis 3

I applied the Overall Imperfection Method (OIM) for stability design of a class 4 steel beam-columns at elevated temperatures. Besides, I developed and validated a GMNIA numerical model capable of capturing the response of a class- 4 beam-column behavior in case of fire.

The basic buckling curves of EN 1993-1-2 was used with modifications for class 4 cross-sections published in the research report of Zhao and others (Zhao et al. 2014).

Through a comparison of the buckling load factors calculated using the GMNIA model, the interaction design formula of EN1993-1-2, and the proposed OIM, I have shown that the OIM leads to results that closely match the GMNIA model and surpass the accuracy of the interaction design formula specified in EN1993-1-2. [S3]

## 7. Statistical evaluation of the proposed OIM method for fire global buckling design

This section presents a comparison study between the results of the Overall Imperfection Method proposed in this research and the results of numerical tests conducted by GMNIA on characteristic structural models.

### 7.1. Accuracy assessment of the OIM with exact imperfection factors

First, the Overall Imperfection Method (OIM) and the interaction formula of EN1993-1-2 are initially applied using imperfection factors that are calibrated from the reference results provided by the GMNIA. Excel spreadsheets and associated functions were employed to derive the imperfection factor values for both the Overall Imperfection Method (OIM) and EN1993-1-2 that give the same buckling resistance calculated using the GMNIA for pure cases (flexural buckling and lateral torsional buckling). This is done to ensure that the same buckling capacities are obtained for the pure compression and pure bending cases using the proposed OIM and EN993-1-2 simplified method as those obtained from GMNIA, and then these calibrated imperfection values were used for predicting the buckling capacities of the investigated beam-columns. so that the effect of the imperfection value was excluded and the accuracy of the approaches themselves were compared. The resulting N-M interaction curves for IPE160 and HEA300 cross-sections at temperatures of 500°C and 600°C are then compared between the proposed OIM, EN1993-1-2, and GMNIA in Fig. 44. The OIM and GMNIA curves show very good agreement, while the EN1993-1-2 curves are sometimes conservative. As the next step, the Overall Imperfection Method (OIM) is applied to all members of the investigation program. The comparison between the theoretical value  $r_{t,EN}$  obtained from the EN1993-1-2 interaction formula and the numerical value  $r_e$  obtained from GMNIA is presented in the scatter plot on the left side of Fig. 45. On the right side of the fig. 45, a comparison is made between the theoretical value  $r_{t,OIM}$  derived from the proposed OIM results and the numerical value  $r_e$  obtained from GMNIA. It is important to note that the values of  $r_e$  correspond to the numerical results provided by GMNIA, while  $r_{t,EN}$  and  $r_{t,OIM}$  represent the theoretical values obtained from the EN1993-1-2 interaction formula and the proposed OIM, respectively.

$$r_e = \sqrt{\left(\frac{M_{u,GMNIA}}{M_{fi,\theta,Rd}}\right)^2 + \left(\frac{N_{u,GMNIA}}{N_{fi,\theta,Rd}}\right)^2} \quad (60)$$

$$r_{t,EN} = \sqrt{\left(\frac{M_{u,EN}}{M_{fi,\theta,Rd}}\right)^2 + \left(\frac{N_{u,EN}}{N_{fi,\theta,Rd}}\right)^2} \quad (61)$$

$$r_{t,OIM} = \sqrt{\left(\frac{M_{u,OIM}}{M_{fi,\theta,Rd}}\right)^2 + \left(\frac{N_{u,OIM}}{N_{fi,\theta,Rd}}\right)^2} \quad (62)$$

where  $(Nu, Mu)_{GMNIA}$  is the global buckling resistance given by GMNIA,  $(Nu, Mu)_{EN}$  by EN1993-1-2 interaction formula, while  $(Nu, Mu)_{OIM}$  by the proposed OIM method. Each value is normalized by the corresponding cross-sectional resistances  $N_{fi,\theta,Rd}$ ,  $M_{fi,\theta,Rd}$  defined by the EN1993-1-2.

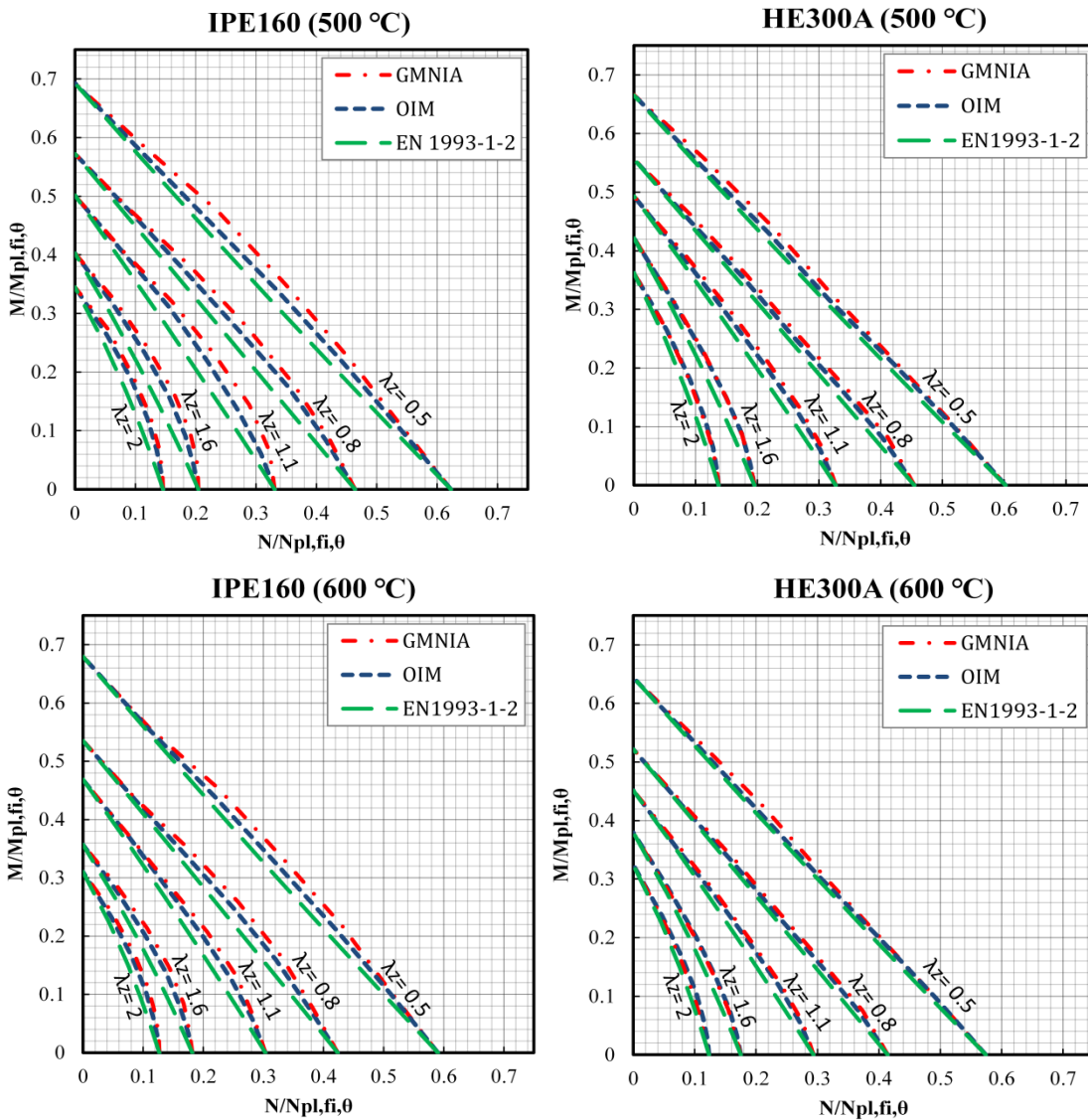


Fig. 44. Interaction curves given by: (i) proposed OIM and EN1993-1-2 with calibrated imperfection factors, (ii) GMNIA

Based on the results presented in Fig. 45 and the statistical analysis presented in Table. 17, it can be observed that the mean value of  $r_e/r_t$  of the proposed OIM is 1.017 on the safe side. The minimum and maximum values are 0.959 and 1.075, respectively. Additionally, it is important to see that in the examined cases, altogether less than 5.0% of the results lied under the unsafe side (mostly for HEA cross-sections), and the coefficient of variation (C.O.V) is very low.

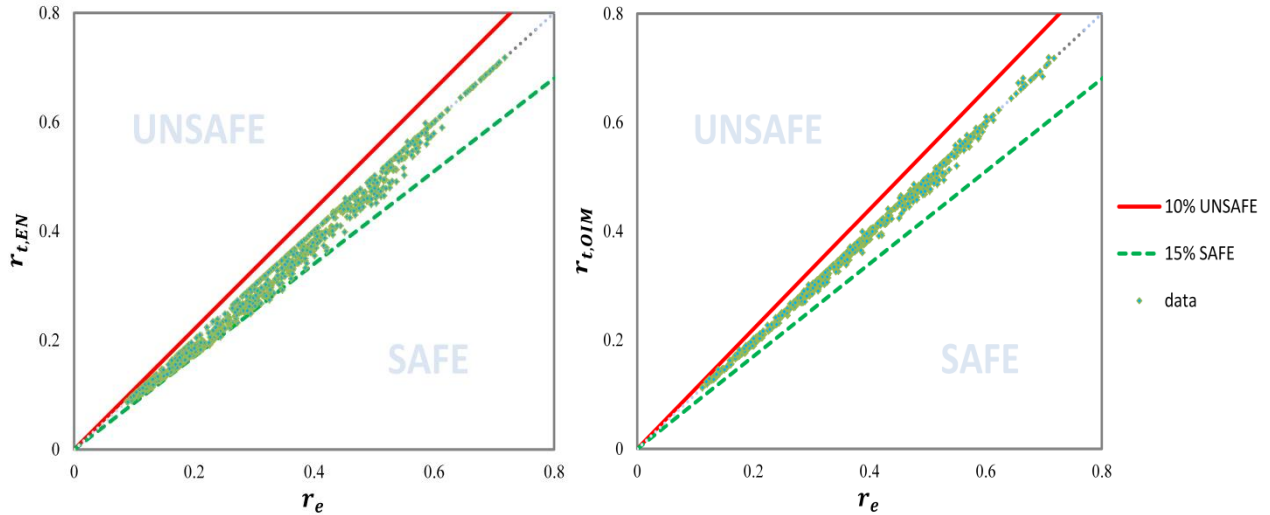


Fig. 45. Statistical evaluation of the results given by (i) the EN1993-1-2 interaction equation (Left) (ii) the proposed OIM method (Right)

On the other side, the interaction method of EN1993-1-2 produce more conservative results, with a mean value of 1.057, and maximum value of 1.19, and a C.O.V is more than twice larger than that of the OIM. The largest deviations from the GMNIA results were observed in the higher slenderness region, where the OIM results remain accurate.

Table 17. Statistical parameters of the normalized OIM method and EN1993-1-2 interaction curve

	Mean value	C.O.V	Min. value	Max. value	n	n<1	n<0.97
GMNIA/OIM	1.017	2.00%	0.959	1.075	1010	46	3
GMNIA/EN1993-1-2	1.057	4.79%	0.979	1.190	1010	40	0



## 7.2. Thesis 4

Based on the analysis of the results, it can be concluded that the Overall Imperfection Method (OIM) is highly accurate in predicting the buckling capacities of beam-columns, especially when the imperfection coefficients of the pure cases (column buckling and beam buckling curves) are precisely calibrated.

In comparison to the interaction formula of EN1993-1-2, the OIM is capable of accurately reflecting the behavior obtained from numerical modeling and predicting the capacities much closer to the numerical results at elevated temperatures. Therefore, the OIM can be a reliable method for predicting the behavior of beam-columns in practical engineering applications. [S4]

## 7.3. Accuracy assessment of the OIM with imperfection factors specified by EN1993-1-2

The current standard of EN1993-1-2 [1] adopts only one buckling curve with unique imperfection coefficient:

$$\alpha = 0.65 \sqrt{\frac{235}{f_y}} \quad (63)$$

In this subsection, the accuracy and reliability of the proposed OIM with the imperfection coefficient given in Eq. (63) for assessment of buckling resistance of steel beam-columns at elevated temperatures are investigated. The results from the proposed OIM are compared to both the numerical results from (GMNIA) and EN1993-1-2 standard results, see Fig. 46.

First of all, it can be seen from Fig. 46 that the proposed OIM curve and the EN1993-1-2 buckling curve are almost identical for the two fundamental cases of pure compression and pure bending moment.

In addition to that, Fig. 47 shows scatter-plots where the corresponding theoretical values  $r_t$  and numerical values  $r_e$  are compared. It can be seen that there is a relatively good agreement between the proposed OIM and the numerical results, with the data being inside the 10% unsafe and 10% safe range. However, it can be noticed from Fig. 46. that the EN1993-1-2 standard

results in unsafe capacities for short members of low slenderness subjected to axial forces, particularly for HE300A cross-sections. The proposed approach is shown to have relatively good agreement with numerical results, but a calibration of the flexural buckling curve may be necessary to safely perform the stability check of relatively short steel columns at elevated temperatures.

It should be mentioned that these unsafe estimations are bigger in the members made of HE300A cross-section while other investigated cross-sections showed similar behavior to that of IPE160. This discrepancy is may be attributed to the use of single imperfection value in fire design situation, as demonstrated for the case of lateral-torsional buckling by Vila Real et al. in [59], while at room temperature different curves are used for different cross-section types.

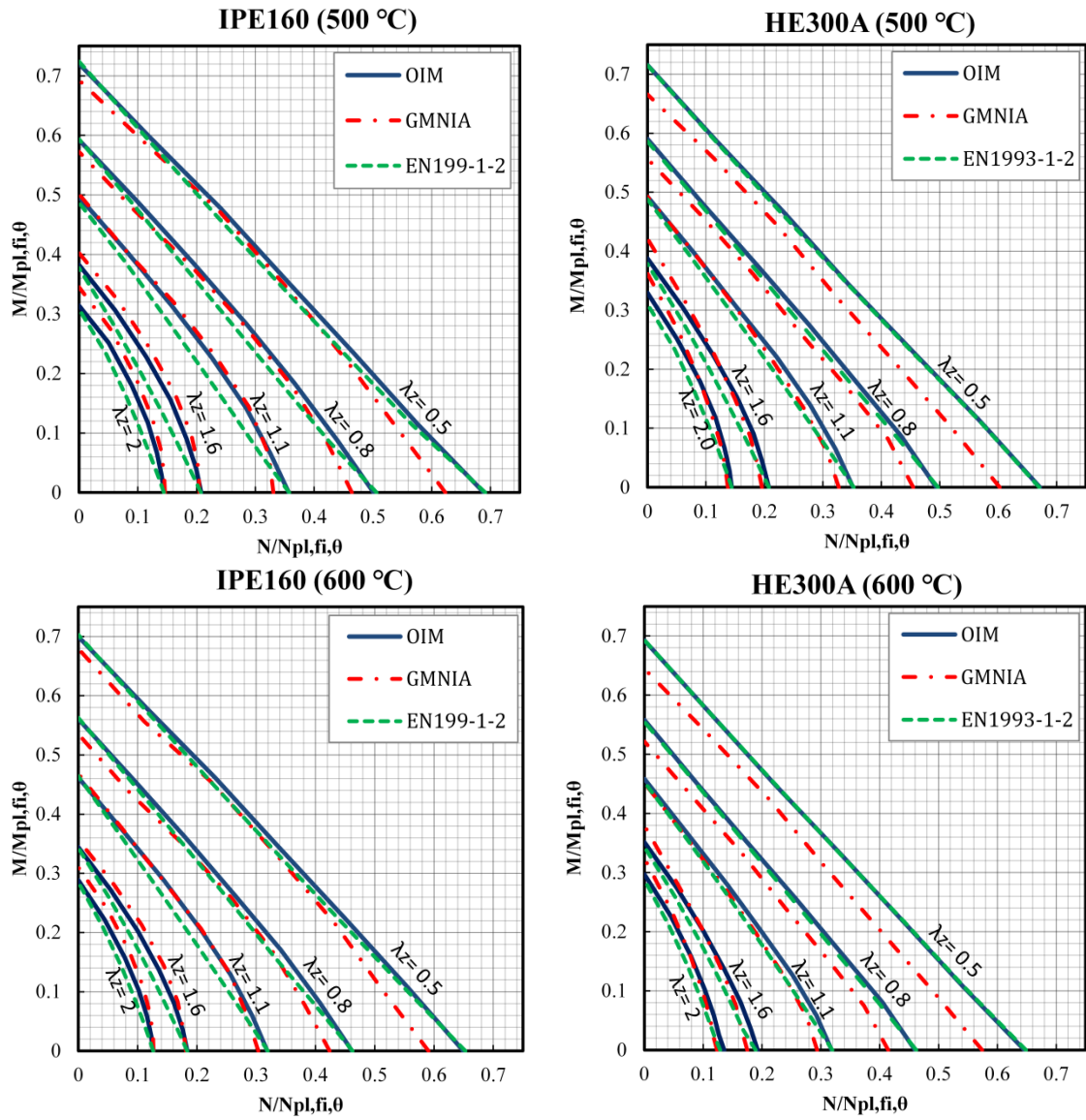


Fig. 46. Interaction curves computed by different methods: (i) proposed OIM with EN1993-1-2's calibrations; (ii) GMNIA; (iii) EN1993-1-2

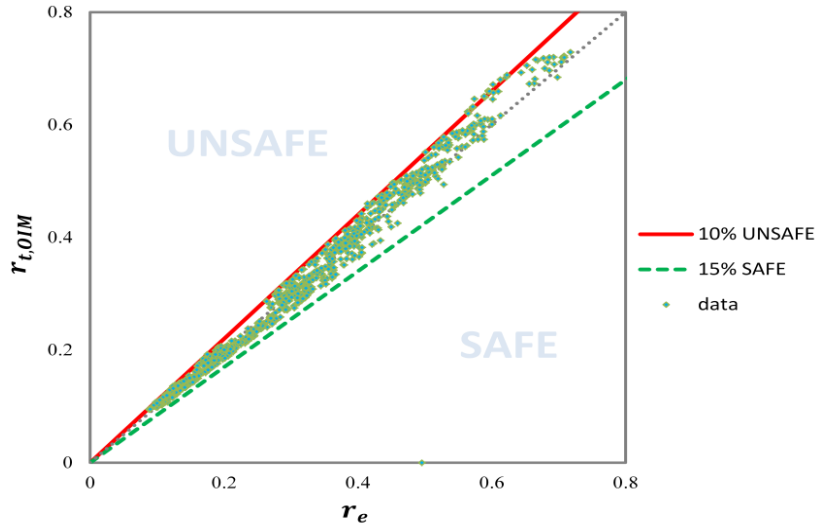


Fig. 47. Validation of the proposed OIM (statistical evaluation)

#### 7.4. Accuracy assessment of the OIM with modified imperfection factor

In the calibration process of buckling resistance, the imperfection coefficient  $\alpha$  is a crucial parameter that serves as the foundation for standard safety calibration. The improvement could be attained by adopting a more conservative imperfection coefficient  $\alpha$  in the AP formula for elevated temperatures, as suggested in [60]:

$$\alpha = 0.85 \sqrt{\frac{235}{f_y}} \quad (64)$$

To validate the proposed OIM approach for beam-column cases, it is important to investigate the fundamental cases of flexural buckling of steel columns under pure compression, and lateral torsional buckling of steel beams under pure bending.

The comparison is made in Fig. 48 shows among the EN1993-1-2 buckling curve, the proposed OIM curve with ( $\alpha=0.65$ ), the modified EN1993-1-2 curve with ( $\alpha=0.85$ ), and the numerical results for (i) members under pure axial compression (left) and for (ii) members under pure bending moment (right). The results indicate that the modified EN1993-1-2 curve with the modified imperfection coefficient of Eq. (64) produces mostly accurate results, except for two cases, as follows:

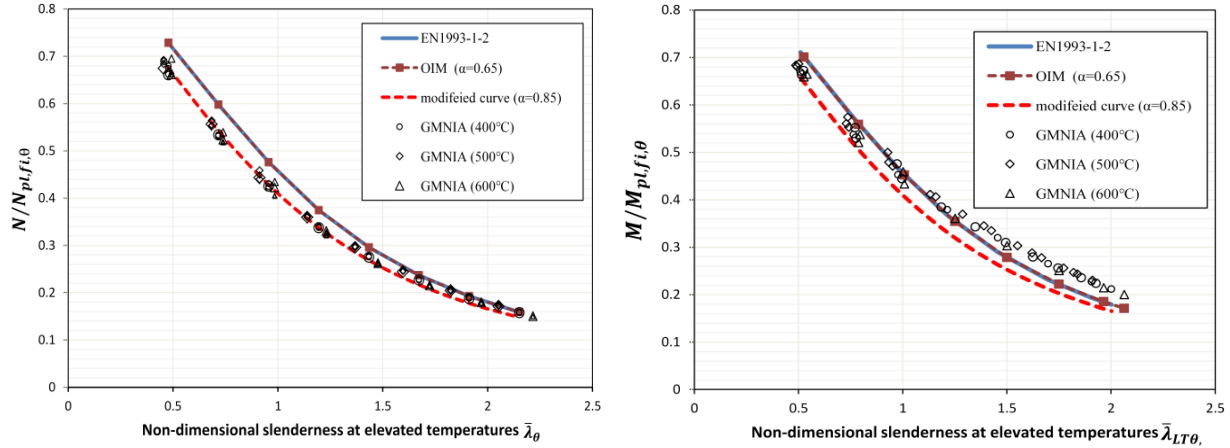


Fig. 48. Comparison of the flexural buckling curves (left) and lateral-torsional buckling curves (right) of EN1993-1-2 and the modified one with  $(\alpha = 0.85\sqrt{235/f_y})$  against numerical results

- (1) for short columns, particularly those made of HEA cross-sections, unsafe predictions of buckling capacity with a maximum difference of 3% are produced
- (2) for members with high slenderness values, relatively conservative results are obtained for lateral torsional buckling.

By introducing the modified value for the imperfection coefficient  $\alpha$  in the AP formula, the results of the proposed OIM are compared with the numerical results, as shown in Fig. 49 and Fig. 50. Based on the statistical evaluation parameters presented in Table 18, it can be seen that:

- the OIM with imperfection coefficient given by EN1993-1-2 is generally unsafe approach with mean value less than 1.00, and minimum value equals to 0.889;
- the OIM with the modified imperfection coefficient  $\alpha = 0.85\sqrt{235/f_y}$  leads to much better results, with a mean value of 1.07 and a better coefficient of variation C.O.V. However, for members with high slenderness under lateral torsional buckling, the method produces conservative results with a maximum value of 1.205;
- the EN1993-1-2 interaction formula produces similar results to the OIM for pure cases, but leads to more conservative results for intermediate slenderness and yields considerably higher C.O.V.

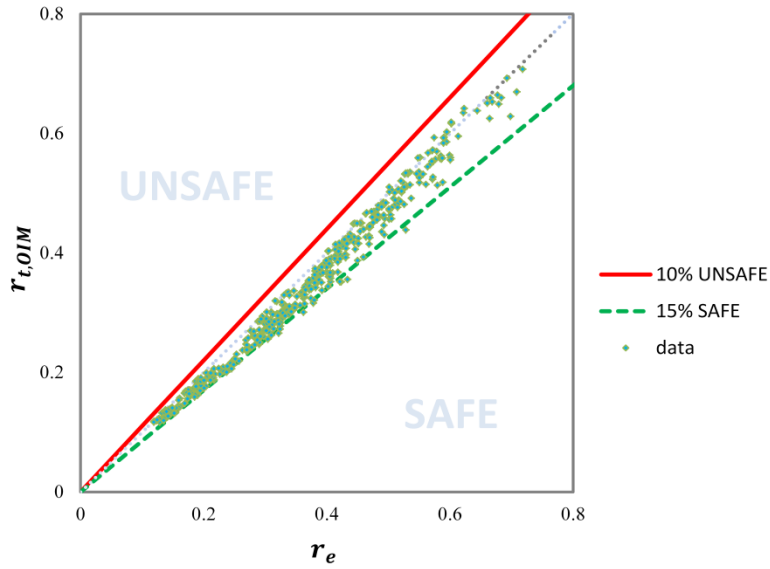


Fig. 49. Statistical evaluation of the proposed Overall Imperfection Method with  $(\alpha = 0.85\sqrt{235/f_y})$

Table 18. Statistical parameters of the proposed OIM method and EN1993-1-2 interaction curve

	GMNIA / OIM( $\alpha=0.65$ )	GMNIA / OIM( $\alpha=0.85$ )	GMNIA / EN1993-1-2 ( $\alpha=0.65$ )	GMNIA / EN1993-1-2 ( $\alpha=0.85$ )
Mean value	0.995	1.070	1.029	1.119
C.O.V	5.07%	4.75%	8.15%	7.81%
Min. value	0.889	0.969	0.882	0.926
Max. value	1.111	1.205	1.226	1.305
n	1010	1010	1010	1010
n<1	462	26	363	57
n<0.97	302	1	229	24

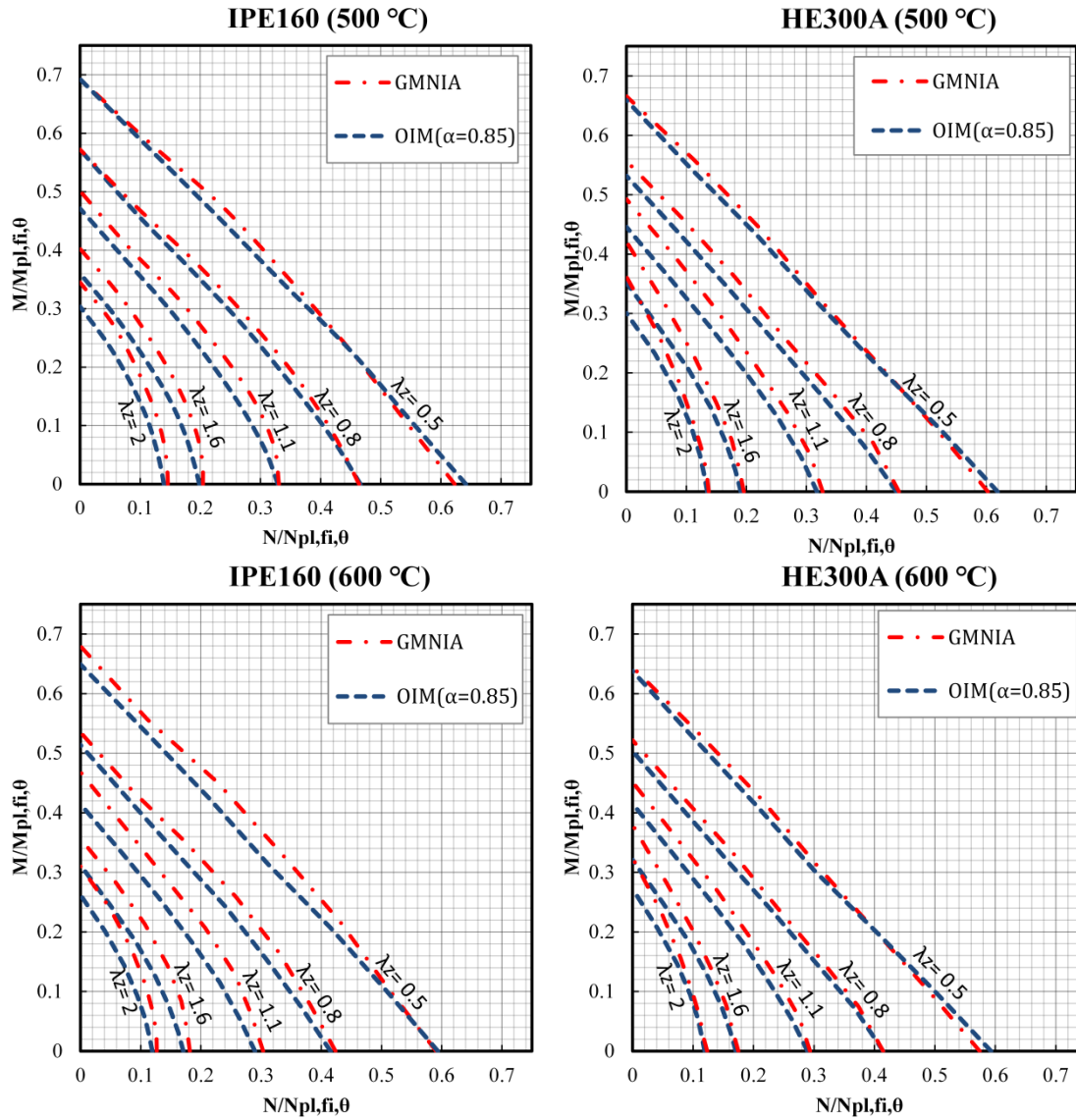


Fig. 50. Comparison between the results of the proposed Overall Imperfection Method with ( $\alpha = 0.85\sqrt{235/f_y}$ ) and the numerical results (GMNIA)

## 7.5. Thesis 5

I investigated the proposed OIM with an imperfection coefficient of  $\alpha = 0.65\sqrt{235/f_y}$ , which is the same value prescribed in EN1993-1-2 for both flexural buckling (FB) and lateral-torsional buckling (LTB) modes. Both the proposed OIM and EN1993-1-2 resulted in unsafe designs mainly for short columns.

Therefore, a more conservative value of the imperfection coefficient at  $\alpha = 0.85\sqrt{235/f_y}$  was examined. Through statistical evaluation, it was observed that the proposed OIM gives significantly improved results compared to the numerical results obtained using  $\alpha = 0.65\sqrt{235/f_y}$ . Nonetheless, conservative predictions were still reported for long members subjected to bending.

These results clearly show the necessity of employing two different imperfection coefficients, one for each buckling mode (flexural buckling and lateral-torsional buckling). [S4]



## 8. Conclusion and future research

.In this chapter, the conclusions and recommendations that stem from the results and methods employed throughout this research project are presented.

### 8.1. Conclusion

- The simplified method prescribed by EN 1993-1-2 results in non-conservative (unsafe) estimations of the buckling strength of steel columns exposed at elevated temperatures, which is influenced by both the cross-section dimensions and slenderness ratio.
- The reason behind this discrepancy may be attributed to the EN1993-1-2 simplified method employing a single buckling curve to estimate the buckling resistance at high temperatures for all types of sections, without considering variations in residual stress magnitudes and distributions among different section types. This approach has been found to be inadequate compared to the numerical results.
- The results indicate that residual stresses have a more significant impact on columns with HEA cross-sections, resulting in a maximum reduction of the buckling resistance of up to 19%. Conversely, for IPE cross-sections, the maximum reduction of the buckling resistance due to residual stresses is around 10%. Additionally, the influence of residual stresses on the buckling capacity of columns is most prominent for intermediate slenderness ratios ( $\bar{\lambda}_z = 1.2 - 1.6$ ), while it becomes less significant for other slenderness ratios and negligible for short columns ( $\bar{\lambda}_{z,\theta} \leq 0.65$ ).
- Based on the analysis of various residual stress patterns at different temperatures, it can be concluded that at room temperature, the ECCS residual stress pattern has the most significant impact on the buckling resistance. However, at 500°C, using either Taras or ECCS residual stress patterns yields nearly identical responses, while the Best-fit Prawel pattern is the most influential (and conservative) case.
- Accurate and consistent results can be obtained through the use of the OIM for fire design of steel members, as long as the imperfection factors applied to the pure buckling modes are precise.
- The semi-probabilistic safety level assessment of the results indicates that the proposed OIM implemented using imperfection coefficients defined in the EN1993-1-2 standard ( $\alpha = \alpha_{LT} = 0.65\sqrt{235/f_y}$ ) produces similar results to those obtained using the EN1993-1-2

design formula. However, both methods can result in unsafe prediction of buckling capacities, particularly for short members and under compression.

- The OIM implemented utilizing a new value of imperfection coefficients, namely using the  $\alpha=\alpha_{LT}=0.85\sqrt{235/f_y}$  proposal gives accurate results that match well with the numerical results obtained through GMNIA.
- In summary, the findings of this research suggest that the proposed Overall Imperfection Method can serve as an alternative method for predicting the buckling resistance of steel beams, column and beam-columns at elevated temperatures. However, further investigations are needed to enhance the accuracy of the imperfection coefficients or factors for the fundamental pure buckling modes.

To this end, this research proposed the use of the Overall Imperfection Method (OIM) for fire design of steel members. Additionally, the research investigated the influences of several factors (material and geometrical imperfections, cross-section dimensions, slenderness ratio, temperature, residual stress ) on the load capacity of steel members at elevated temperatures, with the aim of better understanding the behavior of steel members and developing the methods outlined in the current EN 1993-1-2 standard.

## **8.2. Recommendations and future research**

The findings of this study highlight several avenues for future research. First, the proposed OIM for fire design of steel members should be extended to irregular structural members with irregular loads and support conditions, such as tapered members. Additionally, it is evident that a single imperfection coefficient value used in the current standard EN199-1-2 for both flexural buckling and lateral-torsional buckling modes is not adequate. Therefore, future research should investigate and propose two different imperfection coefficients for each buckling mode. Finally, further research is necessary to examine the effect of different parameters and imperfections in fire situations on the load capacity of steel members.

## References

- [1] EN 1993-1-2:2005, Eurocode 3, Design of steel structures – Part 1–2: General rules Structural fire design. In: European committee for standardization. Brussels, Belgium; 2005.
- [2] Pauli, J., “The Behaviour of Steel Columns in Fire Material - Cross-sectional Capacity - Column Buckling”. ETH Zurich, Institute of Structural Engineering. <https://doi.org/10.3929/ethz-a-009754421>, Zurich, Switzerland, 2012.
- [3] Zhao, B., Oly, R., Morente, F., Vila Real, P., et al. (2014). “Fire design of steel members with welded and hot-rolled class 4 cross-sections”, Final Report of RFCS project FIDESC4, <https://www.researchgate.net/publication/274711521>.
- [4] EN 1993-1-1:2005, Eurocode 3, Design of steel structures – Part 1–1: General rules and rules for buildings. In: European committee for standardization. Brussels, Belgium; 2005.
- [5] Chladný E., Štujberová M. (2013). Frames with unique global and local imperfection in the shape of the elastic buckling mode (Part1). *Stahlbau* 82, pp. 609-617, <https://doi.org/10.1002/stab.201310080>.
- [6] Agüero, A., Pallarés F.J., Pallares L. (2015). Equivalent geometric imperfection definition in steel structures sensitive to lateral torsional buckling due to bending moment. *Engineering Structures* 96 (1), pp. 41-55. <https://doi.org/10.1016/j.engstruct.2015.03.066>.
- [7] Papp, F. (2016). Buckling assessment of steel members trough overall imperfection method. *Engineering Structures* 106, pp. 124–136, <https://doi.org/10.1016/j.engstruct.2015.10.021>.
- [8] Hajdú, G., Papp, F., Rubert, A., (2017). Vollständige äquivalente Imperfectionsmethode für biege- und druckbeanspruchte Stahlträger. *Stahlbau* (86), pp. 483-496, <https://DOI:10.1002/stab.201710471>.
- [9] Hajdú G., Papp F. (2018). Safety Assessment of different stability design rules for beam-columns. *Structures* (14), pp. 376–388. <https://doi.org/10.1016/j.istruc.2018.05.002>.

[10] Hajdú G. (2019). The Validity of the universal transformation method in global buckling design. In: Jeppe, Jönsson (szerk.) The 14th Nordic Steel Construction Conference. Berlin, Germany: Ernst und Sohn, pp. 1-6. , 6 p. <https://doi.org/10.1002/cepa.1149>.

[11] Szalai J.A., Papp F. (2019). New stability design methodology through overall linear buckling analysis. The 14th Nordic Steel Construction Conference, September 18–20, 2019, Copenhagen, Denmark, Ernst & Sohn Verlag für Architektur und technische Wissenschaften GmbH & Co. KG, Berlin · ce/papers. <https://doi.org/10.1002/cepa.1145>.

[12] Papp F., Szalai J.A., Movahedi R.M. (2019). Out-of-plane buckling assessment of frames through overall stability design method. The 14th Nordic Steel Construction Conference, September 18–20, 2019, Copenhagen, Denmark, Ernst & Sohn Verlag für Architektur und technische Wissenschaften GmbH & Co. KG, Berlin · ce/papers. <https://doi.org/10.1002/cepa.1146>.

[13] Szalai J., Papp F., Hajdú G. (2019). Validation of the overall stability design method (OSDM) for tapered members, Stability and Ductility of Steel Structures. Proceedings of the International Colloquia Stability and Ductility of Steel Structures, Prague.

[14] ENV 1993-2: Design of steel structures – Part 2: Steel bridges. CEN, 1997.

[15] Chladný E., Štjuberová M. (2013). Frames with unique global and local imperfection in the shape of the elastic buckling mode (Part2). *Stahlbau* 82, pp. 684-694. DOI: 10.1002/stab.201310082.

[16] Calgaro J. A., Bijlard F., Kuhlmann U., et al. (2010) Consistency of the equivalent imperfections used in design and the tolerance for geometric imperfections used in execution. Document CEN/TC250-CEN/ TC135-Liaison; Version February 2010.

[17] Boissonnade N., Greiner R., Jaspart JP., Lindner J. (2006) New design rules in EN 1993-1-1 for member stability. ECCS technical committee 8 – structural stability, P119. Brussels: European Convention for Constructional Steelwork; 2006.

[18] Taras A., Greiner R., New design curves for lateral-torsional buckling-Proposal based on a consistent derivation. *J Constr Steel Res* 2010;66:648–63.

- [19] Taras A., Greiner R., New design curves for LT and TF buckling with consistent derivation and code-conform formulation. *Steel Constr* 2010;3(3):176–86.
- [20] Taras A, Gonzalez M, Unterweger H. Behaviour and design of members with monosymmetric cross-section. *Proc ICE: Struct Build* 2013;166(8):413–23.
- [21] Szalai J.A. (2017). Complete generalization of the Ayrton-Perry formula for beam-column buckling problems. *Engineering Structures* 153, pp. 205-223. [DOI:10.1016/j.engstruct.2017.10.031](https://doi.org/10.1016/j.engstruct.2017.10.031).
- [22] Hajdú, G., Papp, F. (2016). Overall imperfection method for beam-columns. *International Journal Of Interdisciplinarity In Theory And Practice*. 2016. Pp. 117-122.
- [23] Knobloch, M. (2014). Stability of steel structures in fire. *Stahlbau*, 83(4), 257–264. doi:10.1002/stab.201410147.
- [24] Kirby, B.R., and Preston, R.R., High Temperature Properties of Hot-Rolled Structural Steels for Use in Fire Engineering Studies. *Fire Safety Journal*, 13(1), pp. 27–37, 1988. With permission from Elsevier.
- [25] Rubert, A. and Schaumann, P., Structural Steel and Plane Frame Assemblies under Fire Action. *Fire Safety Journal*, 10, pp.173 – 184, 1983.
- [26] European Convention for Construction Steelwork. Calculation for Fire Resistance of Composite Structures. Technical Note No. 55, ECCS Technical Committee 3, 1989.
- [27] British Standard Institution. British Standard BS 5950, Part 8, Code of Practice for Fire Resistance Design. British Standard Institution, 2000.
- [28] Kay, T. R., Kirby, B. R., Preston, R. R. (1996) Calculation of the heating rate of an unprotected steel member in a standard fire resistance test. *Fire Safety Journal*, 26(4):327–350, 1996.
- [29] Wang Y., Burgess I, Wald F, Gillie M. (2012). Performance-Based Fire Engineering of Structures. 10.1201/b12076.

- [30] Ramberg, W. - Osgood, W. R. (1943) Description of stress-strain curves by three parameters. NACA Technical note 902.
- [31] Outinen, J., Kesti, J., Mäkeläinen, P. (1997) Fire Design Model for Structural Steel S355 Based Upon Transient State Tensile Test Results. *Journal of Constructional Steel Research*. 42(3), pp 161-169.
- [32] Pauli J., Somaini D., Knobloch M., Fontana M. (2012). Experiments on steel columns under fire conditions. ETH Zurich, Institute of Structural Engineering. IBK test report No. 340, Zurich, Switzerland, <https://doi.org/10.3929/ethz-a-007600651>.
- [33] Couto C., Vila Real P., Lopes N., Zhao B. “Local buckling in laterally restrained steel beam-columns in case of fire “. *Journal of Constructional Steel Research* Volume 122, July 2016, Pages 543-556.
- [34] Maraveas, C. “Local Buckling of Steel Members Under Fire Conditions: A Review”. *Fire Technol* 55, 51–80 (2019). <https://doi.org/10.1007/s10694-018-0768-1>.
- [35] Kaitila, O., Imperfection sensitivity analysis of lipped channel columns at high temperatures, *Journal of Constructional Steel Research*, 2002, 58(3), 333-51.
- [36] Vila Real P., Lopes N., Simões da Silva L., Franssen, J.-M. (2007) Parametric analysis of the lateral-torsional buckling resistance of steel beams in case of fire”. *Fire Safety Journal*, vol. 42, iss. 6-7, SEP-OCT, pp. 416-424, 2007.
- [37] Kodur, V., Dwaikat, M.. (2010), Effect of high temperature creep on the fire response of restrained steel beams. *Materials and Structures*. 43. 1327-1341. [10.1617/s11527-010-9583-y](https://doi.org/10.1617/s11527-010-9583-y).
- [38] Morovat, M., Engelhardt, M., Taleff, E., Helwig, T. (2011). Importance of Time-Dependent Material Behavior in Predicting Strength of Steel Columns Exposed to Fire. *Applied Mechanics and Materials*. 82. [10.4028](https://doi.org/10.4028).
- [39] Kuo Chen, Y., Sheng-Jin C., Cun-Ci L., Hung-Hsin, L. (2005). Experimental study on local buckling of fire-resisting steel columns under fire load. *Journal of Constructional Steel Research* - *J CONSTR STEEL RES*. 61. 553-565. [10.1016/j.jcsr.2004.07.001](https://doi.org/10.1016/j.jcsr.2004.07.001).

- [40] Hajdú G. (2021). Buckling resistance of steel beam-columns - the verification of Overall Imperfection Method with numerical method. (In Hungarian), dissertation, 2021.
- [41] Kindmann R., Kraus M.(2011) Steel structures design using FEM. Ernst & Sohn. Online ISBN:9783433600771, [DOI:10.1002/9783433600771](https://doi.org/10.1002/9783433600771).
- [42] Abaqus/Standard, Version 5.8, User's manual, Hibbitt, Karlsson and Sorensen, Inc, USA, 1998.
- [43] BS EN 1090 2. (2008). Execution of steel structures and aluminium structures Part 2: Technical requirements for steel structures. BSI, London, UK.
- [44] ECCS European Convention for Constructional Steelwork. (1976). Manual on stability of steel structures, 2nd ed. Technical Committee 8, Structural stability, [www.eccspublications.eu](http://www.eccspublications.eu).
- [45] Franssen, J. M. Residual stresses in steel profiles submitted to the fire: an analogy, in Proceedings of the 3<sup>rd</sup> CIB/W14 FSF Workshop on Modelling, 25–26 January 1993, Rijswijk, the Netherlands, 103–112.
- [46] Prachař, M., Hricak, J., Jandera, M., Wald, F., Zhao, B., (2016). Experiments of Class 4 open section beams at elevated temperature. *Thin-Walled Structures*, V. 98 (2016), p. 2–18.
- [47] P.M.M. Vila Real, N. Lopes, L. Simões da Silva, P. Piloto, J.-M. Franssen, Numerical modelling of steel beam-columns in case of fire—comparisons with Eurocode 3, *Fire Safety Journal*, Volume 39, Issue 1, 2004.
- [48] Couto, C., Vila Real, P., Lopes, N., Zhao, B., Numerical investigation of the lateral–torsional buckling of beams with slender cross sections for the case of fire, *Engineering Structures*, Volume 106, 2016, Pages 410-421, ISSN 0141-0296, <https://doi.org/10.1016/j.engstruct.2015.10.045>.
- [49] Couto C., Vila-Real, P., “Numerical investigation on the influence of imperfections in the lateral-torsional buckling of beams with slender I-shaped welded sections”, *Thin-Walled Structures*, vol. 145, paper no. 106429, 2019.

[50] EN 1993-1-5, Eurocode 3, Design of steel structures, Part 1-5: Plated structural elements, CEN, Brussels, 2006.

[51] Taras, A. “Contribution to the development of consistent stability design rules for steel members”, Doctoral Thesis, Technical University Graz, 2010.

[52] Greiner R., Salzgeber G., Ofner, R. “New lateral torsional buckling curves  $\chi_{LT}$  - Numerical simulations and design formulae”, European Convention for Constructional Steelwork Technical Committee, Technical report, No. 8, TC-8-2000-014, 2000.

[53] Barth, K. E., White, D. W., “Finite element evaluation of pier moment-rotation characteristics in continuous-span steel I girders”, *Engineering Structures*, vol. 20, pp. 761–778, 1998.

[54] Chacón, R., Serrat, M., Real, E., “The influence of structural imperfections on the resistance of plate girders to patch loading”, *Thin-Walled Structures*, vol. 53, pp. 15–25, 2012.

[55] Kim, Y., “Behavior and design of metal building frames using general prismatic and web-tapered steel I-section members”, PhD Thesis, Georgia Institute of Technology, 2010.

[56] Trahair NS. (1993). Flexural-torsional buckling of structures. CRC Press; 1st edition (July 20, 1993), p. 388, URL: [h`tp://worldcat.org/isbn/0849377633](http://worldcat.org/isbn/0849377633).

[57] Markus Knobloch, Alain Bureau, Ulrike Kuhlmann, Luís Simões da Silva, Hubertus H. Snijder, Andreas Taras, Anna-Lena Bours, Fabian Jörg (2020). Structural member stability verification in the new Part 1-1 of the second generation of Eurocode 3. Part 2: Member buckling design rules and further innovations. *Steel Construction* 13, pp 1-14. DOI:10.1002/stco.20200027.

[58] Szalai, J., Nemer, S., Papp, F. (2021). “The use of the Overall Imperfection Method for fire design situation”. In *Proceedings of the 8th International Conference on Coupled Instabilities in Metal Structures (CIMS 2021)*.

[59] Vila Real, P. M. M.; Lopes, N.; Simões Da Silva, L.; Franssen, J.-M. (2007). Parametric analysis of the Lateral-torsional buckling resistance of Steel beams in case of fire, *Fire Safety*



Journal, Volume 42, Issues 6-7, Pages 416-424, ISSN 0379-7112,  
<https://doi.org/10.1016/j.firesaf.2006.11.010>.

[60] Maia É., Vila Real P., Lopes N., Couto C.. (2020). The General Method for the fire design of slender I-section web-tapered columns. *Thin-Walled Structures*, Volume 155, 2020, 106920, ISSN 0263-8231, <https://doi.org/10.1016/j.tws.2020.106920>.

## List of publications:

[S1] Nemer, S., Papp, F. (2021). “Influence of imperfections in the buckling resistance of steel beam-columns under fire”, *Pollack Periodica*, Vol. 16(2), pp. 1-6. doi: <https://doi.org/10.1556/606.2021.00303>. (cited by 8).

[S2] Nemer, S., Papp, F. (2021). “Numerical Investigation on Flexural Buckling Behavior of Hot-rolled Steel Columns at Elevated Temperatures”, *Periodica Polytechnica Civil Engineering*, 65(3), pp. 918–927, 2021. <https://doi.org/10.3311/PPci.17799>.

[S3] Szalai, J., Nemer, S., Papp, F. (2021). “The use of the Overall Imperfection Method for fire design situation”. In *Proceedings of the 8th International Conference on Coupled Instabilities in Metal Structures (CIMS 2021)*.

[S4] Nemer, S., Szalai J.A., Papp, F. (2023). “The overall imperfection method for fire design situation”, *Engineering Structures*, Vol. 283, 2023, 115884, ISSN 0141-0296, <https://doi.org/10.1016/j.engstruct.2023.115884>

[S5] Nemer, S., (2020) “Numerical study on flexural buckling behavior of steel hot-rolled section columns under elevated temperatures”. In *9th Interdisciplinary Doctoral Conference 2020 book of abstracts*. Conference: Pécs, Hungary 2020.11.27. - 2020.11.28. (PTE) Pécs: Doctoral Student Association of the University of Pécs, pp 247-247 (2020).

[S6] Nemer, S., (2020) “Numerical study on the influence of imperfections in the buckling resistance of steel beam-columns with welded class 4 cross-section at elevated temperatures”. In: *Abstract book for the 16th MIKLÓS IVÁNYI INTERNATIONAL PHD & DLA SYMPOSIUM*. Conference: Pécs, Hungary 2020.10.26. - 2020.10.27. Pécs: Pollack Press, p. 67. (2020).

[S7] Nemer, S., (2023) “ Verification of the Ramberg-Osgood material model for fire design of steel members”. *Slovak Journal of Civil Engineering*, Vol. 31, 2023, No. 2, pp 9–15 (2023). DOI: 10.2478/sjce-2023-0008.

## List of figures:

Fig. 1. Lateral imperfection according to the proposal in [6]and Eurocode 3.....	9
Fig. 2. Fundamental case of Lateral Torsional Buckling according to [7] .....	10
Fig. 3. Relationship between temperature and 0.2% (left) & 1.0% (right) proof stress for BS4360: Grade 50B structural steels [24].....	17
Fig. 4. Stress-strain model for steel at elevated temperature as shown in EN 1993-1-2:2005[1] .....	18
Fig. 5. Alternative stress-strain relationship for steel allowing for strain hardening at temperatures below 400°C as shown in Appendix A of EN 1993-1-2:2005 [1] .....	19
Fig. 6. Reduction factors for the stress-strain relationship of carbon steel at elevated temperatures.....	20
Fig. 7. Modified Ramberg-Osgood material model for steel S355 [31].....	25
Fig. 8. Equivalent uniform moment factor to EN1993-1-2 [1] .....	29
Fig. 9. ABAQUS model and meshing details.....	35
Fig. 10. (Left) Real section vs. FE model section; (Right) modelled cross-section .....	36
Fig. 11. Considered residual stress patterns for $h/b \leq 1.2$ (left) and $h/b > 1.2$ (right) [49].....	37
Fig. 12. EN1993-1-2 Stress-strain relationship for S235 carbon steel at elevated temperatures .....	38
Fig. 13. Comparison of the axial load- displacement curves for S19 column [9] .....	40
Fig. 14. Comparisons of numerical load–vertical displacement curves for three different tests given in [46] .....	41
Fig. 15. Comparison of results obtained by Vila Real et al. [47] using SAFIR, and the results of the developed GMNIA model for the IPE220 cross-section steel column .....	42
Fig. 16. Comparison of results obtained by Vila Real et al. [47] using SAFIR, and the results of the developed ABAQUS model for the IPE220 cross-section steel beam.....	42
Fig. 17. Tested beam: a) scheme; b) test set-up .....	43
Fig. 18. Deformed shape of beam from both a) ABAQUS model and b) real test [46].....	44
Figure 19. Comparison of load–displacement curves as obtained from different numerical analyses [46] .....	44
Fig. 20. Comparison of numerical results obtained by Couto et al. [48], and the results of the developed ABAQUS model steel beams with slender cross section. ....	45
Fig. 21. Details of the beam-column with the applied loads used for residual stress sensitivity analysis ..	47
Fig. 22. First global and first local buckling modes of the studied member .....	48
Fig. 23. Load capacity of the studied member at 500 °C with initial local imperfection $b/200$ and different initial global imperfection values .....	50
Fig. 24. Load capacity of the studied member at 500 °C with fixed global imperfection and two different initial local imperfection values .....	50
Fig. 25. Influence of different residual stresses distributions at 500°C.....	51
Fig. 26. Influence of different residual stresses distributions at ambient temperature .....	52
Fig. 27. Global failure mode of columns.....	55
Fig. 28. Local failure mode of columns .....	55
Fig. 29. Comparison of EN 1993-1-2 buckling curves and GMNIA results for IPE180 cross section.....	56
Fig. 30. Comparison of EN 1993-1-2 buckling curves and GMNIA results for IPE300 cross section.....	56
Fig. 31. Comparison of EN 1993-1-2 buckling curves and GMNIA results for HE240A cross-section ....	57
Fig. 32. Comparison of EN 1993-1-2 buckling curves and GMNIA results for HE300A cross-section ....	57

Fig. 33. Influence of residual stress on buckling resistance of columns with IPE180 cross section.....	58
Fig. 34. Influence of residual stress on buckling resistance of columns with IPE300 cross section.....	58
Fig. 35. Influence of residual stress on buckling resistance of columns with HE240A cross section.....	59
Fig. 36. Influence of residual stress on buckling resistance of columns with HE300A cross section.....	60
Fig. 37. Influence of residual stress on buckling resistance of columns with different cross sections at 500°C.....	60
Fig. 38. Influence of residual stress on buckling resistance of columns with different cross-sections at 600°C.....	61
Fig. 39. Influence of residual stress on buckling resistance of column with of IPE300 cross section.....	62
Fig. 40. Influence of residual stress on buckling resistance of column with of HE300A cross section....	62
Fig. 41. Influence of residual stress on buckling resistance of column with different cross sections at 500 °C.....	63
Fig. 42. The illustration of the ‘Structural Member →ERM’ transformation.....	67
Fig. 43. The structural model of the examined structural member (beam-column).....	74
Fig. 44. Interaction curves given by: (i) proposed OIM and EN1993-1-2 with calibrated imperfection factors, (ii) GMNIA.....	79
Fig. 45. Statistical evaluation of the results given by (i) the EN1993-1-2 interaction equation (Left) (ii) the proposed OIM method (Right).....	80
Fig. 46. Interaction curves computed by different methods: (i) proposed OIM with EN1993-1-2’s calibrations; (ii) GMNIA; (iii) EN1993-1-2.....	83
Fig. 47. Validation of the proposed OIM (statistical evaluation).....	84
Fig. 48. Comparison of the flexural buckling curves (left) and lateral-torsional buckling curves (right) of EN1993-1-2 and the modified one with ( $\alpha = 0.85235/f_y$ ) against numerical results.....	85
Fig. 49. Statistical evaluation of the proposed Overall Imperfection Method with ( $\alpha = 0.85235/f_y$ ).....	86
Fig. 50. Comparison between the results of the proposed Overall Imperfection Method with ( $\alpha = 0.85235/f_y$ ) and the numerical results (GMNIA).....	87

***List of Tables:***

Table 1. Reduction factors for stress-strain relationship of carbon steel at elevated temperatures taken from EN1993-1-2 :2005 [1] .....	21
Table 2. Properties of the cross-sections used in the numerical investigation .....	34
Table 4. Comparison of FE and experimental results from Pauli et al. [32] .....	39
Table 5. Dimensions of the cross-section of the studied member [46] .....	43
Table 6. Dimensions of the cross-section of the studied member [48] .....	45
Table 3. Parameters used for residual stress sensitivity analysis .....	48
Table 7. Results of initial global and local imperfections sensitivity analysis.....	49
Table 8. Results of residual stress sensitivity analysis .....	52
Table 9. The scheme of the generalized OIM .....	66
Table 10. The fundamental Buckling Mode Classes (BMC) in case of double symmetric cross-sections .	68
Table 11. Imperfection factor for flexural buckling at elevated temperature.....	70
Table 12. Imperfection factor for lateral-torsional buckling at elevated temperature.....	70
Table 13. The step-by-step procedure of the OIM at design situation of elevated temperature.....	72
Table 14. The results of the step-by-step OIM calculation in case of the example in Fig. 43. ....	74
Table 15 : Notes to the steps in Table 14 .....	76
Table 16. Comparing the buckling load factors computed with different methods .....	77
Table 17. Statistical parameters of the normalized OIM method and EN1993-1-2 interaction curve .....	80
Table 18. Statistical parameters of the proposed OIM method and EN1993-1-2 interaction curve.....	86